



**TECHNICAL REPORT 0-7095-1**  
TxDOT PROJECT NUMBER 0-7095

# Flood Assessment System for TxDOT

University of Texas at Austin: David Maidment, Paola Passalacqua, Matt Bartos, Sujana Timilsina, Jeil Oh, Andy Carter, Tim Whiteaker, Harry Evans, Christine Thies, Larry Jantzen; KISTERS: Matt Ables, Attila Bibok; Aqua Strategies: Barney Austin, Tim Osting.

US Geological Survey: Scott Grzyb, Jody Avant, Jon Thomas, Michael Nyman, Kristine Blickenstaff

December 2024

Published May 2025

<https://library.ctr.utexas.edu/ctr-publications/0-7095-1.pdf>



Technical Report Documentation Page

|  |  |  |  |                            |           |
|--|--|--|--|----------------------------|-----------|
| 1. Report No.<br>FHWA/TX-25/0-7095-1   |  | 2. Government Accession No.                          |  | 3. Recipient's Catalog No. |           |
| 4. Title and Subtitle<br>Flood Assessment System for TxDOT   |  |  | 5. Report Date<br>Submitted: 31 Oct 2023, Amended 13 Dec 2024  |                            |           |
|  |  |  | 6. Performing Organization Code  |                            |           |
| 7. Author(s)<br><b>University of Texas at Austin:</b> David Maidment, Paola Passalacqua, Matt Bartos, Sujana Timilsina, Jeil Oh, Andy Carter, Tim Whiteaker, Harry Evans, Christine Thies, Larry Jantzen; <b>KISTERS:</b> Matt Ables, Attila Bibok; <b>Aqua Strategies:</b> Barney Austin, Tim Osting.<br><br><b>US Geological Survey:</b> Scott Grzyb, Jody Avant, Jon Thomas, Michael Nyman, Kristine Blickenstaff.  |  |  | 8. Performing Organization Report No.<br>0-7095-1  |                            |           |
|  |  |  | 9. Performing Organization Name and Address<br>Center for Transportation Research<br>The University of Texas at Austin<br>3925 W. Braker Lane, 4 <sup>th</sup> Floor<br>Austin, TX 78759 |                            |           |
| 11. Contract or Grant No.<br>TxDOT RTI Project 0-7095  |  |  |  |                            |           |
| 12. Sponsoring Agency Name and Address<br>Texas Department of Transportation<br>Research and Technology Implementation Division<br>125 E. 11 <sup>th</sup> Street<br>Austin, TX 78701  |  |  | 13. Type of Report and Period Covered<br>Technical Report<br>September 2020 to October 2023  |                            |           |
|  |  |  | 14. Sponsoring Agency Code   |                            |           |
| 15. Supplementary Notes<br>Project performed in cooperation with the Texas Department of Transportation and the Federal Highway Administration.  |  |  |  |                            |           |
| 16. Abstract<br>The National Weather Service (NWS) operates a National Water Model that continually forecasts water flow throughout the stream network of the United States, including 190,000 miles of streams divided into 100,000 stream reaches in Texas. The NWS has also deployed real-time flood inundation mapping to about half of Texas, and is will complete coverage of the state by 2025. This project builds on these services to show flood impact on the road and bridge system. To help densify the streamflow observation network for Texas, 80 radar streamflow gauges were installed on TxDOT bridges, whose data are now ingested by the NWS. The researchers created a data assimilation scheme that adjusts the forecasts of the National Water Model in real-time using data from the TxDOT gauges. A Flood Assessment System for TxDOT was created that comprises a web-based overlay of current and predicted flood information. This system includes a prototype bridge warning service describing real-time water levels at 19,000 span bridges in Texas. A road elevation model was created for the 11-county TxDOT Austin District which comprises 3.8 billion LiDAR points covering 38,000 miles of roadway. The state-wide bridge warning system and the road elevation model are a first for TxDOT and for Texas. |  |  |  |                            |           |
| 17. Key Words<br>Flood emergency operations, real-time information, flood map services, highway maintenance.   |  |  | 18. Distribution Statement<br>No restrictions. This document is available to the public through the National Technical Information Service, Alexandria, Virginia 22312; www.ntis.gov.    |                            |           |
| 19. Security Classif. (of report)<br>Unclassified  |  | 20. Security Classif. (of this page)<br>Unclassified |  | 21. No. of pages<br>123    | 22. Price |



**THE UNIVERSITY OF TEXAS AT AUSTIN  
CENTER FOR TRANSPORTATION RESEARCH**

## **Flood Assessment System for TxDOT**

**Prepared by:**

**University of Texas at Austin:** David Maidment, Paola Passalacqua, Matt Bartos, Sujana Timilsina, Jeil Oh, Andy Carter, Tim Whiteaker, Harry Evans, Christine Thies, Larry Jantzen; **KISTERS:** Matt Ables, Attila Bibok; **Aqua Strategies:** Barney Austin, Tim Osting,

**US Geological Survey:** Scott Grzyb, Jody Avant, Jon Thomas, Michael Nyman, Kristine Blickenstaff.

---

|                       |   |
|-----------------------|---|
| CTR Technical Report: | 0-7095-1  |
| Report Date:          | Submitted: October 2023   |
| Project:              | 0-7095  |
| Project Title:        | Flood Assessment System for TxDOT                                       |
| Sponsoring Agency:    | Texas Department of Transportation                                      |
| Performing Agency:    | Center for Transportation Research at The University of Texas at Austin |

Project performed in cooperation with the Texas Department of Transportation and the Federal Highway Administration.

Center for Transportation Research  
The University of Texas at Austin  
3925 W. Braker Lane, 4<sup>th</sup> floor  
Austin, TX 78759

<http://ctr.utexas.edu/>

## **Disclaimers**

---

**Author's Disclaimer:** The contents of this report reflect the views of the authors, who are responsible for the facts and the accuracy of the data presented herein. The contents do not necessarily reflect the official view or policies of the Federal Highway Administration or the Texas Department of Transportation (TxDOT). This report does not constitute a standard, specification, or regulation.

**Patent Disclaimer:** There was no invention or discovery conceived or first actually reduced to practice in the course of or under this contract, including any art, method, process, machine manufacture, design or composition of matter, or any new useful improvement thereof, or any variety of plant, which is or may be patentable under the patent laws of the United States of America or any foreign country.

## **Engineering Disclaimer**

---

NOT INTENDED FOR CONSTRUCTION, BIDDING, OR PERMIT PURPOSES.

Project Engineer: David Maidment

Professional Engineer License State and Number: Texas No. 53819

P.E. Designation: Research Supervisor

## **Acknowledgments**

---

The project team wishes to thank the RTI Project Managers, Shelley Pridgen and Jadé Adediwura, and the Hydrology and Hydraulics Division Director, Rose Marie Klee, for their direction and guidance of this project. Rose Marie, in particular, has been tireless in facilitating getting gauge permits, and in fostering the relationship between the USGS and the various TxDOT Districts during gauge installations in their area of responsibility. The guidance of the Project Management Committee and the Project Advisory Committee is also gratefully acknowledged.

The Project 0-7095 research team wishes to acknowledge the privilege of working with TxDOT to conduct this research, and to be able to contribute to the safety of our fellow Texans during flood events.

# Table of Contents

---

|   |    |
|---|----|
| Chapter 1. Introduction .....   | 1  |
| Chapter 2. Stream Gauge Network Assessment .....                          | 6  |
| 2.1 Introduction.....   | 6  |
| 2.2. Gauge Equipment Assessment.....                                      | 11 |
| 2.2.1. Installation.....  | 11 |
| Equipment setup.....  | 13 |
| 2.2.2. Equipment Resilience .....   | 15 |
| 2.3. Data Assessment .....  | 16 |
| 2.3.1. Properties of Recorded Data .....                                  | 17 |
| 2.3.2. Cross Sections .....   | 18 |
| 2.3.3. Stage.....   | 21 |
| 2.3.4. Velocity.....  | 23 |
| 2.3.5. Raw Velocity .....   | 23 |
| 2.3.6. Learned Velocity.....  | 24 |
| 2.3.7. Discharge .....  | 26 |
| 2.3.8. Raw Discharge .....  | 26 |
| 2.3.9. Learned Discharge .....  | 27 |
| 2.3.10. Discharge Calibration .....                                       | 28 |
| 2.4. Conclusions.....   | 31 |
| Chapter 3. Flood Assessment System for TxDOT (FAST) .....                 | 33 |
| 3.1. Introduction.....  | 33 |
| 3.2. NWS Flood Inundation Mapping.....                                    | 35 |
| 3.3. Flood Map Services .....   | 37 |
| 3.4. Flood Emergency Response Exercises .....                             | 38 |
| 3.5. Flooded Roads Hydrograph .....                                       | 40 |
| Chapter 4. Bridge Warning Service .....                                   | 42 |
| 4.1. Introduction.....  | 42 |
| 4.2. Inputs for TX-Bridge .....   | 44 |
| 4.2.1. Statewide input staging for high-performance computing (HPC) ..... | 45 |
| 4.2.2. Elevation Dataset Staging .....                                    | 47 |
| 4.2.3. Running TX-Bridge on a High-Performance Computer.....              | 51 |
| 4.2.4. TX-Bridge Output.....  | 53 |
| 4.2.5. Statewide Database – TX-Bridge.....                                | 55 |

|  |     |
|--|-----|
| 4.2.6. Flood Forecaster for TX-Bridge .....  | 57  |
| 4.3. Bridge Warning Service in KISTERS Datasphere .....                            | 63  |
| Chapter 5. Road Flooding .....   | 65  |
| 5.1. Introduction .....  | 65  |
| 5.2. Road Elevation Model .....  | 65  |
| 5.2.1. TxDOT Roadway Inventory .....   | 67  |
| 5.2.2. Open Street Map .....   | 67  |
| 5.2.3. Ecopia .....  | 68  |
| 5.2.4. Other Alternatives .....  | 70  |
| 5.3. Road Elevation Model using the TxDOT Roadway Inventory .....                  | 71  |
| 5.4. Road Elevation Model using Open Street Map .....                              | 74  |
| 5.5. Integration with Bridge Information .....                                     | 76  |
| 5.6. Assessment of Road Elevation Modeling Approaches .....                        | 78  |
| 5.7. Flood Mapping Tutorials .....   | 79  |
| 5.8. Base Level Engineering Modeling in Texas .....                                | 82  |
| 5.9. Bridge-Class Culverts .....   | 84  |
| 5.10. Low-Water Crossings .....  | 85  |
| Chapter 6. Error Analysis and Data Assimilation .....                              | 87  |
| 6.1. Introduction .....  | 87  |
| 6.2. Error analysis at network scale .....   | 88  |
| 6.3. Modeling of discharge in river networks .....                                 | 91  |
| 6.3.1. State-space Muskingum-Cunge routing .....                                   | 91  |
| 6.4. Probability of road overtopping .....   | 92  |
| 6.4.1. Ensemble model for probabilistic forecast with data assimilation .....      | 92  |
| 6.5. Software implementation and web architecture .....                            | 94  |
| 6.6. Data assimilation for improved forecasting .....                              | 95  |
| 6.7. Data assimilation for improved estimation at ungauged bridges and roads ..... | 97  |
| 6.8. Analysis and modeling of hysteresis patterns .....                            | 100 |
| 6.9. Conclusions .....   | 104 |
| Chapter 7. Conclusions .....   | 106 |
| References .....   | 114 |

## List of Tables

---

|  |     |
|--|-----|
| Table 2.1 List of 80 RQ-30 gauges with station identifications, coordinates, and installation information. ....              | 7   |
| [USGS, U.S. Geological Survey; N/A, not applicable; TxDOT, Texas Department of Transportation] .....                         | 7   |
| Table 5.1. Classification of roads into functional levels.....   | 74  |
| Table 6.1 Performance evaluation for National Water Model, Data Assimilation with 6-hour and 1-hour update frequencies ..... | 97  |
| Table 6.2 Mean flows, RMSE and percent reduction in RMSE after data assimilation in New Year Creek watershed.....            | 98  |
| Table 6.3 Mean flows, RMSE and percent reduction in RMSE after data assimilation in Llano watershed.....                     | 98  |
| Table 6.4 Performance of the model at validation sites.....  | 100 |

## List of Figures

---

|   |    |
|---|----|
| Figure 1.1 TxDOT Districts and Road Transportation System .....   | 1  |
| Figure 1.2 National Water Model forecasts flow in the nation’s streams and rivers .....   | 2  |
| Figure 1.3 Stream and river reaches forecast by the National Water Model in Texas .....   | 3  |
| Figure 1.4 Distribution of bridges in Texas.....  | 4  |
| Figure 1.5 Selected RQ-30 gauge locations and USGS gauge locations.....   | 5  |
| Figure 2.1 Diagram of A traditional USGS rating curve developed using direct field measurements to create a stage-discharge relation.....       | 6  |
| Figure 2.2 Image of a completed RQ-30 gauge installation. Photograph by Scott Grzyb, U.S. Geological Survey.....                                | 12 |
| Figure 2.3 Equipment housed in the gauge enclosure. Photograph by Jody Avant, U.S. Geological Survey.....                                       | 13 |
| Figure 2.4 Transmission of data from the gauge to the public. ....  | 14 |
| Figure 2.5 Conceptual drawing of an RQ-30 gauge and sensor. Modified from Sommer Messtechnik (2023b; Figure 2). Figure used by permission. .... | 15 |
| Figure 2.6 Example of a cross section survey involving multiple techniques (Levesque and Oberg, 2012). Used by permission. ....                 | 19 |

|  |    |
|--|----|
| Figure 2.7 Example of a typical cross section comparison plot for computing differences in area. This example is from Manson Creek at SH 294 near Elkhart, Tex. (08065080) (U.S. Geological Survey, 2023).   | 20 |
| Figure 2.8 Example of a cross section comparison plot where channel modifications were made between surveys. This example is from Carters Creek at FM 60 near College Station, Tex. (08111051) (U.S. Geological Survey, 2023).   | 21 |
| Figure 2.9 Photographs showing A, U.S. Geological Survey crest-stage gauge, looking downstream, and B, close-up of a typical enclosed wooden staff and cork line. The cork line marks the heights of a high-water mark during a flood event. Photographs by U.S. Geological Survey.  | 22 |
| Figure 2.10 Graph of continuous velocity data in feet per second at Goose Creek near McNair, Tex. (08067520) illustrating fluctuations in raw velocity values from May 15, 2023, through May 19, 2023 (U.S. Geological Survey, 2023).  | 24 |
| Figure 2.11 Graph of continuous velocity values in feet per second at Goose Creek near McNair, Tex. (08067520) illustrating how learned velocity can minimize fluctuations in recorded data when compared to raw velocity values. (U.S. Geological Survey, 2023).  | 25 |
| Figure 2.12 Example of USGS traditional discharge and RQ-30 Gauge raw discharge  | 27 |
| Figure 2.13 Example of USGS traditional discharge and RQ-30 gauge sensor Learned discharge.  | 27 |
| Figure 2.14 Example of a 13-point calibration of the k-factor profile in Q-Commander.  | 28 |
| Figure 2.15 Chart showing the range of errors between the RQ-30 gauge computed discharge and the USGS verification measurements as calibrations are performed sequentially at New Year Creek at FM 1155 near Chappell Hill, Tex. (USGS site number 08111110) (U.S. Geological Survey, 2023; Grzyb and others, 2025). Note: Discharge values of less than 20 cubic feet per second were removed.  | 29 |
| Figure 2.16 Channel geometries are targeted to constrain the k-factor profile. ...   | 30 |
| Figure 2.17 Chart showing the range of errors for discharge measurements using the targeted calibration approach at New Year Creek at FM 1155 near Chappell Hill, Tex. (USGS site number 08111110) (U.S. Geological Survey, 2023; Grzyb and others, 2025). Note: Discharge values of less than 20 cubic feet per second were removed. Targeted calibration approach refers to measurements made at specific water levels based on geometry of the cross section. | 31 |
| Figure 3.1 Flood Assessment System for TxDOT (FAST)  | 33 |
| Figure 3.2 Reactive and Proactive Flood Emergency Response   | 34 |
| Figure 3.3 Beaumont District Flood Organization, as of February 2022   | 35 |
| Figure 3.4 NWS Flood Inundation Mapping Services Implementation. Source of Figure – National Weather Service   | 36 |

|   |    |
|---|----|
| Figure 3.5 Flood Inundation Map showing inundated roads at bridge locations   |    |
| Source of Figure – National Weather Service .....   | 37 |
| Figure 3.6 Flood map services viewer .....  | 38 |
| Figure 3.7 Austin flood emergency response exercise .....   | 39 |
| Figure 3.8 Flooded Roads Hydrograph for Tropical Storm Imelda.....  | 41 |
| Figure 3.9 Historical Flood Impact on the Road Transportation System of Texas,<br>May 2014 to August 2021.....  | 41 |
| Figure 4.1 Tx-Bridge Flood Forecaster .....   | 42 |
| Figure 4.2 Bridge envelope.....   | 43 |
| Figure 4.3 Sample excerpt from the TX-Bridge “global configuration” INI file .  | 46 |
| Figure 4.4 LiDAR Collections provided by TxGIO (Aug 14, 2023).....  | 47 |
| Figure 4.5 LiDAR Collections-“Best-in-time-and-space” (Aug 14, 2023) .....  | 48 |
| Figure 4.6 “001_bridge_merge.copc.laz” representing the bridges within the<br>‘Ellis, Hill, Johnson, & Navarro Counties LiDAR’ .....                    | 49 |
| Figure 4.7 Graphical representation of “R-Tree” index and properties for a portion<br>of the ‘Ellis, Hill, Johnson, & Navarro Counties’ collection..... | 50 |
| Figure 4.8 Computation Packaging – HUC-8 12070203 for ‘North and Central<br>Texas’ Collection .....   | 52 |
| Figure 4.9 Example of ‘Local Input Configuration’ JSON for TX-Bridge .....  | 52 |
| Figure 4.10 Sample KMZ of Tx-Bridge Output .....  | 54 |
| Figure 4.11 Major Axis Line and Bridge Hull for Bridge .....  | 55 |
| Figure 4.12 Extracted bridge Cross Section. ....  | 55 |
| Figure 4.13 TX-Bridge Statewide database (2023.09.19) .....   | 56 |
| Figure 4.14 NOMADS ‘channel_rt’ streamflow forecast files.....  | 58 |
| Figure 4.15 Bridge Forecast Points.....   | 58 |
| Figure 4.16 Forecast Point Color Coding .....   | 59 |
| Figure 4.17 TX-Bridge Flood Forecasting Web Mock-up showing only warnings<br>.....  | 60 |
| Figure 4.18 Realtime Cross Section Plot .....   | 60 |
| Figure 4.19 TX-Bridge Flood Forecaster Web Service .....  | 61 |
| Figure 4.20: Flow diagram of the architecture of the WMS service .....  | 63 |
| Figure 4.21: Bridge Warning WMS layers displayed in QGIS .....  | 64 |
| Figure 5.1 LIDAR tiles covering the TxDOT Austin District.....  | 66 |
| Figure 5.2. TxDOT Roadway Inventory roads for the Austin District (18,173<br>miles).....  | 67 |
| Figure 5.3. Open Street Map lines in the Austin District (41,095 miles) .....   | 68 |

|  |    |
|--|----|
| Figure 5.4. Ecopia road coverage of the Austin District (37,879 miles) .....   | 68 |
| Figure 5.5. Ecopia classification of land cover classes.....   | 69 |
| Figure 5.6. Ecopia classification distinguishes the public road system from driveways, parking lots and buildings .....                                      | 69 |
| Figure 5.7. Comparison of NBI and Ecopia Road Widths .....   | 70 |
| Figure 5.8. Spurious road features in a field identified by the ESRI Road Extraction Deep Learning model.....  | 71 |
| Figure 5.9. Road Elevation Models for the Pennybacker bridge.....  | 71 |
| Figure 5.10. Comparison of Road Elevation Models at Highway 183 and Loop 1, Austin, Texas. ....  | 72 |
| Figure 5.11. Comparison of the location of road lines from the TxDOT Roadway Inventory, Open Street Map and Ecopia, overlaid on the Ecopia road polygons. 73 |    |
| Figure 5.12. Coverage of the TxDOT Roadway Inventory and Ecopia Road Elevation models for Travis County.....   | 73 |
| Figure 5.13. Minimum, Median and Maximum Road Bed Width for the TxDOT Roadway Inventory.....   | 75 |
| Figure 5.14. Comparison of road widths on Anderson Lane at Shoal Creek in Austin, Texas. ....  | 75 |
| Figure 5.15. Geospatial data for bridges extracted from LIDAR data using Tx-Bridge.....  | 76 |
| Figure 5.16. Road and Bridge Elevation Points on Anderson Lane at Shoal Creek .....  | 77 |
| Figure 5.17. Bridge Deck Template Created with Data from the National Bridge Inventory.....  | 77 |
| Figure 5.18 First tutorial – road elevation points in a watershed.....   | 79 |
| Figure 5.19 Second tutorial -- road inundation mapping at street scale .....   | 80 |
| Figure 5.20 100-year flood depth map for Anderson Lane at Shoal Creek developed using water depth at LIDAR points.....                                       | 80 |
| Figure 5.21 Third tutorial – flood impact at the watershed scale. ....   | 81 |
| Figure 5.22 Inventory of roads impacted by a 100-year flood on Shoal Creek....   | 81 |
| Figure 5.23 Connecting the road representation in (x,y,z) with that in (x,y,m) ...   | 82 |
| Figure 5.24 Base Level Engineering modeling in Texas.....  | 83 |
| Figure 5.25 Description of a bridge-class culvert in the TxDOT AssetWise system .....  | 84 |
| Figure 5.26 3D Bridge-class culvert positioned beneath the Road Elevation Model for Anderson Lane at Shoal Creek in Austin, Texas. ....                      | 85 |
| Figure 5.27 Survey information acquired in the rapid field assessment for culverts .....   | 85 |

|  |     |
|--|-----|
| Figure 5.28 Low-water crossing on Onion Creek at FM 150 .....  | 86  |
| Figure 6.1. RMSE map for Texas for period 2020-2022. Dots represent gage locations. The size of the dot indicates the magnitude of the RMSE (in m <sup>3</sup> /s). ...  | 90  |
| Figure 6.2. Percent Bias map for Texas for period 2020-2022. Dots indicate the location of the gage. The color indicates whether the NWM is underestimating (yellow) or overestimating (blue) with respect to the observed discharge. ....   | 91  |
| Figure 6.3. RMSE versus mean discharge. ....   | 91  |
| Figure 6.5 Hydrological Forecast and Overtopping Probability Analysis.....   | 94  |
| Figure 6.6. Adjusted forecasts displayed in Datasphere. ....   | 95  |
| Figure 6.7 Forecasted streamflow with data assimilation, New York Creek at FM 1155 near Chapell Hill, Tx.....  | 96  |
| Figure 6.8 Changes in flow due to data assimilation in the New Year Creek watershed. ....  | 99  |
| Figure 6.9 Changes in flow due to data assimilation in the Llano watershed .....   | 99  |
| Figure 6.10 Streamflow comparison for validation site at New Year Creek watershed. ....  | 100 |
| Figure 6.11: Stage and velocity data at a sensor in Carters Creek near College Station, TX.....  | 101 |
| Figure 6.12: Plots of stage vs. velocity for four streams, where each curve is a unique flow event.....  | 102 |
| Figure 6.13. (Top): Depth and velocity hydrographs for a flood wave at a single point in a rectangular channel, simulated using the Saint-Venant equations. (Bottom): Forces acting on the control volume, including inertial, hydrostatic, gravitational, and frictional forces. .... | 103 |

# Chapter 1. Introduction

The Texas Department of Transportation (TxDOT) is responsible for construction and maintenance of the backbone road transportation system of the state. These are the principal routes connecting the cities and counties of Texas and comprise a little over 100,000 miles of roads, termed “On-System” because their maintenance is the responsibility of TxDOT. In addition, Texas has about 25,000 span bridges over water whose condition is documented in the National Bridge Inventory. During flood events, TxDOT is responsible for managing the closing and opening of flooded On-System roads, and for ensuring the integrity of the state’s bridge system.

To accomplish this task, as shown in Figure 1.1, TxDOT has divided Texas into 25 Districts, which are themselves subdivided into 265 Maintenance Sections, where Maintenance Supervisors manage the operations on their road and bridge system. On average a Maintenance Section is responsible for 50 routes, 100 bridges, 400 miles of roads and 1000 square miles of area. When a significant flood occurs, an Emergency Operations Center is opened at the District Office to coordinate field Maintenance operations, and interactions with other emergency response agencies, including public safety, public works, and state-wide emergency coordination through the Texas Division of Emergency Management.

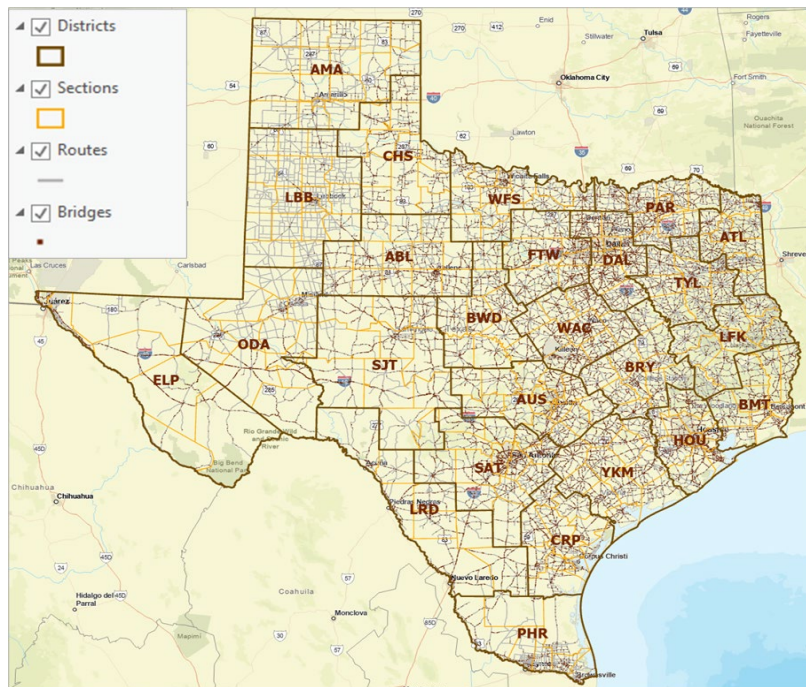
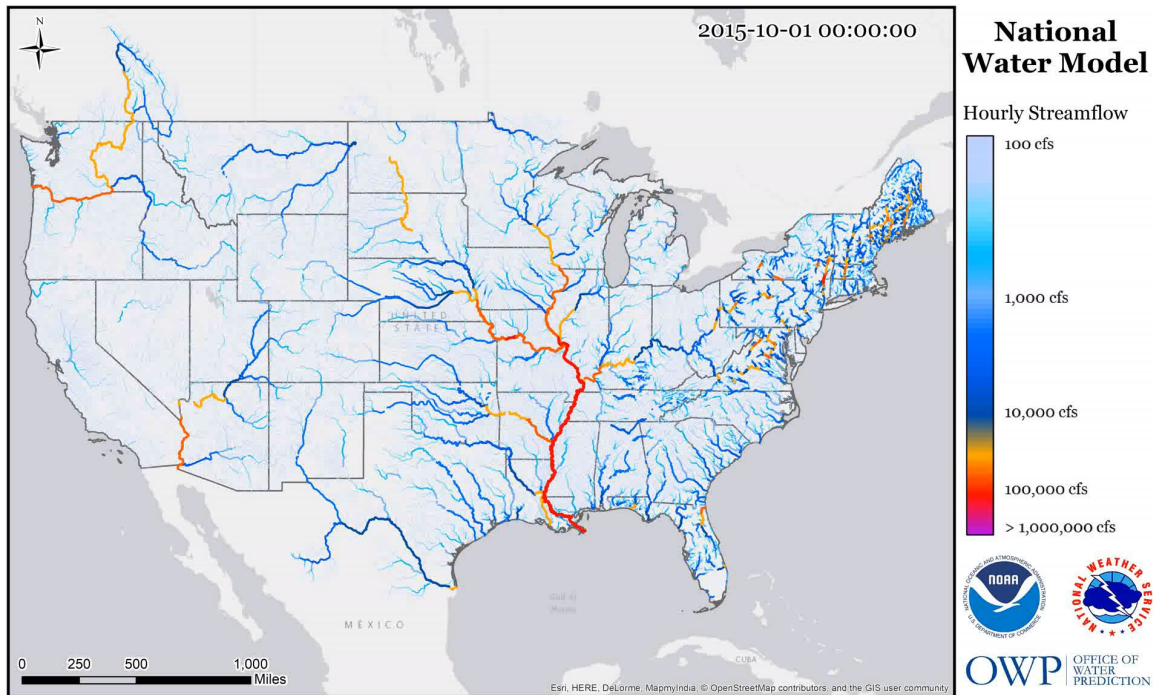


Figure 1.1 TxDOT Districts and Road Transportation System

The National Weather Service (NWS) began the operation of a National Water Model across the United States in 2016. This forecasts flow in the nation's stream and river network continuously, as shown in Figure 1.2. Four versions of the forecast model operate, which provide information on current conditions, over the next 18 hours, over the next 10 days, and over the next 30 days. Since 2016, a series of updates to the National Water Model have been made, most recently in September 2023, when Version 3.0 was released that combines river flow forecasts with forecasts of coastal flood inundation from storm surge.



*Figure 1.2 National Water Model forecasts flow in the nation's streams and rivers*

For Texas, the National Water Model provides streamflow forecasting to about 190,000 miles of streams and rivers divided in 102,000 stream reaches, as shown in Figure 1.3.

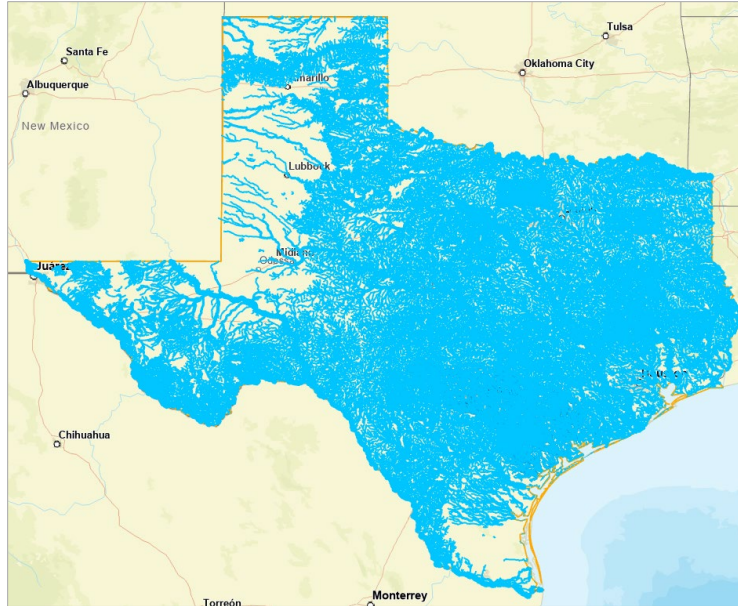


*Figure 1.3 Stream and river reaches forecast by the National Water Model in Texas*

This stream mapping is taken from a set of stream lines called the Medium Resolution National Hydrography Dataset Plus developed by the US Geological Survey and USEPA. There is a lower density of stream lines in West Texas because that is a wind-formed landscape rather than a water-formed landscape as in the remainder of Texas.

TxDOT maintains documentation of about 55,000 bridges in the National Bridge Inventory, as shown in Figure 1.4. These comprise about 25,000 span bridges over water, 20,000 bridge-class culverts, and about 10,000 grade-separated bridges, or bridges over railroads. A span bridge has an elevated bridge deck supported on piers and beams and the river or stream flows beneath the bridge deck. A bridge-class culvert is generally a set of multiple concrete box culverts set into the road itself, where the culverts support the overlying road surface. A grade-separated bridge is where a bridge carries one road over another. To be included in the National Bridge Inventory, a bridge needs to be at least 20 feet in length measured along the roadway centerline. TxDOT reports to the federal government on the condition of the bridges in the National Bridge Inventory, and has a team of inspection crews who inspect each bridge at regular intervals.

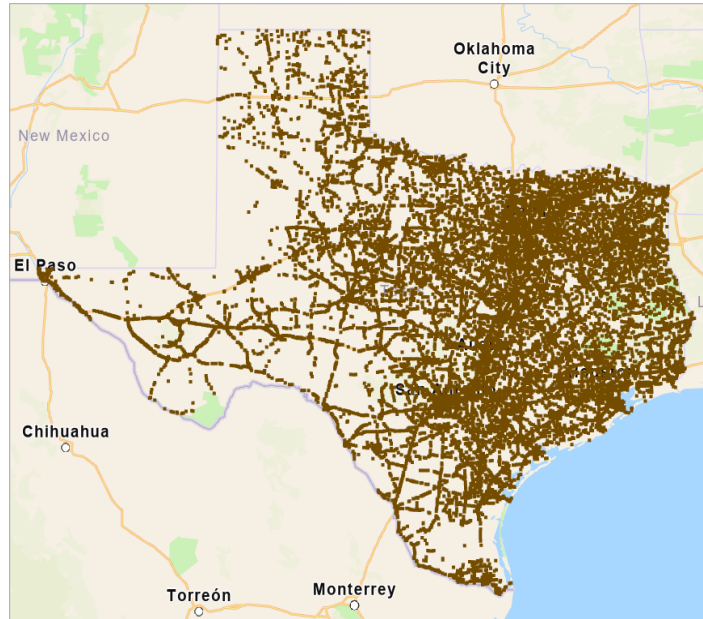


*Figure 1.4 Distribution of bridges in Texas.*

For several decades, the National Weather Service has maintained river forecasts at point locations along the main rivers of Texas, issued by River Forecast Centers, of which the main one for Texas is located in Fort Worth. There are currently about 500 NWS river forecast or observation points at USGS stream gauging locations in Texas. The National Water Model provides streamflow forecasts on about 100,000 individual stream reaches in Texas, an increase in forecast density of about 200 times. Densified forecasting requires densified streamflow measurement, and the TxDOT bridge system is the obvious foundation for extending the state’s streamflow measurement system to support flood operations.

In an earlier TxDOT research project 5-9054-01<sup>1</sup> conducted from 2017 to 2019, 20 RQ-30 radar streamflow gauges were installed along IH-10 between the San Antonio and Beaumont Districts. The request for proposals for this project called for 60 more RQ-30 gauges to be installed using a watershed-based approach to gauge siting. A gauge siting study was carried out, summarized in Technical Memorandum 2<sup>2</sup>, that located the 80 gauges according to three criteria: (1) that TxDOT receives early warning of potential bridge and roadway inundation; (2) that the gauges are grouped so that they are mutually supportive and data assimilation can be used to correct the flow on adjacent ungauged streams; (3) that there are ideal measurement locations on high bridges on generally straight reaches where the water is contained in the channel and the velocity is greater

<sup>1</sup><https://library.ctr.utexas.edu/ctr-publications/5-9054-01-1.pdf>

<sup>2</sup>[https://www.caee.utexas.edu/prof/maidment/StreamflowII/Documents/0\\_7095\\_TM2\\_Final.pdf](https://www.caee.utexas.edu/prof/maidment/StreamflowII/Documents/0_7095_TM2_Final.pdf)

than 1 ft/sec. Some of the original 20 RQ-30 gauges were relocated to new sites as part of this siting study.

The resulting distribution of selected RQ-30 gauge locations is shown in Figure 1.5 along with existing USGS gauges in these areas. Gauges are located in data sparse-areas of flood-prone southeast Texas, with about half the gauges on tributaries of inland Brazos and Trinity basins and the other half in coastal basins where flat terrain makes gauging by traditional USGS methods challenging. The resulting gauging distribution approximately doubles the existing USGS gauging density in the chosen watersheds. Considering both the TxDOT and USGS gauges, the gauging density is approximately one gauge per HUC10 watershed unit.

The Hydrologic Unit Code (HUC) system is a hierarchical collection of watersheds where smaller watersheds are grouped within larger ones. In particular, in Texas, the larger HUC8 watersheds are considered a standard unit for hydrologic and hydraulic modeling. It is shown in Chapter 6 of this report how data assimilation can be used within a HUC8 watershed to improve the streamflow estimates for a larger stream network around the gauges as well as at the gauges themselves.

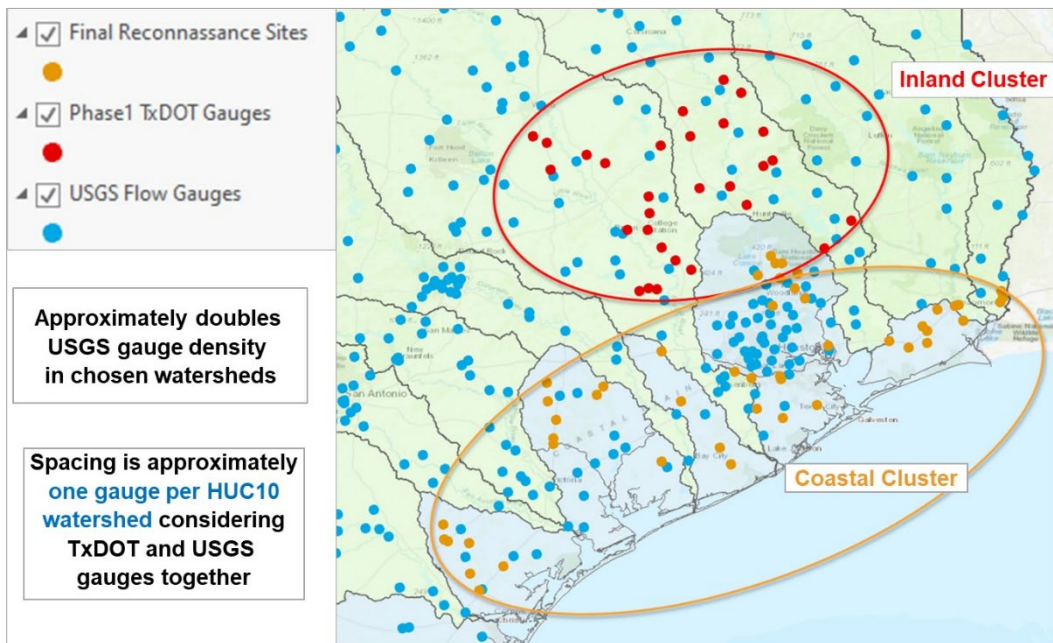


Figure 1.5 Selected RQ-30 gauge locations and USGS gauge locations.

The operation of the RQ-30 stream gauging network is described in Chapter 2 of this report, followed in Chapter 3 by an outline of the Flood Assessment System for TxDOT, in Chapter 4 by bridge warning services, in Chapter 5 by the road elevation model and road flooding, in Chapter 6 by forecast error assessment and data assimilation, and in Chapter 7 by conclusions.

# Chapter 2. Stream Gauge Network Assessment

Prepared by Scott Grzyb<sup>1</sup>, Jody Avant<sup>2</sup>

<sup>1</sup> U.S. Geological Survey, Austin, Texas

<sup>2</sup> U.S. Geological Survey, The Woodlands, Texas

## 2.1 Introduction

The purpose of this chapter is to assess the current (2023) performance and capabilities of the streamgauge network installed for the “Evaluate Improved Streamflow Measurement Technologies at TxDOT Bridges” project.

The U.S. Geological Survey (USGS) traditionally employs a method of discharge computation relating continuously measured stage to an associated discharge (Rantz and others, 1982). This stage-discharge relation is built using numerous physical discharge measurements, which is labor-intensive. A primary research objective of this project is to evaluate the feasibility of methods alternative to the traditional USGS stage-discharge relation for computing discharge, namely the computation of discharge using surface velocimetry.

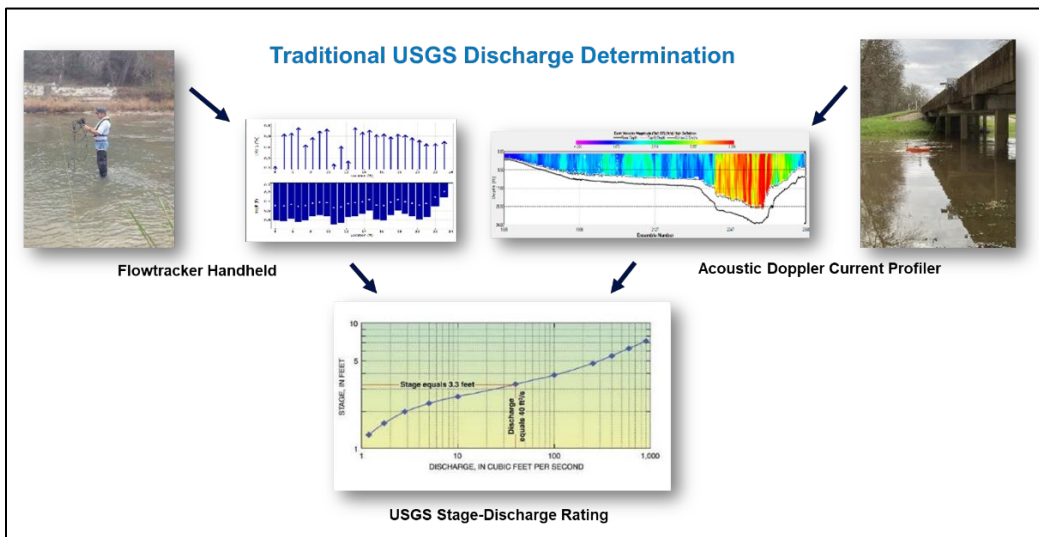


Figure 2.1 Diagram of A traditional USGS rating curve developed using direct field measurements to create a stage-discharge relation.

To augment traditional streamgauging methods, the USGS Next Generation Water Observing System (NGWOS) is actively investigating a wide range of innovative methods for measuring streamflow discharge including radar and

image velocimetry for remotely sensing surface velocities, and drone-mounted ground-penetrating radar for discharge measurements (<https://www.usgs.gov/mission-areas/water-resources/science/next-generation-water-observing-system-ngwos>). The project described herein to compute discharge using surface velocimetry is consistent with the goals of USGS to advance the science of streamgauging. A total of 80 surface velocimetry gauges were used to record and compute stage and discharge data, respectively, for comparison with traditional USGS methods. Several velocimetry gauges have become available in recent years. The RQ-30 surface velocimetry gauge (Sommer Messtechnik, 2021b) (hereinafter referred to as the “RQ-30 gauge”) was selected by the Texas Department of Transportation (TxDOT) for use in this project. The RQ-30 gauge measures both water-surface elevation at a streamgauge (also known as gauge height or stage) and water velocity in a single instrument (Sommer Messtechnik, 2021b). The primary purpose of installing the RQ-30 gauges is to provide streamflow information to water managers and safety personnel during large stormwater runoff events.

This status update reflects the current progress of the project as of July 31, 2023. Because of delays in the site selection, equipment delivery, and permit processes, there were also delays in the installation of the streamgauges, which reduced the amount of data that were collected as of July 2023 compared to the planned amount.

**Table 2.1 List of 80 RQ-30 gauges with station identifications, coordinates, and installation information.**

**[USGS, U.S. Geological Survey; N/A, not applicable; TxDOT, Texas Department of Transportation]**

| USGS Site Number | Station Name                                    | Latitude (decimal degrees) | Longitude (decimal degrees) | Date Installed | Data Start Date | Bridge Identification Number | TxDOT District |
|------------------|---|----------------------------|-----------------------------|----------------|-----------------|------------------------------|----------------|
| 08173210         | Plum Creek at US183 near Luling, Tex.           | 29.654922                  | -97.599771                  | 11/15/2021     | 07/27/2022      | N/A                          | Austin         |
| 08042539         | Spindletop Bayou at SH 65 near Stowell, Tex.    | 29.792666                  | -94.423832                  | 06/23/2022     | 07/06/2022      | 200360036801046              | Beaumont       |
| 08042515         | Rhodair Gully at US 69 near Nederland, Tex.     | 29.982018                  | -94.029553                  | 03/08/2022     | 03/08/2022      | 201240020015158              | Beaumont       |
| 08042468         | Willow Marsh Bayou at US 90 near Beaumont, Tex. | 30.063885                  | -94.217924                  | 03/10/2022     | 03/10/2022      | 201240002806043              | Beaumont       |
| 08042455         | Hillebrandt Bayou at HWY 90 near Beaumont, Tex. | 30.067742                  | -94.157113                  | 06/24/2022     | 07/20/2022      | 201240002807063              | Beaumont       |
| 08041970         | Mayhaw Bayou at SH 73 near Hamshire, Tex.       | 29.825332                  | -94.295082                  | 06/23/2022     | 06/23/2022      | 201240050804322              | Beaumont       |

| USGS Site Number | Station Name                                       | Latitude (decimal degrees) | Longitude (decimal degrees) | Date Installed | Data Start Date | Bridge Identification Number | TxDOT District |
|------------------|--|----------------------------|-----------------------------|----------------|-----------------|------------------------------|----------------|
| 08041945         | N. Fork Taylors Bayou at IH 10 near Hamshire, Tex. | 29.912350                  | -94.292116                  | 06/21/2022     | 06/22/2023      | 201240073902445              | Beaumont       |
| 08041940         | Green Pond Gully at FM 365 near Fannett, Tex.      | 29.945485                  | -94.325837                  | 03/10/2022     | 03/10/2022      | 201240093202144              | Beaumont       |
| 08031005         | Cow Bayou at IH 10 near Vidor, Tex.                | 30.130924                  | -93.915754                  | 03/09/2022     | 03/09/2022      | 201810002811260              | Beaumont       |
| 08067505         | Cedar Bayou at I-10 near Mont Belvieu, Tex.        | 29.821514                  | -94.909705                  | 07/12/2021     | 09/22/2021      | 200360050802327              | Beaumont       |
| 08067280         | Turtle Bayou at I-10 near Hankamer, Tex.           | 29.840581                  | -94.654225                  | 07/09/2021     | 07/12/2021      | 200360050802347              | Beaumont       |
| 08042470         | Willow Marsh Bayou at I-10 near Beaumont, Tex.     | 30.014729                  | -94.181207                  | 07/08/2021     | 09/21/2021      | 201240073902040              | Beaumont       |
| 08041790         | Neches River at Beaumont, Tex.                     | 30.094509                  | -94.091129                  | 06/22/2022     | 08/07/2020      | 201810002809504              | Beaumont       |
| 08041788         | Bairds Bayou at I-10 near Beaumont, Tex.           | 30.095538                  | -94.076771                  | 07/07/2021     | 08/07/2020      | 201810002809145              | Beaumont       |
| 08031020         | Cole Creek at I-10 near Orange, Tex.               | 30.131653                  | -93.863733                  | 04/15/2021     | 04/15/2021      | 201810002811263              | Beaumont       |
| 08030530         | Sabine River at I-10 near Orange, Tex.             | 30.127301                  | -93.701415                  | 07/06/2021     | 09/21/2021      | 201810002814243              | Beaumont       |
| 08111110         | New Year Creek at FM 1155 near Chappell Hill, Tex. | 30.212309                  | -96.242983                  | 08/20/2021     | 08/20/2021      | 172390140504004              | Bryan          |
| 08111090         | Rocky Creek at SH 105 near Brenham, Tex.           | 30.220000                  | -96.303172                  | 07/28/2021     | 08/12/2021      | 172390031507022              | Bryan          |
| 08111085         | New Year Creek at Tex. 105 near Brenham, Tex.      | 30.195803                  | -96.365403                  | 07/28/2021     | 08/23/2021      | 172390031507072              | Bryan          |
| 08111080         | Grassy Creek at SH 105 near Navasota, Tex.         | 30.353306                  | -95.996278                  | 07/27/2021     | 09/08/2021      | 170940033801107              | Bryan          |
| 08111070         | Navasota River at SH 6 near Navasota, Tex.         | 30.418459                  | -96.106686                  | 07/29/2021     | 03/08/2022      | 170210005002014              | Bryan          |
| 08111056         | Peach Creek at SH 6 near Millican, Tex.            | 30.512415                  | -96.206711                  | 07/30/2021     | 08/12/2021      | 170210005002170              | Bryan          |
| 08111051         | Carters Creek at FM 60 near College Station, Tex.  | 30.641733                  | -96.308125                  | 08/24/2021     | 08/24/2021      | 170210050601016              | Bryan          |
| 08111006         | Mathis Creek at US 190 near Kurten, Tex.           | 30.757619                  | -96.297513                  | 08/24/2021     | 08/24/2021      | 170210011701088              | Bryan          |
| 08110520         | Brushy Creek at SH. 7 near Marquez, Tex.           | 31.247303                  | -96.215594                  | 08/05/2021     | 08/12/2021      | 171450033503014              | Bryan          |
| 08109310         | Thompson Creek at SH 47 near Bryan, Tex.           | 30.637589                  | -96.452461                  | 08/06/2021     | 08/12/2021      | 170210313802002              | Bryan          |

| USGS Site Number | Station Name                                       | Latitude (decimal degrees) | Longitude (decimal degrees) | Date Installed | Data Start Date | Bridge Identification Number | TxDOT District |
|------------------|--|----------------------------|-----------------------------|----------------|-----------------|------------------------------|----------------|
| 08108710         | Walnut Creek at FM 46 near Bremond, Tex.           | 31.121486                  | -96.617242                  | 08/25/2021     | 08/25/2021      | 171980054001046              | Bryan          |
| 08065925         | Nelson Creek at FM 247 near Huntsville, Tex.       | 30.822323                  | -95.594525                  | 08/02/2021     | 08/12/2021      | 172360057802024              | Bryan          |
| 08065820         | Larrison Creek at FM 1428 near Midway, Tex.        | 30.949757                  | -95.716466                  | 08/19/2021     | 08/19/2021      | 171540172201001              | Bryan          |
| 08065700         | Caney Creek at HWY 21 near Madisonville, Tex.      | 30.937116                  | -95.935596                  | 08/20/2021     | 08/19/2021      | 171540011704061              | Bryan          |
| 08065420         | Lower Keechi Creek at IH 45 near Centerville, Tex. | 31.310172                  | -96.002127                  | 08/05/2021     | 08/12/2021      | 171450067503133              | Bryan          |
| 08065310         | Upper Keechi Creek at FM 542 near Oakwood, Tex.    | 31.405486                  | -95.764372                  | 08/18/2021     | 08/18/2021      | 171450042603016              | Bryan          |
| 08189718         | Chiltipin Creek at US 77 near Sinton, Tex.         | 28.045897                  | -97.525013                  | 03/22/2022     | 03/22/2022      | 162050037104055              | Corpus         |
| 08189590         | Poesta Creek at Beeville, Tex.                     | 28.399012                  | -97.747530                  | 03/24/2022     | 03/24/2022      | 160130010107020              | Corpus         |
| 08189585         | Poesta Creek at FM 351 near Beeville, Tex.         | 28.411383                  | -97.780581                  | 03/24/2022     | 08/24/2022      | 160130241202001              | Corpus         |
| 08189520         | Devils Run Creek at US 77 near Woodsboro, Tex.     | 28.217455                  | -97.351605                  | 03/22/2022     | 08/14/2022      | 161960037103088              | Corpus         |
| 08189320         | Medio Creek at SH 202 near Beeville, Tex.          | 28.381407                  | -97.595170                  | 02/23/2022     | 03/23/2022      | 160130044703053              | Corpus         |
| 08189298         | Medio Creek near Normanna, Tex.                    | 28.515367                  | -97.781265                  | 03/23/2022     | 03/23/2022      | 160130010008054              | Corpus         |
| 08117857         | Linnville Bayou at SH 35 near Van Vleck, Tex.      | 29.070228                  | -95.789030                  | 03/31/2022     | 03/30/2022      | 120200017903086              | Houston        |
| 08078935         | Oyster Creek at FM 1462 near Rosharon, Tex.        | 29.352686                  | -95.519393                  | 03/30/2022     | 03/31/2022      | 120200141404013              | Houston        |
| 08078910         | Oyster Creek at FM 1092 near Missouri City, Tex.   | 29.573602                  | -95.564272                  | 06/08/2022     | 06/08/2022      | 120800125701006              | Houston        |
| 08078890         | Oyster Creek at FM 1464 near Sugar Land, Tex.      | 29.618915                  | -95.683813                  | 06/09/2022     | 06/10/2022      | 120800141502194              | Houston        |
| 08078400         | Austin Bayou at SH 35 near Liverpool, Tex.         | 29.281050                  | -95.331489                  | 03/31/2022     | 03/31/2022      | 120200017803361              | Houston        |
| 08077888         | Mustang Bayou at SH 6 near Alvin, Tex.             | 29.436575                  | -95.266566                  | 05/18/2022     | 05/18/2022      | 120200019202029              | Houston        |
| 08077670         | Highland Bayou at FM 646 near Santa Fe, Tex.       | 29.380862                  | -95.089742                  | 05/25/2022     | 05/25/2022      | 120850097801057              | Houston        |

| USGS Site Number | Station Name   | Latitude (decimal degrees) | Longitude (decimal degrees) | Date Installed | Data Start Date | Bridge Identification Number | TxDOT District |
|------------------|--|----------------------------|-----------------------------|----------------|-----------------|------------------------------|----------------|
| 08077640         | Dickinson Bayou at FM 517 near Alvin, Tex.           | 29.436074                  | -95.170130                  | 05/17/2022     | 05/17/2022      | 120850100202001              | Houston        |
| 08077110         | Hickory Slough at FM 865 near Pearland, Tex.         | 29.566379                  | -95.350470                  | 05/19/2022     | 05/19/2022      | 120200097602487              | Houston        |
| 08076990         | Clear Creek at FM 865 near Pearland, Tex.            | 29.585528                  | -95.352136                  | 05/19/2022     | 05/19/2022      | 121020097601488              | Houston        |
| 08070900         | Peach Creek near Cleveland, Tex.                     | 30.327254                  | -95.226551                  | 03/11/2022     | 03/11/2022      | 112040033806069              | Houston        |
| 08070550         | Spring Branch at SH 242 near Splendora, Tex.         | 30.219812                  | -95.249208                  | 03/02/2022     | 03/02/2022      | 121700353801006              | Houston        |
| 08070220         | Caney Creek at FM 1097 near Willis, Tex.             | 30.454969                  | -95.423554                  | 05/26/2022     | 05/26/2022      | 121700125902013              | Houston        |
| 08068025         | Crystal Creek at FM 1314 near Conroe, Tex.           | 30.241385                  | -95.382980                  | 05/26/2022     | 05/26/2022      | 121700198601007              | Houston        |
| 08068020         | E. Fork Crystal Creek at FM 1485 near Conroe, Tex.   | 30.294823                  | -95.352392                  | 02/28/2022     | 02/28/2022      | 121700106203017              | Houston        |
| 08067653         | W. Fork San Jacinto River at FM 2854, Conroe, Tex.   | 30.314535                  | -95.511500                  | 03/01/2022     | 03/11/2022      | 121700274401002              | Houston        |
| 08067520         | Goose Creek near McNair, Tex.                        | 29.800721                  | -95.004551                  | 06/07/2022     | 06/07/2022      | 121020050801332              | Houston        |
| 08066380         | Big Creek at SH 150 near Shepherd, Tex.              | 30.502180                  | -95.031258                  | 08/16/2021     | 08/16/2021      | 112040039503017              | Lufkin         |
| 08066138         | Tantabogue Creek at FM 230 near Lovelady, Tex.       | 31.102494                  | -95.472217                  | 08/17/2021     | 08/17/2021      | 111140093101031              | Lufkin         |
| 08066087         | Gail Creek at FM 1280 near Lovelady, Tex.            | 31.137375                  | -95.407312                  | 08/17/2021     | 08/17/2021      | 111140093102020              | Lufkin         |
| 08065340         | Hurricane Bayou at US-287 near Crockett, Tex.        | 31.344679                  | -95.472576                  | 08/18/2021     | 08/18/2021      | 111140010904006              | Lufkin         |
| 08180990         | Leon Creek at I-10 near San Antonio, Tex.            | 29.593168                  | -98.599722                  | 8/31/2021      | 10/11/2021      | 150150007208155              | San Antonio    |
| 08169778         | Geronimo Creek at I-10 near Seguin, Tex.             | 29.599612                  | -97.939171                  | 07/15/2021     | 09/21/2021      | 150950053501065              | San Antonio    |
| 8167000          | Guadalupe River at Comfort, Tex.                     | 29.965285                  | -98.897213                  | 8/30/2021      | 10/30/2020      | 151310007204020              | San Antonio    |
| 08065080         | Manson Creek at SH 294 near Elkhart, Tex.            | 31.629817                  | -95.634297                  | 08/04/2021     | 08/16/2021      | 100010005802015              | Tyler          |
| 08064990         | Town Creek at FM 645 near Palestine, Tex.            | 31.723022                  | -95.759138                  | 08/04/2021     | 08/23/2021      | 100010170701008              | Tyler          |
| 08102730         | Leon River at FM 436 near Little River Academy, Tex. | 30.993444                  | -97.393556                  | 12/14/2022     | 12/15/2022      | 090500159402007              | Waco           |

| USGS Site Number | Station Name  | Latitude (decimal degrees) | Longitude (decimal degrees) | Date Installed | Data Start Date | Bridge Identification Number | TxDOT District |
|------------------|---|----------------------------|-----------------------------|----------------|-----------------|------------------------------|----------------|
| 08100950         | Cowhouse Creek at FM 1783 near Purmela, Tex.        | 31.377956                  | -97.917341                  | 01/10/2023     | 01/10/2023      | 090140023116393              | Waco           |
| 08108705         | Little Brazos River at SH 6 near Reagan, Tex.       | 31.177897                  | -96.751533                  | 08/25/2021     | 08/25/2021      | 090740004904165              | Waco           |
| 08098295         | Pond Creek at SH 53 near Rosebud, Tex.              | 31.073453                  | -97.006397                  | 08/26/2021     | 08/26/2021      | 090740023202091              | Waco           |
| 08097000         | Cow Bayou at FM 2643 near Mooreville, Tex.          | 31.312647                  | -97.138425                  | 08/23/2021     | 08/23/2021      | 090740107801007              | Waco           |
| 08164410         | W Sandy Creek at FM 2437 near Sheridan, Tex.        | 29.451055                  | -96.673573                  | 02/25/2022     | 02/26/2022      | 131430234902001              | Yoakum         |
| 08163900         | Little Brushy Creek at US 77 near Yoakum, Tex.      | 29.135953                  | -96.986590                  | 02/24/2022     | 02/26/2022      | 131430037002055              | Yoakum         |
| 08163880         | Chicolette Creek at US 77 near Yoakum, Tex.         | 29.094174                  | -96.987181                  | 02/24/2022     | 02/28/2022      | 132350037004047              | Yoakum         |
| 08163720         | Clarks Creek at US 77 near Hope, Tex.               | 29.268823                  | -96.972823                  | 02/23/2022     | 02/24/2022      | 131430037001014              | Yoakum         |
| 08162580         | Juanita Creek at SH 71 near Midfield, Tex.          | 28.973436                  | -96.208478                  | 03/29/2022     | 03/29/2022      | 131580026607051              | Yoakum         |
| 08117858         | Linnville Bayou at FM 521 near Cedar Lane, Tex.     | 28.951552                  | -95.711354                  | 05/24/2022     | 05/24/2022      | 131580084701022              | Yoakum         |
| 08117403         | West Bernard Creek at US 59 near Hungerford, Tex.   | 29.400593                  | -96.068209                  | 05/23/2022     | 05/23/2022      | 132410008908253              | Yoakum         |
| 08174545         | Peach Creek at I-10 near Waelder, Tex.              | 29.692646                  | -97.231495                  | 07/14/2021     | 07/14/2021      | 130900053505167              | Yoakum         |
| 08164200         | E. Navidad River at US90 near Weimar, Tex.          | 29.697693                  | -96.838002                  | 07/13/2021     | 09/21/2021      | 130760002603190              | Yoakum         |
| 08164150         | W Navidad River at I-10 near Schulenburg, Tex.      | 29.689957                  | -96.938262                  | 07/13/2021     | 10/14/2021      | 130760053507075              | Yoakum         |
| 08117375         | Little Bernard Creek at I-10 WB FR near Sealy, Tex. | 29.761620                  | -96.205309                  | 06/10/2022     | 06/10/2022      | 130080027102800              | Yoakum         |

## 2.2. Gauge Equipment Assessment

### 2.2.1. Installation

The RQ-30 gauge (Sommer Messtechnik, 2021a ,b) used for this project requires less time to install than a traditional USGS streamgauge. Installation

infrastructure for the RQ-30 gauge was either furnished by Kisters North America (Boerne, Tex.) or was fabricated by the USGS before installation to improve consistency and reduce time and effort while on-site. Once bridge attachment permitting is complete, traditional USGS gauges can take up to one week to install whereas the authors of this chapter found that the typical RQ-30 gauge can be installed and operational in less than 4 hours, often allowing the opportunity for one crew to install two complete gauges in a single day. Quicker installation results in less roadway exposure time for installation crews as well as a potential reduction in gauge installation costs.



*Figure 2.2 Image of a completed RQ-30 gauge installation. Photograph by Scott Grzyb, U.S. Geological Survey.*

A steel bracket was fabricated and hot-dip galvanized to secure a 24” by 24” powder coated aluminum enclosure to the bridge guardrail. All bridge attachments are held in place with concrete anchor bolts. USGS reference gauges are installed and periodically surveyed to North American Vertical Datum of 1988 (NAVD 88) datum to ensure water-surface elevations are consistent and repeatable through the life of the gauge.

## Equipment setup

Each RQ-30 gauge consists of the following components:

- **Data Logger:** A data-collection platform for recording and transmitting sensor data,
- **Sensors:** Measuring devices used to observe stage and velocity,
- **Equipment Enclosure:** A weatherproof housing used to store and protect gauging equipment,
- **Wire Weight Gauge:** A calibrated measuring device for determining water-surface elevation, and
- **Power Supply:** A solar charged, 12-volt power source to run the gauging equipment.



*Figure 2.3 Equipment housed in the gauge enclosure. Photograph by Jody Avant, U.S. Geological Survey.*

The data logger selected for this project was the Sommer Messtechnik MRL-7 data-collection platform (Sommer Messtechnik, 2021a) because of its compatibility with the sensor used on RQ-30 gauges and its ability to transmit data wirelessly via cellular modems. The MRL-7 also allows for two-way communication, which allows technicians to troubleshoot or change internal settings on both the RQ-30 gauge sensor and data logger remotely if necessary. Data are transmitted over File Transfer Protocol (FTP) to data servers, where R scripts are used to automatically retrieve and distribute the data to the USGS National Water Information System (NWIS) (USGS, 2023).

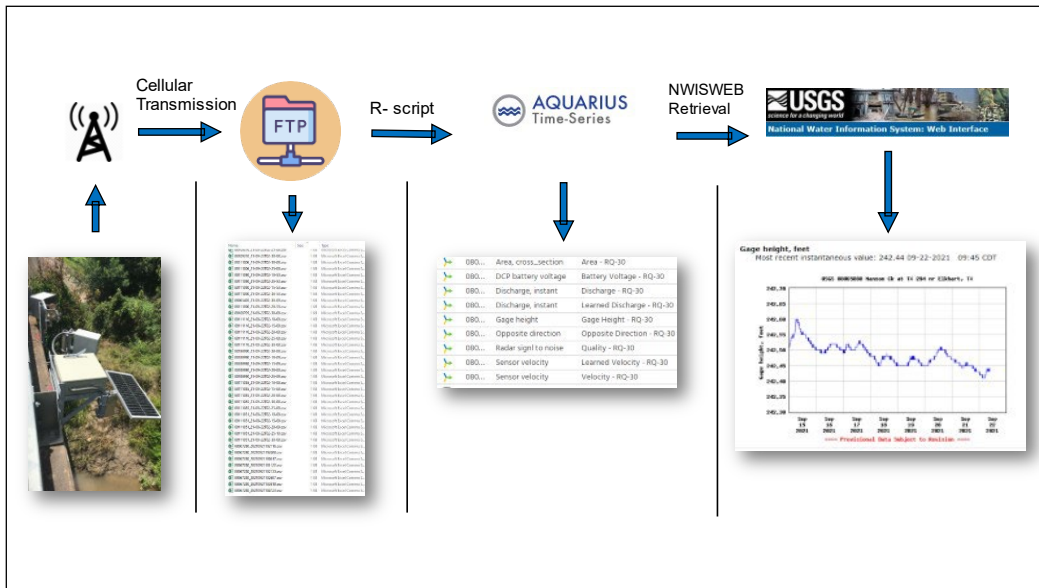


Figure 2.4 Transmission of data from the gauge to the public.

Each data logger controls a dual sensor on the RQ-30 gauge featuring a non-contact water-level sensor to measure the stage and a surface-velocity radar sensor. This dual sensor is mounted at the RQ-30 gauge to the bridge guardrail and communicates to the MRL-7 via a wired RS-485 connection. The RQ-30 gauge is set to record stage and velocity values at 5-minute intervals and transmit the data at 15-minute intervals. Velocity values are a continuous measurement of surface velocity over a user-determined timeframe specified during setup. During the RQ-30 gauge setup, the user also defines which side (upstream or downstream) of the bridge the unit is installed. By entering this starting location, the RQ-30 gauge can determine the flow direction based on the Doppler shift frequencies it is receiving.

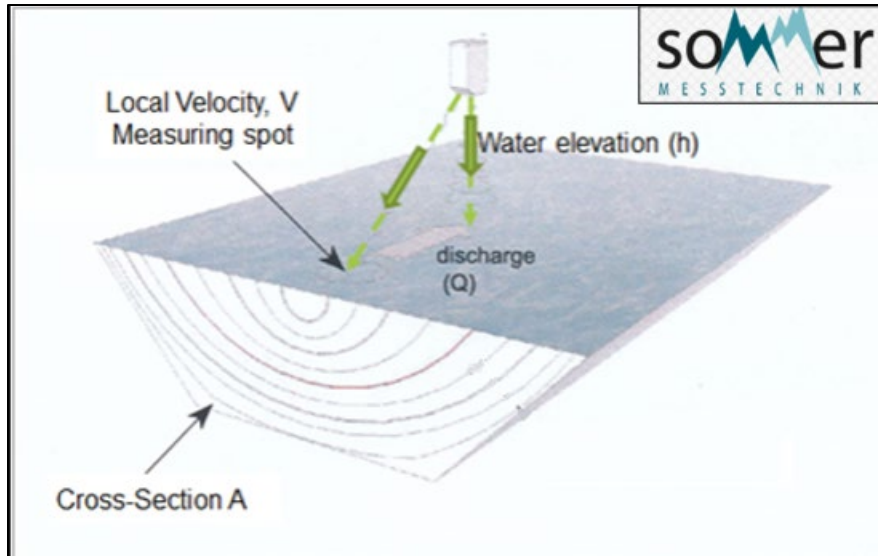


Figure 2.5 Conceptual drawing of an RQ-30 gauge and sensor. Modified from Sommer Messtechnik (2023b; Figure 2). Figure used by permission.

The gauge is powered by a 35 amp-hour 12-volt battery which is charged with a 20-volt solar panel attached to the gauge enclosure. Batteries are considered a consumable part of the streamgauge and are expected to be replaced as needed.

A wire-weight gauge, surveyed to NAVD 88, serves as the reference to the non-contact water-level method used to measure the stage. The wire-weight gauge can be used to manually determine the water surface by lowering a weight attached to a steel cable to the water surface. When the weight contacts the water surface, a calibrated dial is read to determine the stage at that time.

### 2.2.2. Equipment Resilience

Data loggers, sensors, solar panels, batteries, and transmission components run continuously throughout the life of a streamgauge. These components reside outdoors and are subject to temperature fluctuations, bridge vibration, and equipment malfunction that can affect the reliability of the system.

As of July 2023, the 80 RQ-30 gauges have been operational 1–3 years. During this time, the MRL-7 data loggers installed at each gauge have functioned well when no external issues were present. External issues such as incorrect or loose wiring, user error, incorrect settings, limited cellular signal coverage, sensor malfunction, and system power loss can cause temporary outages of data that are not attributed to the overall function of the data logger. The most common problem observed with the MRL-7 data logger is the temporary loss of cellular function in areas of weak cellular data services.

Transmissions were reliant on the signal quality of the cellular data network. Efforts were made during the reconnaissance phase of the project to ensure data could be sent and received onsite using cellular phone speed test applications.

The RQ-30 gauge sensor functioned according to its manufacturer specifications (Sommer Messtechnik, 2021b) except for low-velocity resolution. Large variances were often observed by the authors of this chapter in the final recorded data (Grzyb and others, 2025). The intended use of these gauges is to provide information to better inform TxDOT regarding flood related decisions, therefore limitations identified during low-flow conditions were of little concern for the practicality of the network for its primary intended purpose as a flood support streamgauge.

Stage and velocity components of the sensor functioned correctly during the study with one exception. There was a malfunction in the stage data from five of the 80 RQ-30 gauges; these five gauges were recording a single stage value repeatedly regardless of any changes in the actual stage (Grzyb and others, 2025). USGS personnel were able to remedy all of stage malfunctions by rebooting the RQ-30 gauge sensors remotely, which reset the sensors and allowed them to resume normal operation.

### **2.3. Data Assessment**

---

The USGS initially considered separating the 80 gauges into three groups to evaluate differences in the data depending on the frequency of site visits and differences in instrumentation and data collection methods. Because of ongoing drought conditions and other considerations, all gauges were ultimately visited every 6- to 8-weeks. There was an emphasis on visiting the site to collect data whenever the stage was elevated (such as during runoff events). This stage verification process is consistent with procedures used throughout the USGS. The USGS also installed one or more passive crest-stage gauges (CSGs) considering site-specific hydraulics to manually record the highest stage between successive site visits.

### 2.3.1. Properties of Recorded Data

Nine properties are monitored by each RQ-30 gauge. Of these nine properties, only the stage data are published on NWIS web (USGS, 2023). The data for following six properties used to assess the performance and capabilities of the RQ-30 gauge network are available in the companion data release (Grzyb and others, 2025):

1. **Stage (ft):** Level of the water surface, measured every 5 minutes,
2. **Velocity (ft/s):** Water surface velocity in-line with the RQ-30 gauge sensor,
3. **Learned velocity (ft/s):** Water surface velocity determined internally by machine learning algorithms built into the RQ-30 gauge sensor,
4. **Area (ft<sup>2</sup>):** Cross section area computed by the channel geometry input into the RQ-30 gauge sensor,
5. **Discharge (ft<sup>3</sup>/s):** Instantaneous discharge value as calculated by the RQ-30 gauge sensor with velocity, and
6. **Learned Discharge (ft<sup>3</sup>/s):** Instantaneous discharge value as calculated by the RQ-30 gauge sensor with Learned velocity.

The remaining three properties are used as internal quality control; because they have no application in the computation of streamflow, they were not included in the companion data release.

**Quality:** A signal-to-noise ratio determined internally by the RQ-30 gauge sensor that evaluates the velocity return signal to the level of background noise interfering with the radar signal during a reading,

**Opposite Direction:** The ratio of velocity distributions in the forward and opposite directions, and

**DCP battery voltage (V):** Voltage of the gauge battery at the time of transmission.

### 2.3.2. Cross Sections

To compute discharge using velocimetry, a cross-sectional area must be determined in order to enter the area into the standard discharge equation

$$Q = V_{Average} \times A \quad (1)$$

where

$Q$  is volumetric flow rate (discharge) in cubic feet per second (ft<sup>3</sup>/s),

$V_{Average}$  is the average velocity at the gauge cross section, in feet per second (ft/s),

and  $A$  is the cross-sectional area at the streamgauge, in cubic feet (ft<sup>3</sup>).

For this project, cross sections were determined by using light detection and ranging (lidar) data, global navigation satellite systems (GNSS), and total station surveying. All datums were referenced to NAVD 88.

During the establishment of each RQ-30 gauge, the channel at each site was surveyed to create a cross section which was entered into the RQ-30 gauge sensor for discharge computation. The above-water portions of the cross-sectional survey were obtained by using a total station to define features within the channel. Below-water portions of the cross-sectional survey were obtained by means of acoustic Doppler current profiler (ADCP) bathymetry data when on-site conditions, such as excessive water depths, prevented direct observations of the channel geometry and water-surface elevations.

When multiple survey methods were required to complete a cross section survey, data were entered into the USGS program AreaComp3 (Knight, 2023) to assist in computing a cross-sectional area. For instance, combining ADCP data with traditional level and stadia or depth-sounding observations to create a stage area-rating curve.

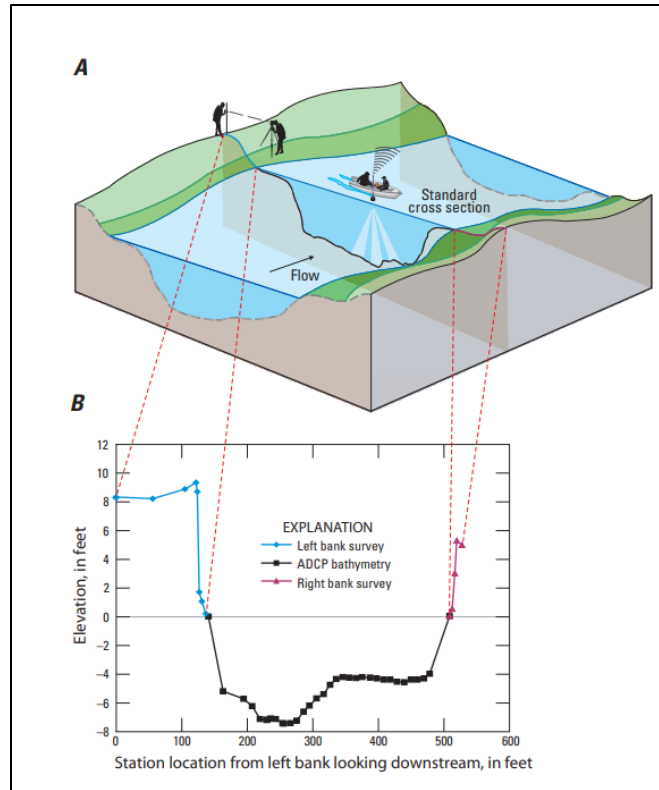


Figure 2.6 Example of a cross section survey involving multiple techniques (Levesque and Oberg, 2012). Used by permission.

The cross-sectional area of a stream is determined by the geometry and the stage at any given time. If the surveyed cross-section undergoes a scour or fill condition, either natural or manmade, a change in the velocity distribution could occur. Changes in cross-sectional area commonly occur because of flood events and often require a resurvey of the cross-section to maintain an accurate velocity-discharge relation.

The Stage-Area Rating Validation section of Levesque and Oberg (p.34, 2012) explains

The standard cross section should be re-surveyed and documented annually for the first 3 years that a station is operated. If less than 1 year has elapsed since the previous survey and a change in the cross section is suspected, the standard cross section should be re-surveyed. After 3 years, the frequency of re-surveys can be reduced to that used for station levels (typically every 3 years) if the following conditions are met:

1. The standard cross-section does not show substantial change in geometry. This evaluation of the channel cross section is often based on direct observations made onsite by the hydrographer.

2. A comparison of the stage-area rating created from the annual surveys indicates no substantial percentage difference from the initial survey.

The USGS program AreaComp3 (Knight, 2023) was also used to compare cross sections and determine any differences in channel geometry over time. An emphasis was made on high-flow comparisons of channel geometries because low-flow channel geometries are sensitive to minor variations in the survey location. The results of each comparison were assessed for substantial area differences, as described in the USGS Techniques and Methods 3–A23 report entitled “Computing Discharge Using the Index Velocity Method” (Levesque and Oberg, 2012).

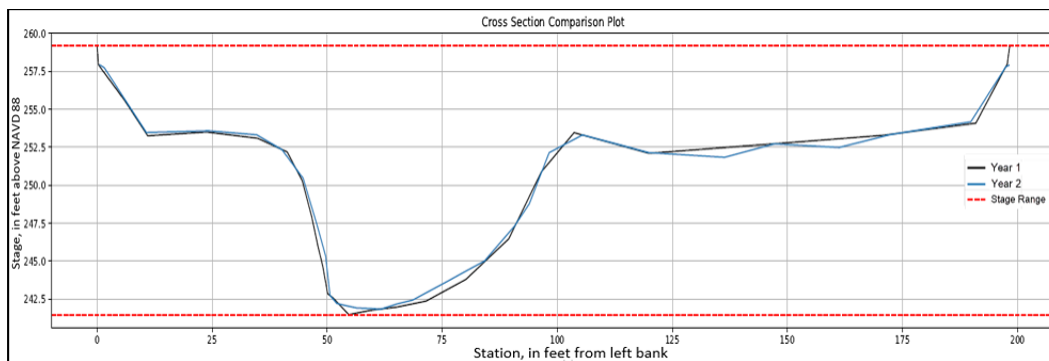


*Figure 2.7 Example of a typical cross section comparison plot for computing differences in area. This example is from Manson Creek at SH 294 near Elkhart, Tex. (08065080) (U.S. Geological Survey, 2023).*

In Figure 2.7 , an example of two annually surveyed cross sections at one gauge are compared by using the USGS program AreaComp3 (Knight, 2023). The difference in area at lower stages is greater from year to year because the percent change in area is highly sensitive to small variations in low flow channel geometry. Minor variations are also observed in the overbank geometry because of differing survey points within the cross section.

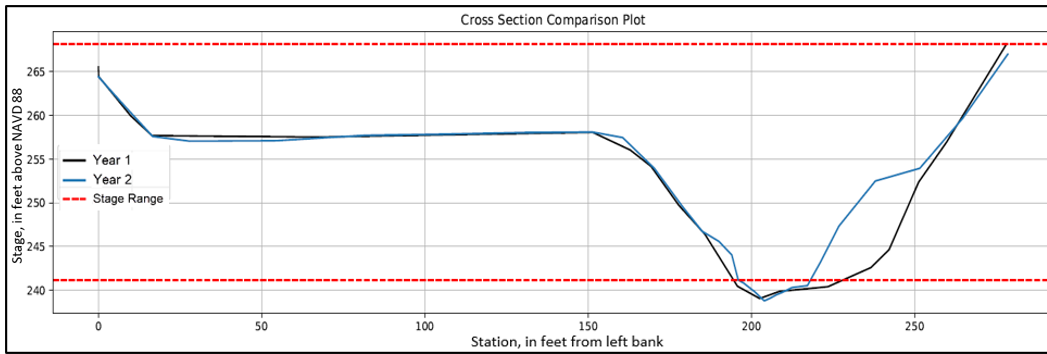


Figure 2.8 Example of a cross section comparison plot where channel modifications were made between surveys. This example is from Carters Creek at FM 60 near College Station, Tex. (08111051) (U.S. Geological Survey, 2023).

The largest cross-section area changes were found in channels where channel modifications were made by local entities. Modifications in the form of the addition of rip-rap banks, concrete channelization, or channel clearing caused the largest bank-full area differences year over year. Figure 2.8 shows how the cross section in year 2 changed from the cross section in year 1 because of the addition of rip rap on the right bank between the stations at 200 and 250 feet from the left bank. In this example, bank-full area was decreased by approximately 30 percent. Cross sections that are observed to have changed because of human modifications are re-surveyed as soon as possible to keep the stage-area relation up-to-date. Three sites were identified and resurveyed during the project because of human modifications to the channel.

### 2.3.3. Stage

The accuracy of each stage reading is significant because stage, coupled with a cross sectional survey, determines the area component necessary to compute discharge. The accuracy of measured water-surface elevations made using the RQ-30 gauge sensor was evaluated for each of the 80 installed streamgauges. An initial sensor calibration was performed for each instrument and was verified against a wire weight reference gauge at an interval of 8–12 weeks or when higher flow verification was possible. If water was not present in the channel during installation, stage was set to a dry channel bottom and later verified and calibrated when water was present. Gauges set to a dry channel are expected to be reading incorrectly during the first verification visit.

In addition to physical verifications made by field technicians during a range of flows, passive verifications were made using a CSG to verify peaks when field staff was not present. A CSG is a 2-inch metal pipe installed near the gauge that holds a wooden staff made of cedar and ground cork. As water rises on the pipe,

intake holes allow water to enter the pipe elevating cork onto the staff. Technicians later measure these marks for peak verification.



*Figure 2.9 Photographs showing A, U.S. Geological Survey crest-stage gauge, looking downstream, and B, close-up of a typical enclosed wooden staff and cork line. The cork line marks the heights of a high-water mark during a flood event. Photographs by U.S. Geological Survey.*

Raw, unedited stage data are received and stored in an internal USGS database called Aquarius. Once a stage verification is made in the field, data are then corrected manually in the Aquarius software by technicians. The method of correction is dependent on the nature of the discrepancy but is often attributed to instrument drift. Once a correction is performed and validated with the USGS approval process, a “corrected” data set is published in the USGS NWIS database (USGS, 2023).

To assess the overall drift in calibration of each water-level radar sensor used to measure the stage, a difference was calculated between raw stage values and corrected, published stage values at the time of each verification. To use this approach, stage corrections that were known to be attributed to gauge malfunction, datum error, user error, or incorrect siting were omitted from the assessment.

For the 45 sites used in the drift assessment, 396 independent stage verifications were made comparing raw stage values to the correct observed values. The mean error ranged from -0.06 feet to 0.05 feet. The mean and median were both 0.00 feet with a standard deviation of 0.02 feet, indicating that the stage values

measured by the RQ-30 in general appeared to closely replicate manually measured stages.

#### **2.3.4. Velocity**

Velocity is not commonly measured as a continuous property at traditional USGS streamgauges; because velocity varies throughout the water column in a stream, it is typically measured discretely at different depths as part of a traditional discharge measurement. The RQ-30 gauge sensor measures surface velocity using the Doppler frequency shift method. The addition of continuously measured velocity allows for the non-contact computation of discharge after accounting for how the velocity profile varies with depth throughout the water column and adjusting the surface velocity to represent the average velocity in the entire stream cross section (Sommer Messtechnik, 2021b).

#### **2.3.5. Raw Velocity**

Raw velocity is the unaltered measurement of surface velocity recorded by the RQ-30 gauge. Gauges are typically sited so that velocity is observed where water flows the fastest within the main channel. When the velocity sensor is triggered by the MRL-7 data logger, it records the average of continuous velocity values over a specific time. The averaging time used for this project was 40 seconds.

The RQ-30 gauge manufacturer specifications state an operational range of 0.08 to 16 meters per second, or about 0.26 to 52 feet per second (Sommer Messtechnik, 2021b). Unless ideal conditions were met, it was observed that velocities less than approximately 0.8 feet per second were often not registered. Velocities greater than 0.8 feet per second fluctuated, which was attributed to variable flow characteristics in the measurement location. Wave action, turbulence, debris, and eddy velocities caused minor to major variations in consistent velocity values illustrated in Figure 2.10. Increasing the velocity averaging times helped to alleviate these fluctuations, but erroneous spikes in velocity data still occurred.

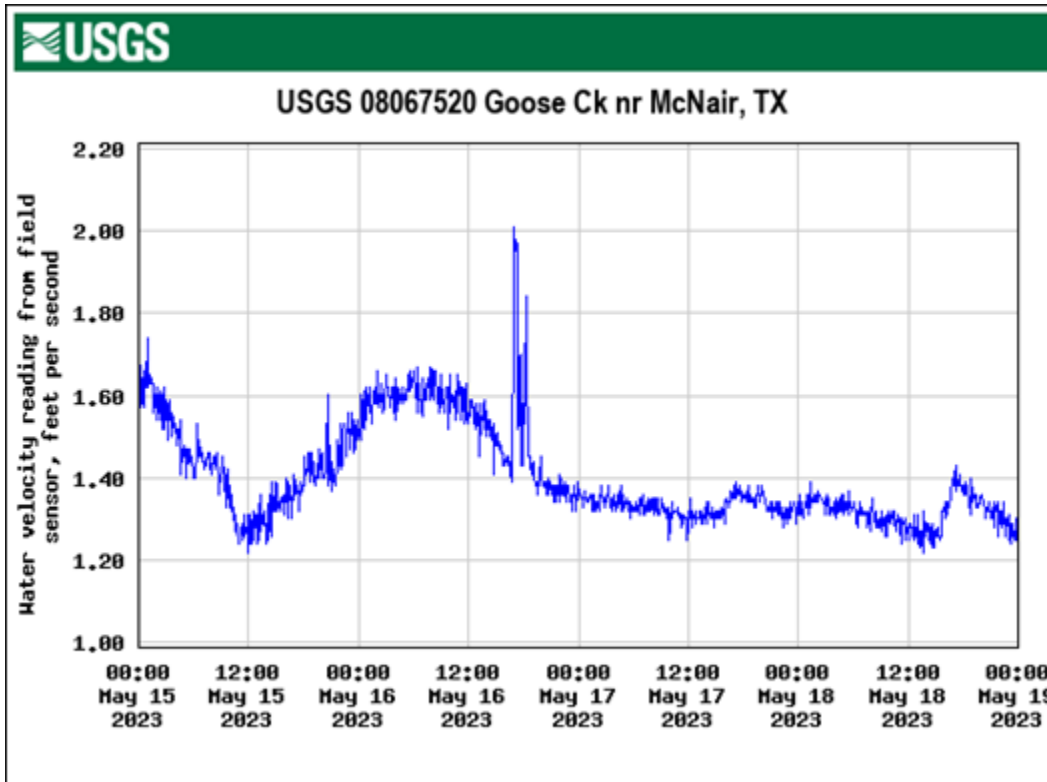


Figure 2.10 Graph of continuous velocity data in feet per second at Goose Creek near McNair, Tex. (08067520) illustrating fluctuations in raw velocity values from May 15, 2023, through May 19, 2023 (U.S. Geological Survey, 2023).

### 2.3.6. Learned Velocity

Learned velocity refers to an adaptive relationship between water level and velocity, continually refined with ongoing measurements (Sommer Messtechnik, 2021b). The RQ-30 gauge sensor internally retains this water level/velocity correlation, allowing it to offer the most likely velocity estimation for a given water level by leveraging previously recorded values. A notable advantage of learned velocity is its capacity to reduce outlier raw velocity data, particularly in instances of turbulent flows, eddy velocities, or the presence of heavy debris in the waterway. Learned velocity has limitations when there are rapid changes in the stage-velocity relation caused by backwater, loop ratings, or substantial changes in channel geometry. In situations where rapid changes in the stage-velocity relation occur, the learned velocity may differ from the actual velocity because it is based on previous observed conditions.

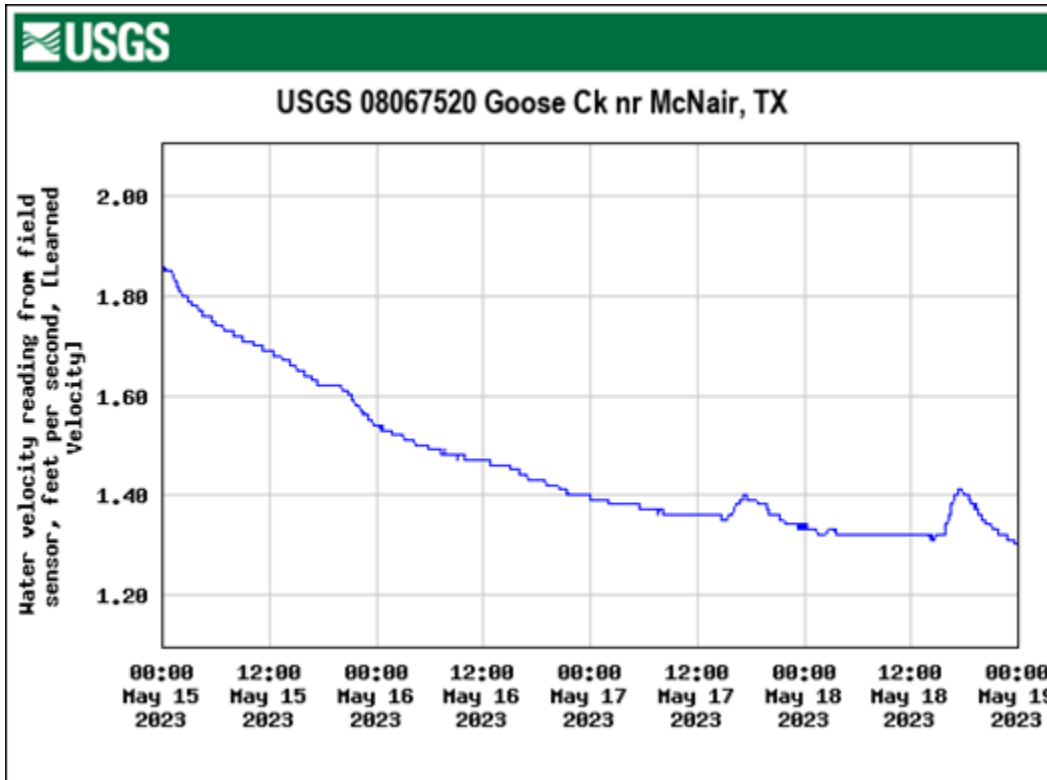


Figure 2.11 Graph of continuous velocity values in feet per second at Goose Creek near McNair, Tex. (08067520) illustrating how learned velocity can minimize fluctuations in recorded data when compared to raw velocity values. (U.S. Geological Survey, 2023)

Figure 2.11 illustrates a learned velocity hydrograph for the data depicted in Figure 2.10. Unlike raw velocity, spikes and fluctuations are removed, but resolution can be sacrificed if velocities are dynamic from one event to another. For instance, if the learned velocity relation was created using backwater affected raw velocity values, the learned velocity may be biased low. Likewise, if the learned velocity is based on normal unimpeded flows, backwater affected flows may be overestimated.

### 2.3.7. Discharge

The RQ-30 gauge sensor computes discharge from the volumetric flow rate equation (eq. 1).-The term  $V_{Average}$  in equation 1 is determined by using machine learning algorithms built into the RQ-30 gauge sensor to multiply the surface velocity at the gauge by a coefficient called the “k-factor.” The k-factor adjusts a surface velocity to an average velocity dependent on the observed stream height and channel roughness properties. k-factors are determined by using RQ-30 gauge software Q-Commander (Sommer Messtechnik, 2021b). Q-commander is used to create an initial k-factor from a user-derived roughness coefficient and the surveyed geometry of the cross section. For all installed sites, an appropriate Manning’s roughness coefficient was selected; the Manning’s roughness coefficient represents the resistance to flow in channels and flood plains (Arcement and Schneider, 1989). Following the initial setup, calibrations are made to adjust the k-factor profile accordingly. As of July 2023, 202 discharge measurements have been made. Of those 202 measurements, 136 measurements were made at discharges greater than 20 ft<sup>3</sup>/s.

### 2.3.8. Raw Discharge

Raw discharge is a direct discharge calculation made by using the instantaneous raw velocity measured by the RQ-30 gauge sensor and multiplying it by the cross-sectional area. The initial setup in the Q-Commander software requires a cross section, the location of the radar, and a user selected Manning’s roughness coefficient. These three inputs are used by Q-Commander to determine the k-factor relation between surface velocity and mean velocity. Once a k-factor relation is created, discharge is computed for all stages, regardless of its accuracy.

Because uncalibrated raw discharge was computed using raw velocity, the same fluctuations observed in raw velocity values were observed in the raw discharge values. The fluctuations in discharge are directly proportional to those in raw velocity, which can cause large variations in discharge.

Figure 2.12 shows a high-water event recorded using the uncalibrated RQ-30 gauge to compute high-flow discharge. The USGS discharge unit values are truncated on the rising leg of the event whereas the RQ-30 gauge computes the event to its entirety. The USGS discharge is truncated because the stage-discharge relation relies on measurements to complete an initial rating curve, and the rating curve was not available for the stage at the onset of the high-flow event. Because of the “flashy” nature of streamflow, measurements representing a wide range of stage heights can be difficult to obtain, and stations can go years before a rating curve representing all ranges of stage can be developed.

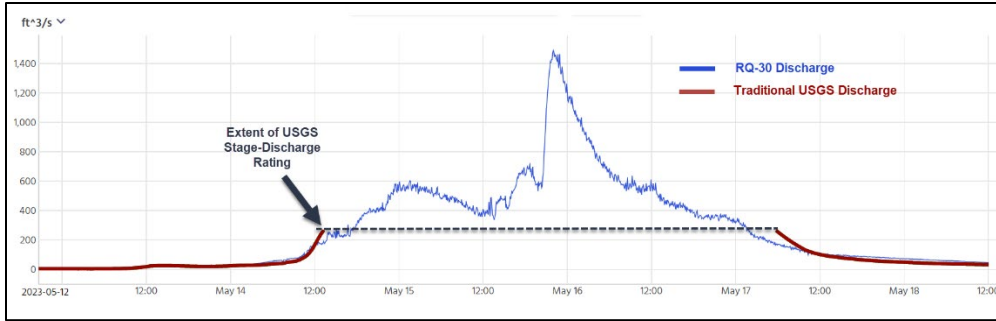


Figure 2.12 Example of USGS traditional discharge and RQ-30 Gauge raw discharge

The accuracy of the selected Manning’s roughness coefficient was found to be the largest source of error in computing a discharge before the RQ-30 gauge is calibrated. On-site roughness coefficients were selected using Cowan’s method as described in Arcement and Schneider (1989). The Manning’s roughness coefficient was then updated in the Q-Commander software to best fit the k-factor profile to the observed ADCP discharge measurements.

### 2.3.9. Learned Discharge

Learned discharge (Sommer Messtechnik, 2021b) is computed by multiplying the learned velocity by the cross-sectional area. The output from learned discharge is generally smoother than the raw discharge as is derived from the learned velocity. There are many types of smoothing functions, and smoothing functions are widely used in statistical analyses to reduce the amount of “noise” or random variations in environmental data (Helsel and others, 2020). Figure 2.13 illustrates an overall smoother hydrograph with less “noise” in the hourly data when compared to the raw discharge in Figure 2.12.

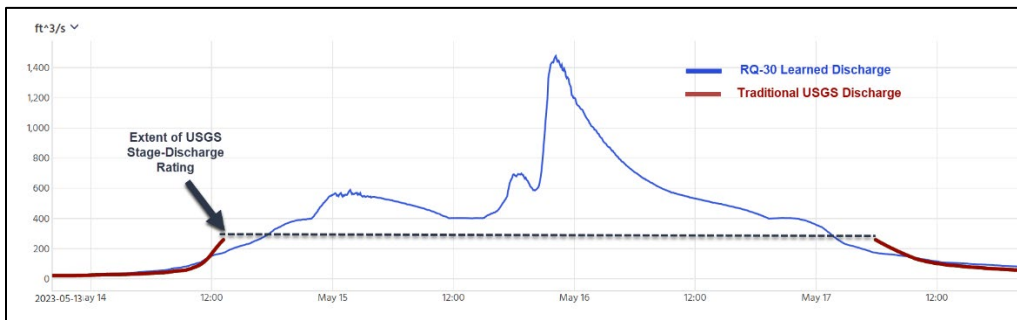


Figure 2.13 Example of USGS traditional discharge and RQ-30 gauge sensor Learned discharge.

Similar to learned velocity, learned discharge has limitations when there are rapid changes in the stage-velocity relation caused by backwater, loop ratings, or substantial changes in channel geometry.

### 2.3.10. Discharge Calibration

The initial setup of the RQ-30 gauge allows for the measurement of stage and discharge immediately, but a calibration of the sensor yields more accurate results as new discharge measurements are made. To perform a calibration, a stage, surface velocity and physically measured discharge must be available. The measurement information is entered into Q-commander, which creates a constraint on the k-factor profile relating surface velocity to the average velocity for the measurement stage. Changes to the initial roughness coefficient can then be used to adjust the k-factor profile to the measurement via the Q-commander software. Subsequent measurements are then used to provide additional constraints to adjust the k-factor profile manually, if necessary, as seen in Figure 2.14.

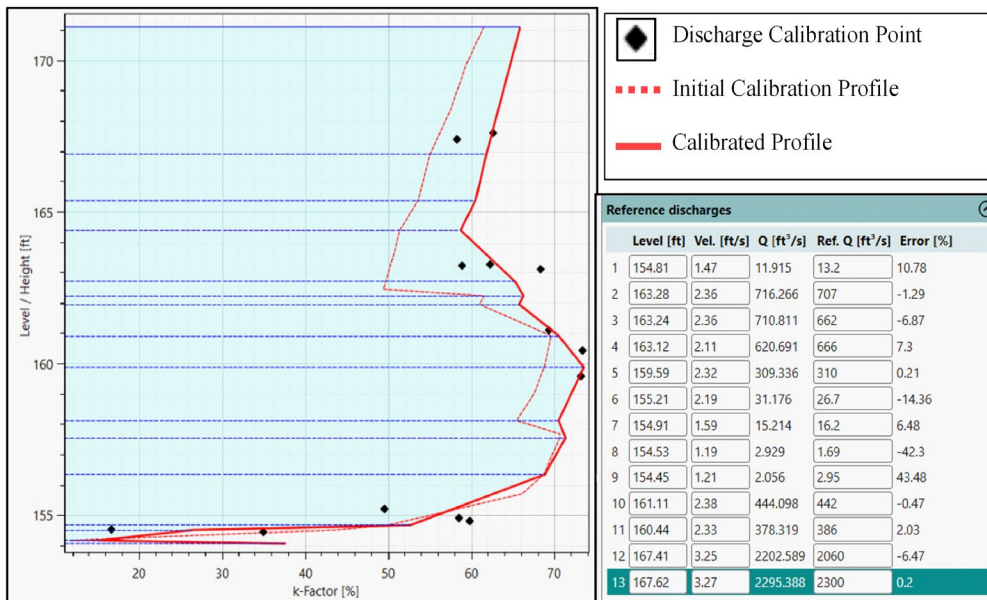
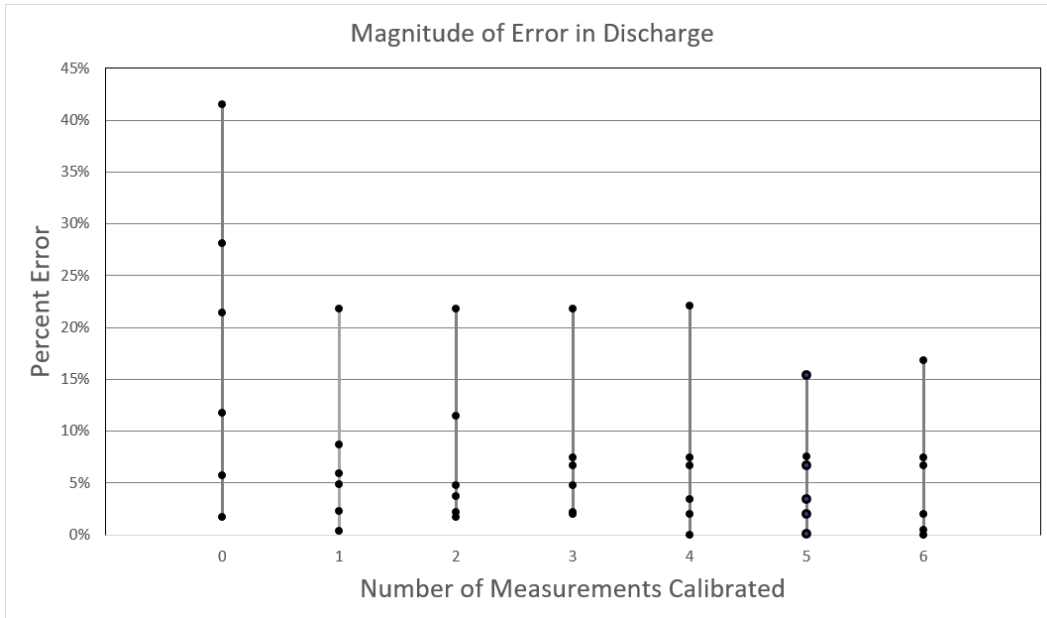


Figure 2.14 Example of a 13-point calibration of the k-factor profile in Q-Commander.

Discharge measurements were made at all stages to determine how many measurements were needed to calibrate the gauge for accurate discharge throughout the entire range of observed flow. Prior to calibrating, the initial k-factor profile was used to determine the magnitude of the difference between the RQ-30 gauge sensor derived discharge and the physical verification measurement. A calibration point was then created using the first verification measurement, and all subsequent measurements were assessed against the 1-point calibrated RQ-30 gauge derived discharge. The process was repeated until all measurements had been calibrated and assessed. Since these gauges are being assessed as flood decisions support tools, discharges less than 20 ft<sup>3</sup>/s were omitted from calibration error calculation. Discharges under 20 ft<sup>3</sup>/s were omitted because lower flows are

highly sensitive to small bathymetric changes resulting in large errors that do not represent the high-flow measurement of discharge.



*Figure 2.15 Chart showing the range of errors between the RQ-30 gauge computed discharge and the USGS verification measurements as calibrations are performed sequentially at New Year Creek at FM 1155 near Chappell Hill, Tex. (USGS site number 08111110) (U.S. Geological Survey, 2023; Grzyb and others, 2025). Note: Discharge values of less than 20 cubic feet per second were removed.*

Figure 2.15 shows that calibrating to each individual measurement decreases overall error but may require numerous measurements, which are expensive and dependent on weather conditions. Using this approach, calibration of an RQ-30 gauge sensor may not be any faster than traditional methods.

A second approach was explored after a pattern was recognized in the previous calibration assessment. The overall shape of the initial k-factor profile computed in the Q-Commander software closely resembles the finished, calibrated profile. Rather than making frequent measurements, targeted stages were selected and measured to constrain the original profile. Targeted measurements include the main channel, the transition between main channel and overbank, and overbank stages. Once the targeted measurements are made, the roughness coefficient is adjusted to best fit the calibration points.

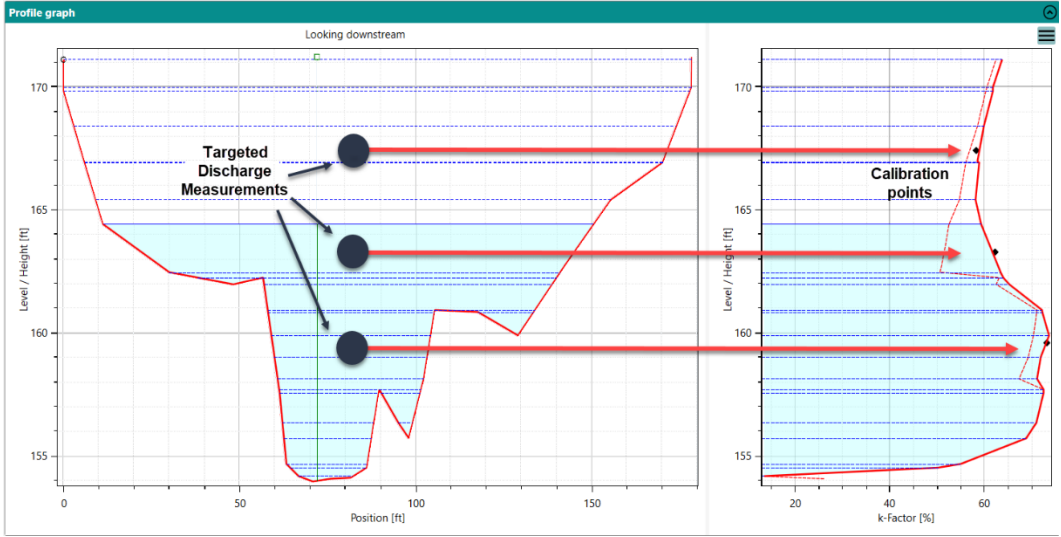


*Figure 2.16 Channel geometries are targeted to constrain the k-factor profile.*

Figure 2.16 demonstrates a typical channel with overbank where three stages are targeted to expedite the calibration process. Each measurement constrains the software derived k-factor profile while closely preserving the original profile shape.

Figure 2.17 shows a calibration for the previous example when the targeted method is followed. In this example, an overall error of less than 10 percent was achieved for measurements greater than 20 ft<sup>3</sup>/s with calibration points.

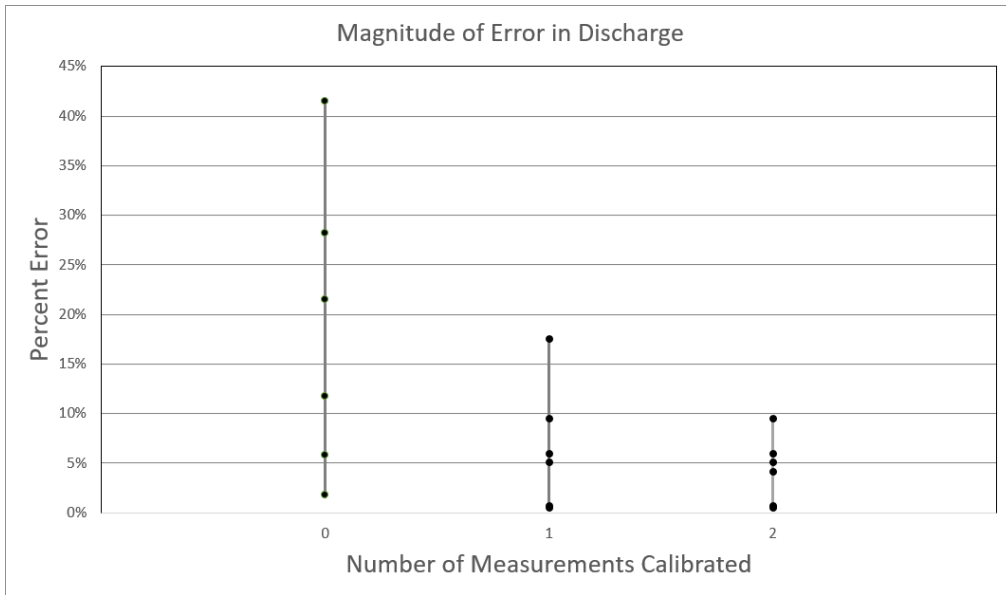


Figure 2.17 Chart showing the range of errors for discharge measurements using the targeted calibration approach at New Year Creek at FM 1155 near Chappell Hill, Tex. (USGS site number 08111110) (U.S. Geological Survey, 2023; Grzyb and others, 2025). Note: Discharge values of less than 20 cubic feet per second were removed. Targeted calibration approach refers to measurements made at specific water levels based on geometry of the cross section.

## 2.4. Conclusions

Water levels recorded by the RQ-30 gauges closely matched the water levels available from nearby stable references if the initial calibration was correct. The water-level sensors used to measure the stage were able to maintain precise water-level elevation values without the need for frequent recalibration. By reducing the need recalibrate the sensors, the standard interval of 8-week routine maintenance visits to service streamgauges could potentially be extended.

Cross sections surveyed during the project have shown little change caused by natural means, preserving the stage-area relation necessary for consistent discharge computation using velocimetry. Modifications made to the gauge cross-section were the only discernable differences that required a resurvey during the project. The Cross-sectional area is subject to change due to flood events, which can directly affect the computation of discharge using velocimetry, especially for base-flow conditions.

Velocity data recorded when flows were greater than approximately 0.8 feet per second were reasonable when compared to manually measured velocity values. Velocities less than 0.8 feet per second were often less available as the velocities

slowed because the measurements were close to the lower bound of the sensor's operational range and high signal to noise ratio at lower velocities. The steadiness of measured velocities was notably influenced by turbulence from bridge piers, debris, and other channel-related eddy velocities which cause fluctuations between consecutive data points.

Although the targeted measurement approach to velocimetry discharge calibration is showing promise in the ability to reduce the time needed to calibrate a streamflow gauge, additional data are needed to ensure the method is valid for all conditions. Extreme site conditions such as large channel slopes, variable bedforms, bridge disturbances, and backwater affected flows have not yet been fully assessed.

# Chapter 3. Flood Assessment System for TxDOT (FAST)

## 3.1. Introduction

The Flood Assessment System for TxDOT (FAST) is a set of web map services that can be viewed using a normal web browser on a computer or hand-held device, as illustrated in Figure 3.1. On the left hand side are map services for precipitation and flood inundation that are part of the NWS Hydrovisualization services.<sup>3</sup> These are augmented by maps of stream gauge locations for both the RQ-30 and normal USGS stream gauge network. On the right hand side are map services created for assessing the impact of flooding on the road and bridge system, including bridge warnings, flooded roads, and flood impact, measured by the length of roads flooded in each District and Maintenance Section.

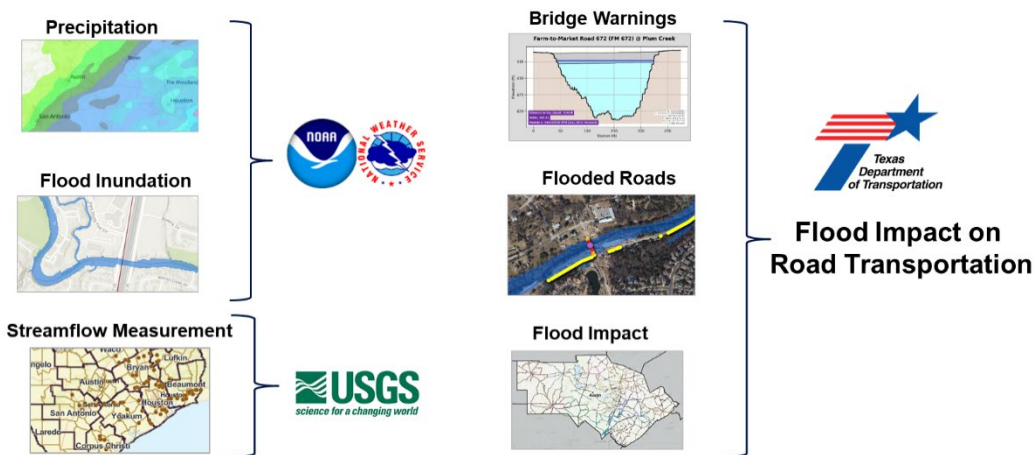


Figure 3.1 Flood Assessment System for TxDOT (FAST)

The goal of having these map services is to enable TxDOT to move from a *reactive* mode to a *proactive* mode in dealing with flood operations. In a reactive mode, as shown on the left hand side of Figure 3.2, the staff in the Emergency Operations Center (EOC) coordinate with the Maintenance Supervisors to dispatch field staff to observe flood conditions at particular points on the road system and call back by telephone or radio to report what they see. Sometimes this results in “babysitting” the roads where the field staff wait in place to observe

<sup>3</sup> <https://maps.water.noaa.gov/server/rest/services>

flood conditions changing over time. Then, decisions are made at the Emergency Operations Center based on flood conditions then prevailing.

In proactive mode, as shown on the right hand side of Figure 3.2, the intent is to assess current and anticipated future flood conditions by means of maps, and thus to be able to get ahead of flood events, closing roads in a timely fashion so that cars and trucks are diverted onto alternative routes and not trapped on a flooded highway. In this way, TxDOT Maintenance staff can themselves be kept safer, and not dispatched unknowingly into a dangerous flooding situation. Forecast information can be used to close roads and divert traffic in a timely manner. The severity and extent of flood conditions can be monitored regionally as the flood rises and falls. After flooding is over, bridges can be inspected and roads reopened in an efficient manner.

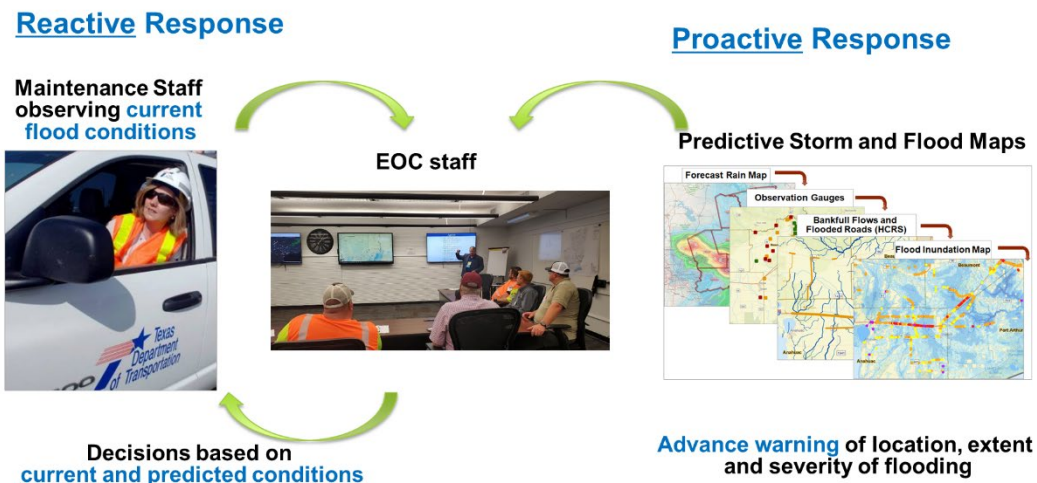


Figure 3.2 Reactive and Proactive Flood Emergency Response

The method of organization of Maintenance staff during a flood event is illustrated in Figure 3.3 for the TxDOT Beaumont District at the time of a flood emergency response exercise that the research team held with the Beaumont District in February 2022. At the heart of this organization is the Emergency Operations Center (EOC) maintained in the District office. All of the staff in the center take on roles defined by the FEMA National Incident Management System (NIMS)<sup>4</sup>, which guides all levels of government, nongovernmental organizations and the private sector in responding to emergency events. The EOC is staffed 24 hours per day with 12 hour shifts that change at 7AM and 7 PM. The most

<sup>4</sup> [National Incident Management System | FEMA.gov](https://www.fema.gov/national-incident-management-system)

critical staff positions have two occupants, one designated for the day shift, the other for the night shift. A schedule of operational and weather briefings is fitted into this schedule to support flood emergency operations.

The EOC staff coordinate with the Maintenance supervisors in each Maintenance section. For the Beaumont District, Maintenance sections follow county boundaries except for Jefferson County, which includes the principal city, Beaumont, which has two Maintenance sections, called Beaumont and Port Arthur, respectively. When additional resources are needed from the state level or from other TxDOT Districts, this is coordinated through the TxDOT Austin Emergency Operations Center.

Additional actions are coordinated with other local agencies. In particular, only the Department of Public Safety has the authority to close roads, so TxDOT must first obtain their permission before erecting road barriers and diverting traffic. Similarly, regional flood rescue and support operations are coordinated by the Texas Department of Emergency Management through its Disaster District Coordinators.

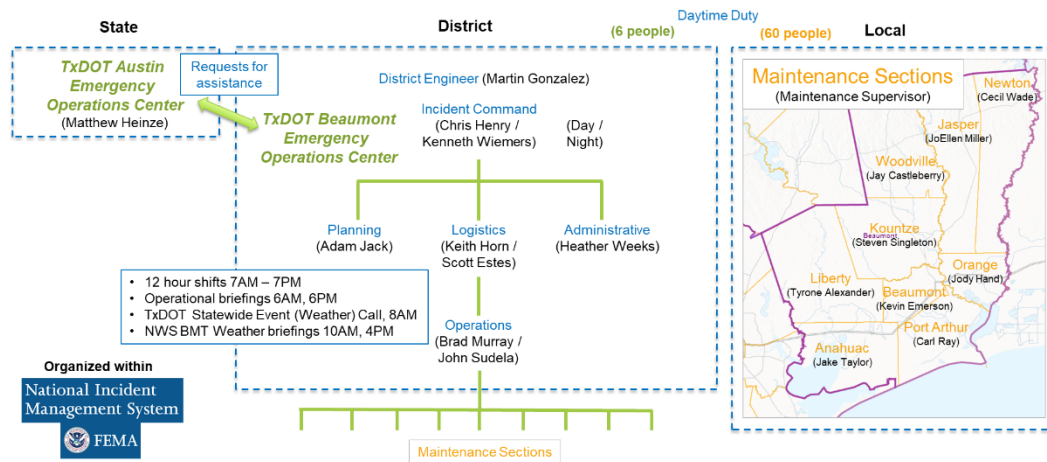


Figure 3.3 Beaumont District Flood Organization, as of February 2022

It can be appreciated that having TxDOT staff at state, District and Section levels coordinating and having coordination with other agencies, a significant need exists for a Common Operating Picture, or “One Water Map” over the landscape that everyone can work from.

### 3.2. NWS Flood Inundation Mapping

The NWS has commenced providing public, real-time flood inundation mapping services, beginning in October 2023. About half of Texas is part of the first 10%

of a national deployment of such services, as shown in Figure 3.4. This affects 20 TxDOT Districts, with complete coverage being provided for 12 Districts. State-wide coverage for Texas is scheduled to be completed in October 2025.

Flood inundation mapping involves two steps: first the discharge in each stream segment is calculated by the National Water Model that operates as part of the NWS weather forecasting system and is calculated in the Weather and Climate Operational Supercomputer System (WCOS), which is managed by the NOAA Environmental Modeling Center, located in College Park, MD. Weather forecasting is first used to calculate forecast precipitation, then this and associated climate variables such as temperature, wind and humidity, are input to the National Water Model to compute streamflow discharge. This exercise is repeated hourly for the current conditions and short-range forecast (18 hours ahead) and every six hours for the medium-range forecast (10 days ahead). The discharge is computed for 2.7 million stream reaches in the continental US, and for additional stream reaches in Alaska, Hawaii, Puerto Rico, and other US territories.

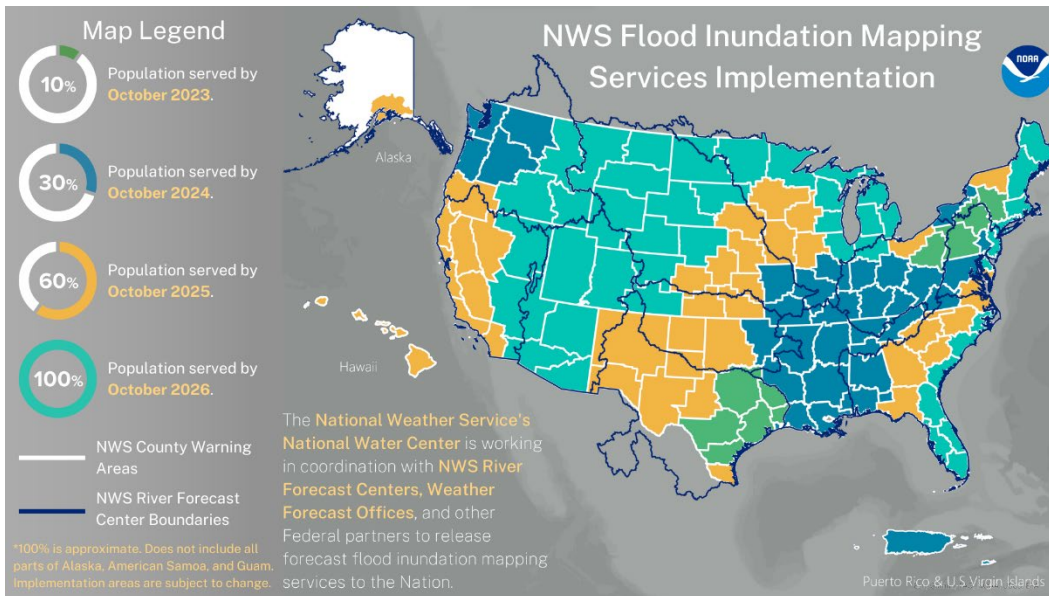


*Figure 3.4 NWS Flood Inundation Mapping Services Implementation.  
Source of Figure – National Weather Service*

Once the discharge in the stream reaches is known, this is converted into a stage-height using a rating curve computed using the Height Above Nearest Drainage (HAND) method or by using a hydraulic engineering model. This, in turn is used to create a flood inundation map for the area flooded around the stream itself. The individual stream reach inundation maps are combined to give a flood inundation map for a watershed and stream network. As a point of reference,

there are about five hundred of these stream reaches in Travis County, Texas, including three reaches on Shoal Creek and one reach on Waller Creek within the City of Austin. The flood inundation mapping service is managed by the NWS National Water Center, located in Tuscaloosa, AL.

The current version of the NWS flood inundation mapping is computed using bare-earth elevation models with all the bridges removed. A consequence is that all bridge locations are shown as being flooded, as shown in Figure 3.5, even though the road on the bridge deck is most often well above the flood waters. This challenge can be overcome through the development of a Road Elevation Model, as described in Chapter 5 of this report.



*Figure 3.5 Flood Inundation Map showing inundated roads at bridge locations  
Source of Figure – National Weather Service*

### 3.3. Flood Map Services

---

Flood Map Services are accessed through a web viewer in which a series of maps are displayed in layers using a set of tabs to separate one layer of maps from another and, and within a given group, to separate one map from another. Each map or layer can be toggled on or off individually. The services utilize the ESRI map server systems and services from different sources can be integrated into a single viewing system<sup>5</sup>, as shown in Figure 3.6.

---

<sup>5</sup> This viewer can be found at: <https://arcg.is/0eGPz4>

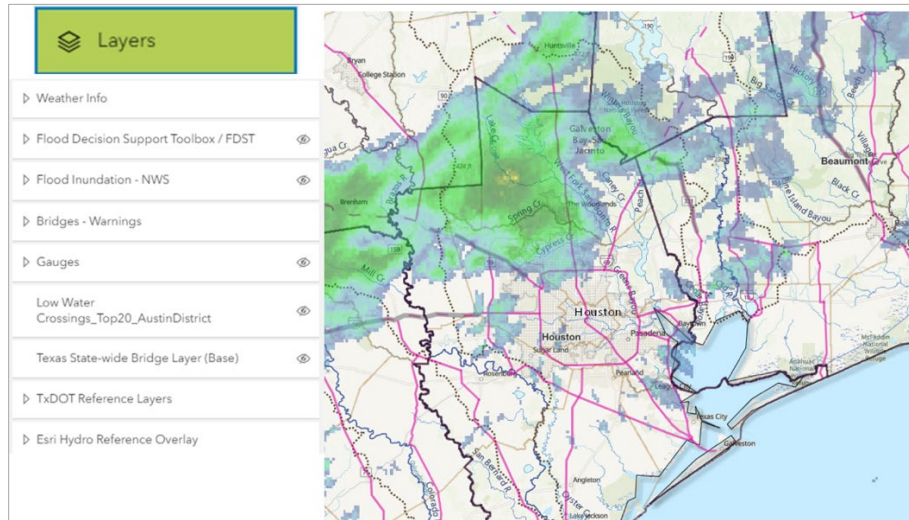


Figure 3.6 Flood map services viewer

In this manner, static information specific to TxDOT, such as the map of District and Maintenance Section boundaries, can be combined with dynamic information, such as NWS precipitation and flood inundation forecasts, and current and forecast conditions at TxDOT bridges. Each map is a light service and the whole system works effectively, even though there are many maps involved – the hierarchical organization in the viewer helps to structure the interaction of the viewer with the maps. At present, the prototype FAST services viewer is maintained as part of the ArcGIS Online system at the University of Texas at Austin. At a later date, this will need to be migrated to another hosting environment, either at TxDOT, or at another support organization for TxDOT.

### 3.4. Flood Emergency Response Exercises

The research team conducted two large-scale emergency response exercises, the first in the Beaumont District in February 2022, and the second in the Austin District in January 2023. About 30-40 TxDOT employees participated in each exercise, drawn mostly from the staff in the various Maintenance sections. These exercises are described in Report P6A1<sup>6</sup> and P6A2<sup>7</sup>, respectively. The Beaumont exercise used Tropical Storm Imelda in 2019 as its case study; the Austin exercise was similarly focused on the Llano flood of 2018. Each of these exercises took

<sup>6</sup><https://www.cae.utexas.edu/prof/maidment/StreamflowII/Documents/ReportP6A1Project07095.pdf>

<sup>7</sup><https://www.cae.utexas.edu/prof/maidment/StreamflowII/Documents/ReportP6A2Project07095.pdf>

many months of preparation to create the flood map products to be evaluated. This work was found to be invaluable in focusing attention on the needs of the ultimate end user of FAST – the TxDOT Maintenance staff.



*Figure 3.7 Austin flood emergency response exercise*

The exercises were conducted using the Homeland Security Exercise and Evaluation Program (HSEEP)<sup>8</sup>, and follow a formal protocol with roles assigned to the various participants, formal records maintained of comments and suggestions, a survey conducted at the end of the exercise to evaluate its effectiveness, and a focus on presenting the flood maps as information products for TxDOT staff to evaluate and determine whether that product would be helpful to them in their work during flood operations.

The discussion was divided into two groups – an Emergency Management group in one room, and Maintenance field staff group and in another room. This division created more freedom for the field staff to speak frankly and a great deal of feedback was received – in the Austin exercise there were more than 100 written “likes” of various kinds and also more than 100 written “suggestions for improvement”. The HSEEP exercise format was effective in creating a discussion and feedback environment in which TxDOT Maintenance staff were able to engage and provide feedback on the prototype flood map products they evaluated.

The key outcomes of the Beaumont Flood Emergency Response Exercise were: (1) The idea was validated that flood information presented as maps provides useful and usable information for TxDOT flood emergency response. (2) Three key maps of greatest interest to the TxDOT Maintenance staff were identified (flooded road depth estimates, rainfall forecasts by TxDOT jurisdictions, bridge warnings) (3) Three reference maps that provide supportive information were

---

<sup>8</sup> <https://www.fema.gov/emergency-managers/national-preparedness/exercises/hseep>

identified (flood inundation, bankfull streams and HCRS flooded roads, gauge conditions)

The key outcomes of the Austin Flood Emergency Response Exercise were: (1) As in the Beaumont Exercise, the Austin Exercise participants found significant value in the flood information being presented in spatial format. The maps provide useful and usable information for TxDOT flood emergency response, which supports situational awareness during a flooding event. (2) While all the presented layers were found to be of value, bridge warnings and flooded roads were of greatest interest to the Austin Maintenance staff. (3) During the exercise, there was discussion about the need to have either spatial or tabular alerts highlighting changes in flooding situations (increased flooding, receding water levels, etc.). Also, the idea of a tabular report of flooded roads / bridges to help with work orders and response by field personnel was popular.

While both the Emergency Management Group and the Maintenance Group found value in all the products, they favored a few of them more than others. In addition, they discussed various data settings and symbology changes to several of the products to match their focus during a flood. If these products are implemented across TxDOT, the research team will need to incorporate several of the symbology requests.

### **3.5. Flooded Roads Hydrograph**

---

An interesting concept arose from the Beaumont exercise following the plotting of maps of road closures as recorded in the TxDOT Highway Conditions Reporting System (HCRS), as shown in Figure 3.8. The HCRS records road closures due to all causes, one of which is flooding. The particular segment of road closed is recorded, along with the beginning time and the ending time of the closure. Thus, at any time, the total length of roads closed can be calculated, and plotted. The time pattern of the total length of road closures closely follows that of a streamflow hydrograph at a gauging station, and is termed here a “flooded roads hydrograph. The area under the flooded roads hydrograph, expressed in [time, length] units such as day-miles summarizes the total impact of the flood as measured by the product of the length and duration of closures summed over the flood event. The combination of the road closure maps and the flooded road hydrograph summarizes the flood severity – How large is it? Where is it? When did it occur?

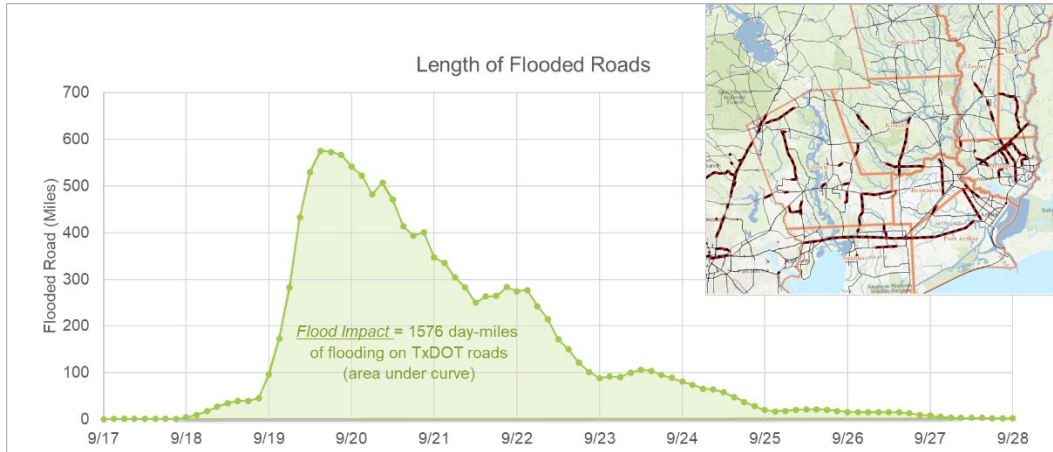


Figure 3.8 Flooded Roads Hydrograph for Tropical Storm Imelda

This pattern becomes even more compelling when a chart of the cumulated day-miles of road flooding is plotted through time, as shown in Figure 3.9. It is very easy to pick out when the major flood events occurred, and to compare the magnitude of their impacts on the road transportation system. For example, although Hurricane Harvey in August 2017 had an intense flood impact on infrastructure in Southeast Texas, the May 2015 flood actually had a larger transportation impact because it covered a larger area and lasted longer.

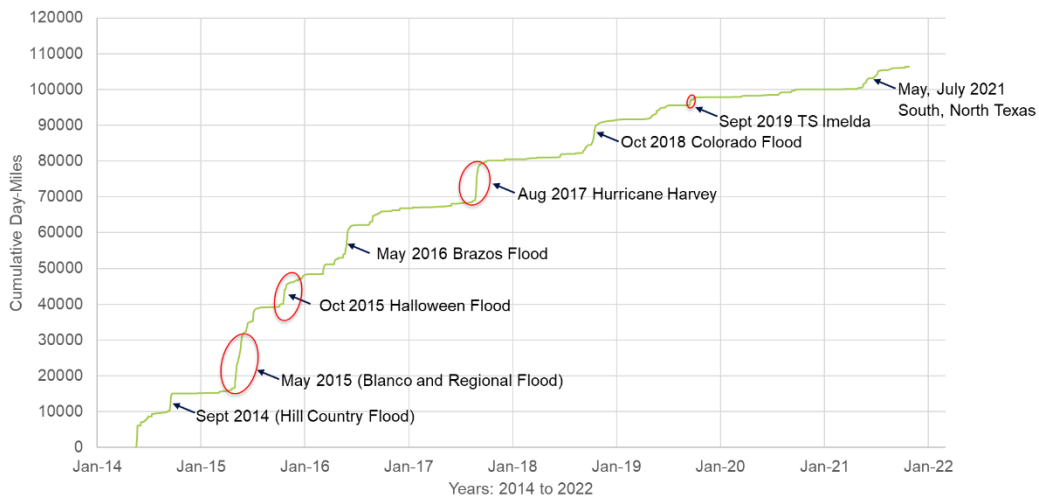


Figure 3.9 Historical Flood Impact on the Road Transportation System of Texas, May 2014 to August 2021

# Chapter 4. Bridge Warning Service

## 4.1. Introduction

A prototype state-wide bridge warning service for TxDOT has been created called Tx-Bridge Flood Forecaster, as illustrated in Figure 4.1. This monitors water conditions and creates short-range forecasts out to 18 hours ahead for about 19,000 span bridges over water whose discharge is forecast by the National Water Model. The underlying geospatial analysis to create the description of each bridge is carried out with an open-source code called Tx-Bridge<sup>9</sup> created as part of this research project.

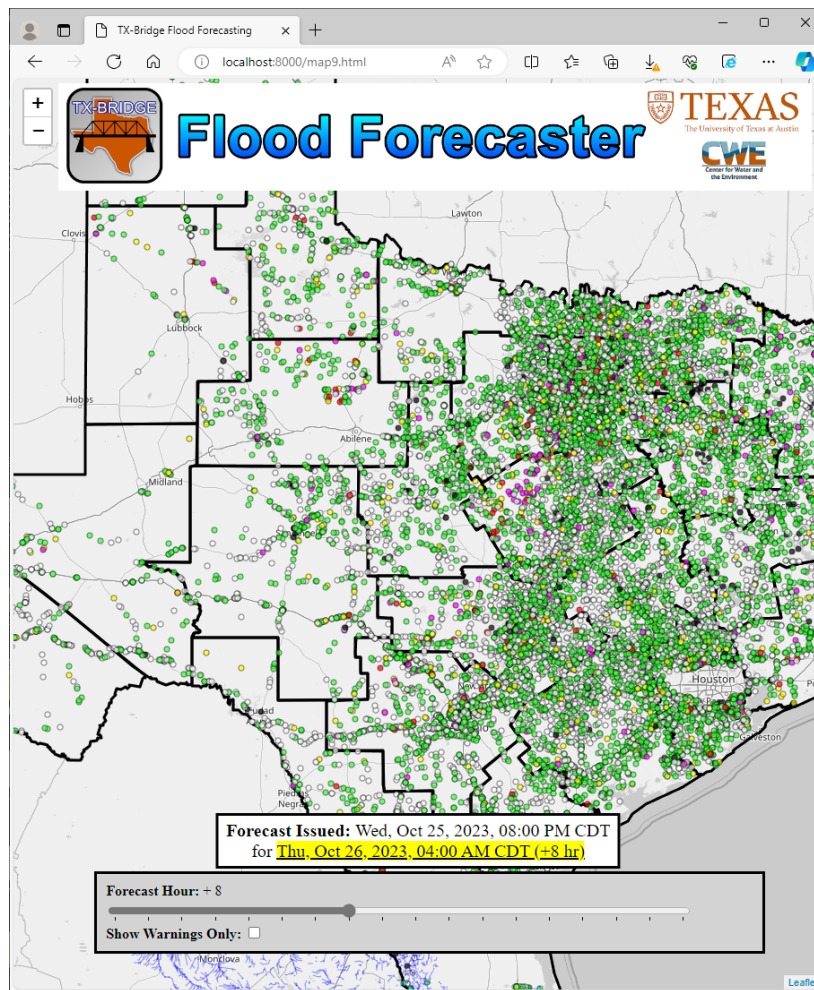


Figure 4.1 Tx-Bridge Flood Forecaster

<sup>9</sup> <https://github.com/andycarter-pe/tx-bridge>

Each bridge is characterized by a “bridge envelope” as illustrated in Figure 4.2. At the top is an elevation profile of the road on the bridge deck, where the elevation above geodetic datum in feet is defined by LIDAR data points collected for Texas. Beneath the bridge deck profile is an estimate of bridge thickness between the bridge deck and the low chord elevation, defined by a set of rules dependent on the main span type and length of the bridge, and described more fully in Technical Memorandum 5B<sup>10</sup>, pages 9-12. Beneath this again, is the water surface elevation profile, determined from the National Water Model discharge and a rating curve linking discharge to water depth created by the Height Above Nearest Drainage (HAND) method. This rating curve is determined for the stream that the bridge is located in using the NWS Flood Inundation Mapping methodology<sup>11</sup>. The bridge envelope is closed by a cross-section profile of the stream itself calculated using 1m Digital Elevation Models for Texas created from LIDAR data collections.

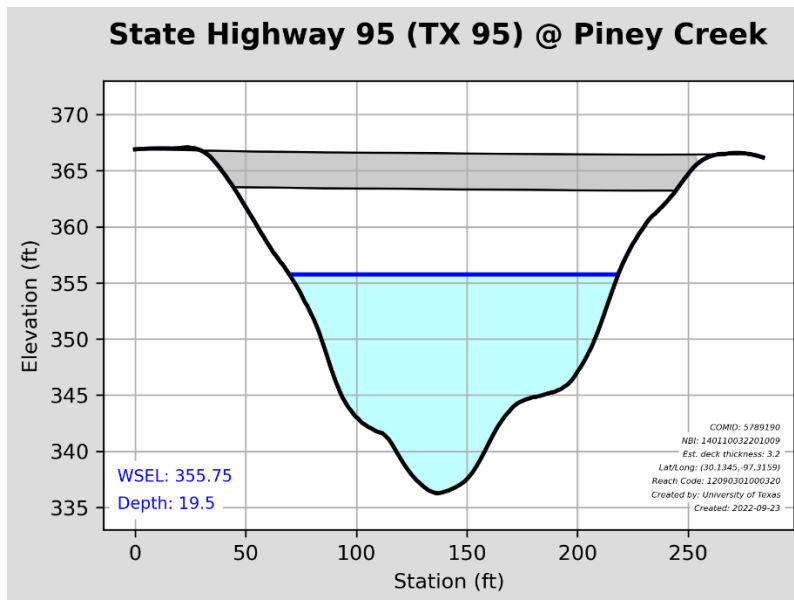


Figure 4.2 Bridge envelope

<sup>10</sup> <https://www.caee.utexas.edu/prof/maidment/StreamflowII/ReferenceDocs/0-7095-TM5B-Final.pdf>

<sup>11</sup> <https://github.com/NOAA-OWP/inundation-mapping>

## 4.2. Inputs for TX-Bridge

---

Initially, when TX-Bridge workflows were created, they were heavily dependent on external web services, including connections to the following remotely hosted data repositories:

- (1) Cloud optimized point clouds (entwine) - <https://raw.githubusercontent.com/hobu/usgs-LiDAR/master/boundaries/boundaries.topojson> leading to Amazon Web Services (AWS) repositories like [https://s3-us-west-2.amazonaws.com/usgs-LiDAR-public/TX\\_Pecos\\_Dallas\\_B3\\_2018/ept.json](https://s3-us-west-2.amazonaws.com/usgs-LiDAR-public/TX_Pecos_Dallas_B3_2018/ept.json)
- (2) OpenStreetMap Roadway Linework - <https://www.openstreetmap.org/>
- (3) USGS 'Bare Earth' digital elevation models (DEM) - <https://elevation.nationalmap.gov/arcgis/services/3DEPElevation/ImageServer/WCSServer?request=GetCapabilities&service=WCS>
- (4) National Hydrography Dataset (NHD) Flowlines - <https://hydro.nationalmap.gov/arcgis/rest/services/nhd/MapServer/6>
- (5) National Water Model Hydrofabric Lines - [https://maps.water.noaa.gov/server/rest/services/reference/static\\_nwm\\_flowlines/FeatureServer](https://maps.water.noaa.gov/server/rest/services/reference/static_nwm_flowlines/FeatureServer)

Furthermore, apart from these remote datasets, the following locally stored input data were also required:

- (6) National bridge inventory points (shapefile) with attributed bridge deck thickness
- (7) Vector stream linework (geopackage) of hydrofabric derived from 3-meter resolution Fathom terrain – statewide for Texas
- (8) Tabular synthetic rating curves derived from 'height above nearest drainage' (HAND) hydraulic calculations for each streamline in the hydrofabric derived from Fathom 3-meter terrain.

Alongside the remote repositories and local files, the user utilizing the TX-Bridge code had to define an area of interest polygon and specify the classification for the desired point cloud containing 'bridge' points. However, this workflow had certain limitations. Firstly, if any of the remote repositories were unavailable, it would hinder the extraction of bridge geometry. Secondly, since this workflow heavily relied on internet connectivity, it couldn't be expanded to leverage high-

performance computing (HPC) node clusters, like the ones accessible at the Texas Advanced Computing Center (TACC).

#### 4.2.1. Statewide input staging for high-performance computing (HPC)

In order to execute the bridge data extraction process on the University of Texas' node cluster located at the Texas Advanced Computing Center (TACC), the initial step involved creating and preparing statewide datasets to replace the reliance on third-party remote services. These datasets can be obtained for download from the following link: <https://web.corral.tacc.utexas.edu/nfiedata/acarter/tx-bridge-global-input-20231027/> .

**texas osm transport dissolve ln 4326.gpkg** – 917 Mb – Geopackage representing a simplified geometry of the vehicular roads and railroads throughout the state of Texas, pulled from OpenStreetMaps in August of 2023.

- 1) **nhd h texas state flowline 4269.gpkg** – 2.9 Gb – Geopackage representing high resolution national hydrography stream centerlines in the state of Texas.
- 2) **nwm flows.gpkg** - 1.8 Gb – Geopackage of National Water Model flowlines for the entire continental United States (CONUS) as of August 2023
- 3) **nwm v20 recurrence flows.nc** - 831 Mb - NetCDF file of National Water Model recurrence interval flows for all reaches in CONUS. Version 2.0.
- 4) **nbi bridges texas 4326.shp** – 205 Mb – Shapefile (cpg, dbf, prj, shp, shx) of the National Bridge Inventory (NBI) points within the state of Texas.
- 5) **demDerived reaches split filtered addedAttributes crosswalked.gpkg** – 3.0 Gb – Geopackage that contains the stream centerlines of the hydrofabric derived from the Fathom 3-meter terrain.
- 6) **hydroTable rp bf lmtdischarge cda.parquet** – 1.0 Gb – Parquet (tabular data) that has the hydraulic calculations from the HAND analysis of the Fathom 3-meter hydrofabric. This contains the synthetic rating curve for each reach.

To extract bridge data from all regions in Texas, these datasets were employed.

The TX-Bridge code underwent modifications to necessitate a global configuration file, Figure 4.3, which both specifies the input file path and defines default variable values. An illustrative sample file, named `config_global.ini`, is accessible at the following link:

[https://web.corral.tacc.utexas.edu/nfiedata/acarter/tx-bridge-global-input-20231027/global\\_config/](https://web.corral.tacc.utexas.edu/nfiedata/acarter/tx-bridge-global-input-20231027/global_config/).

```
# -----
[global_input_files]
# these are the input files that are global for the entire area (like state of Texas)

# OpenStreetMap linework (roads and railroads simplified)
str_osm_gpkg = /work2/08140/acarter/stampede2/tx_bridge_20230901/global_input/texas_osm_transport_dissolve_ln_4326.gpkg

# national hydrography dataset streams
str_nhd_stream_gpkg = /work2/08140/acarter/stampede2/tx_bridge_20230901/global_input/nhd_h_texas_state_flowline_4269.gpkg

# national water model flowlines
str_nwm_flowlines_gpkg = /work2/08140/acarter/stampede2/tx_bridge_20230901/global_input/nwm_flows.gpkg

#national water model lookup table
str_nwm_lookup_netcdf = /work2/08140/acarter/stampede2/tx_bridge_20230901/global_input/nwm_v20_recurrence_flows.nc

# national bridge inventory points with bridge thickness field
str_texas_nbi_filepath = /work2/08140/acarter/stampede2/tx_bridge_20230901/global_input/nbi_bridges_texas_4326.shp

# stream segments used to determine synthetic rating curves
str_hand_stream_ln_gpkg = /work2/08140/acarter/stampede2/tx_bridge_20230901/global_input/demDerived_reaches_split_filtered_addedAttributes_crosswalked.gpkg

# parquet tabular data of the synthetic rating curves
str_hydro_table_parquet = /work2/08140/acarter/stampede2/tx_bridge_20230901/global_input/hydroTable_rp_bf_lmtdischarge_cda.parquet

# field name of the stream segment
str_segment_field_name = HydroID

# kml marker images
str_marker_green_filepath = /work2/08140/acarter/stampede2/tx_bridge_20230901/global_input/marker_green_64.png
str_marker_red_filepath = /work2/08140/acarter/stampede2/tx_bridge_20230901/global_input/marker_red_64.png
str_marker_yellow_filepath = /work2/08140/acarter/stampede2/tx_bridge_20230901/global_input/marker_yellow_64.png
str_marker_white_filepath = /work2/08140/acarter/stampede2/tx_bridge_20230901/global_input/marker_white_64.png
str_marker_purple_filepath = /work2/08140/acarter/stampede2/tx_bridge_20230901/global_input/marker_purple_64.png
# -----
# .....
# [01_points_by_class]

# distance to buffer the input polygon (meters)
int_buffer = 300

# height and width of las tile (meters)
int_tile = 3000

# requested point cloud tile overlap (meters)
int_overlap = 50
# .....
# .....
# [02_polygonize_clusters]

# DBSCAN - distance from point to be in neighborhood in centimeters
flt_epsilon = 250
```

Figure 4.3 Sample excerpt from the TX-Bridge “global configuration” INI file

## 4.2.2. Elevation Dataset Staging

As of August 14, 2023, a survey of the Texas Water Development Board's (TWDB) servers revealed the presence of seventy-six (76) distinct LiDAR datasets covering the entire state of Texas, acquired between 2001 and 2022 (Figure 4.4). The TWDB generously granted permission for both the LiDAR point clouds and bare earth DEMs from all these collections to be duplicated and organized on the Texas Advanced Computing Center's (TACC) file system. These collections exhibit both spatial and temporal overlap, such as the University of Texas' campus in Austin, which possesses LiDAR data from 2003, 2007, 2012, 2017, and 2021.

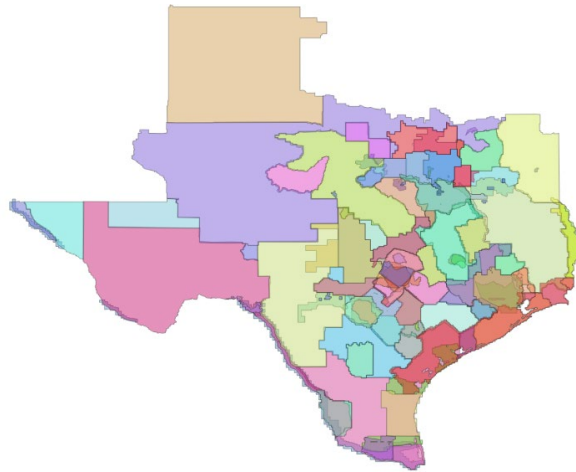


*Figure 4.4 LiDAR Collections provided by TxGIO (Aug 14, 2023)*

From these overlapping spatial datasets, it was essential to establish coverage that reflects the best combination of both temporal and spatial aspects. We refer to this coverage as ‘best-in-time-and-space’. This entails defining a polygon that represents the most recent LiDAR data available for a specific region. For instance, in the Austin metropolitan area, the most recent data stems from the "Bexar & Travis Counties LiDAR," which was acquired in March of 2021.

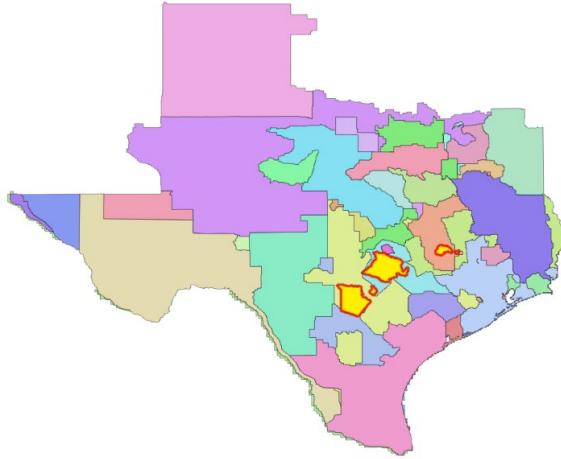


Figure 4.5 LiDAR Collections-“Best-in-time-and-space” (Aug 14, 2023)

From this geospatial process, it was determined that most recent LiDAR data collections is composed of thirty-six (36) different collections as shown in Figure 4.5.

#### 4.2.2.1. Cloud Optimized Point Clouds for Bridges

According to the information provided in Technical Memorandum 5B, "Evaluate Streamflow Measurement at TxDOT Bridges" (dated 03/31/2023 and revised on 04/10/2023), section 2.5, each of the "best-in-time-and-space" collections requires a single Cloud Optimized Point Cloud (COPC) that exclusively represents the 'bridge' classified points. These COPC files are accessible at the following link: <https://web.corral.tacc.utexas.edu/nfiedata/acarter/tx-bridge-copc-20231027/> . These files are organized numerically in descending order, with sizes ranging from 294 Mb to 30 Kb.

For instance, the file named "001\_bridge\_merge.copc.laz" encompasses the bridge data within the 'Ellis, Hill, Johnson, & Navarro Counties LiDAR' collection, acquired in January of 2022, covering the region south of the Dallas-Fort Worth metroplex, Figure 4.6.

Because these COPC files are compatible with cloud-based systems, they can be easily incorporated and visualized through a URI link, such as [https://web.corral.tacc.utexas.edu/nfiedata/acarter/tx-bridge-copc-20231027/001\\_bridge\\_merge.copc.laz](https://web.corral.tacc.utexas.edu/nfiedata/acarter/tx-bridge-copc-20231027/001_bridge_merge.copc.laz) , using geographic information systems like QGIS.

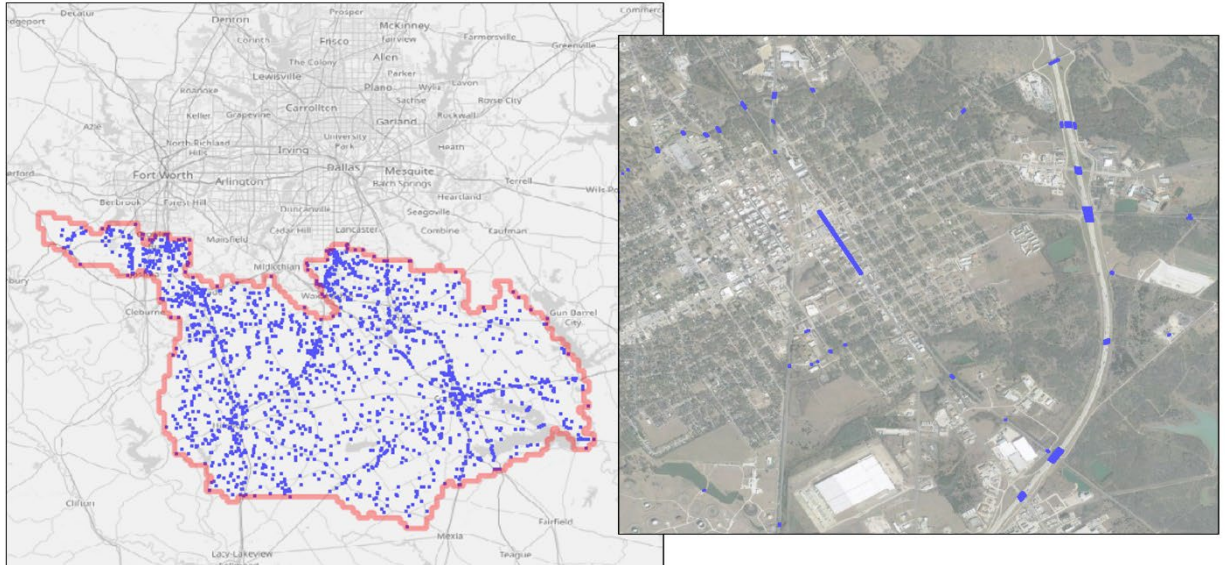


Figure 4.6 "001\_bridge\_merge.copc.laz" representing the bridges within the 'Ellis, Hill, Johnson, & Navarro Counties LiDAR'

#### 4.2.2.2. Digital Elevation Model R-Tree Indexing

DEMs are digital representations of the elevation or topography of the terrain. In this case, they are used to model the ground below a bridge deck and the elevation of the roads leading to the bridge's abutments. To analyze and understand the cross-section of each bridge accurately, the DEM tiles need to be organized in a way that allows for easy and efficient extraction of relevant ground data for a specific bridge area.

The DEM datasets are quite large. Dealing with such large datasets requires an efficient solution that avoids replicating or translating the base geotiff data provided by the Texas Water Development Board (TWDB). The chosen solution for TX-Bridge involves the use of a "Rectangular R-Tree" index. An R-Tree is a data structure commonly used for spatial indexing, which means it organizes spatial data in a way that makes it more efficient to search for specific geographic regions.

This R-Tree index serves as a way to catalog all the geotiff DEMs in each TWDB collection. It stores information about the spatial footprint of each tile and the source location path, which is the file path or reference to where the geotiff DEM data is stored. Though much smaller and quicker, an R-Tree is like a polygon index shapefile that stores both the spatial footprint and source location path for each tile, Figure 4.7.

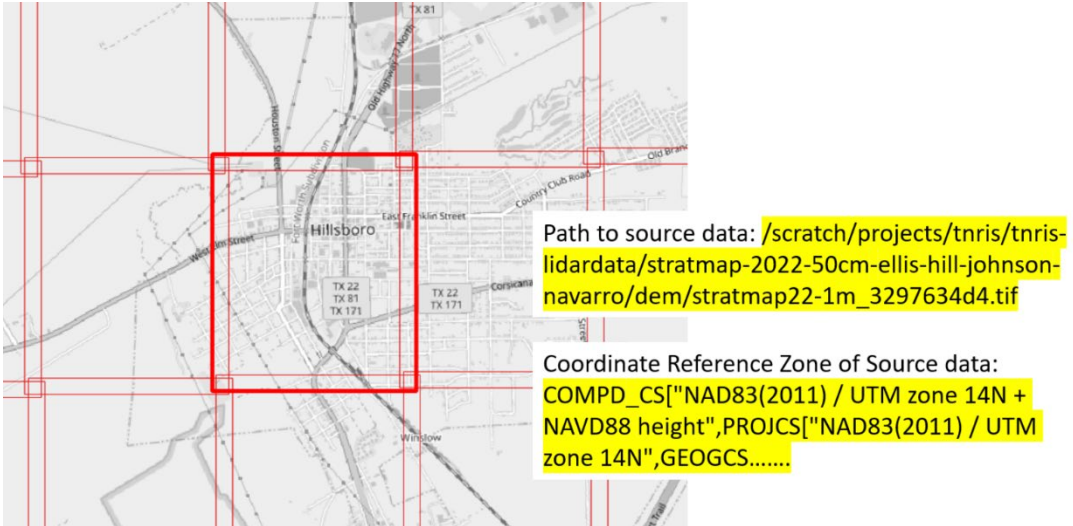


Figure 4.7 Graphical representation of “R-Tree” index and properties for a portion of the ‘Ellis, Hill, Johnson, & Navarro Counties’ collection

#### 4.2.2.3. Elevation Data Staging Scripts

As described in earlier sections, preparing the terrain data for automated extraction using TX-Bridge involved two key steps: (1) creating a Cloud Optimized Point Cloud (COPC) containing points classified as 'bridge,' and (2) generating an "R-Tree" index from a collection of geotiff DEM tiles. Python scripts for executing these tasks can be found at this link:

[https://github.com/andycarter-pe/tx-bridge/tree/hpc\\_run/src/input\\_staging](https://github.com/andycarter-pe/tx-bridge/tree/hpc_run/src/input_staging) .

Workflow to create COPC of bridge points from directory of point cloud LAZ files:

- 1) **01 extract point class from laz directory.py** -- Given an input directory of laz point cloud files, extract and save corresponding bridge deck classification points (las) for each tile
- 2) **02 reproject las directory.py** -- Reproject all LAS files in a given directory to a user supplied coordinate reference system
- 3) Merge the directory of reprojected LAS files into a single LAZ file. This is accomplished using the lasmerge command in the ‘lastools’.. This utilized the pointscene/lastools Docker container:  
<https://hub.docker.com/r/pointscene/lastools>
- 4) **04 convert laz to copc.py** -- convert a single laz to a cloud optimized point cloud

Workflow to create “R-Tree” index of directory of digital elevation models:

- 1) **05 create rtree from dem dir.py** -- Given a directory of geotiffs, create an R-Tree index that contains the limits and the file path to the DEMs. Then create a similar R-Tree that is projected to a desired coordinate reference system (CRS), but retains the file path and CRS of the original DEMs a data in the reprojected R-tree

### 4.2.3. Running TX-Bridge on a High-Performance Computer

TX-Bridge is designed to extract bridge cross-section information from classified LiDAR point clouds. This process involves analyzing large datasets of LiDAR point clouds and other related geospatial data to identify and extract bridge-related information. To perform this extraction across the entire state of Texas, the project requires terabytes of input data. This data includes LiDAR point clouds, digital elevation tiles, and various input vector datasets.

The extraction process is computationally intensive, and this is where high-performance computing (HPC) comes into play. High-performance computing, often referred to as supercomputing, is used to distribute the computational load across multiple nodes. Each node can be thought of as an independent computer with its own processor and RAM. This approach allows for parallel processing, which is essential for handling the massive datasets efficiently.

The TX-Bridge Python algorithms are specifically written to take advantage of multiple cores on each node. In parallel processing, tasks are divided into smaller subtasks that can be processed simultaneously by multiple cores, significantly speeding up the analysis.

#### 4.2.3.1. Computation Packaging

In the effort to extract bridge data across the entire state of Texas, requests were divided into smaller subtasks, which were then concurrently dispatched to multiple nodes within the High-Performance Computing (HPC) system. These subtasks were bundled to encompass a specific "best-in-time-and-space" LiDAR collection within a corresponding Hydrologic Unit Code 8 (HUC-8) watershed boundary. For instance, consider the Lampasas HUC-8 watershed (12070203), which intersects with six distinct "best-in-time-and-space" collection polygons. Each individual computational request entailed identifying and locating all bridges within one of these collections for the specified HUC-8 boundary.

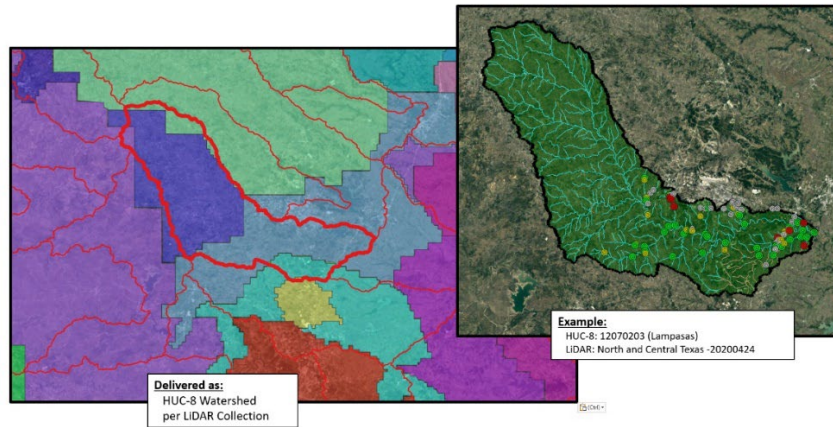


Figure 4.8 Computation Packaging – HUC-8 12070203 for 'North and Central Texas' Collection

Every "computation package" necessitates a JavaScript Object Notation (JSON) file, which outlines the particular resources essential for executing the desired computation. Within the workflow, this is referred to as a 'local input configuration' file. This configuration file generally comprises the following components:

- 1) An 'area-of-interest' polygon – such as a HUC-8 boundary
- 2) A path to write the output from TX-Bridge
- 3) Location of the R-Tree index for a given digital elevation model (DEM) repository
- 4) Path to cloud optimized point cloud of identified bridge points.

Some additional metadata describing these parameters is also required for documentation during the execution of TX-Bridge (Figure 4.9).

```
{
  "str_aoi_shp_filepath": "/work2/08140/acarter/stampede2/tx_bridge_20230901/aoi_huc_8_stateplane/input_huc_12040202_ar_2278.gpkg",
  "str_aoi_name": "run_400_HUC_12040202_collection_018",
  "str_output_folder": "/work2/08140/acarter/stampede2/tx_bridge_20230913/output/400_12040202_018",
  "b_is_feet": true,
  "str_cog_dem_path": "/work2/08140/acarter/stampede2/tx_bridge_20230901/rtree/018/rtree_file_3857",
  "copc_point_cloud": {
    "copc_name": "upper_coast",
    "copc_date": 20180322,
    "copc_short_name": "018",
    "copc_filepath": "/work2/08140/acarter/stampede2/tx_bridge_20230901/bridge_copc/018_bridge_merge.copc.laz",
    "copc_class": 17
  }
}
```

Figure 4.9 Example of 'Local Input Configuration' JSON for TX-Bridge

#### 4.2.3.2. TX-Bridge Containerization

A Docker container serves as an isolated environment that packages not only an operating system but also the specific application code required for its execution. It empowers the bundling of Python code, or any other application code, together with all essential dependencies, libraries, and the underlying operating system into a single cohesive entity. This containerization guarantees the uniform execution

of Python code across diverse environments and streamlines the deployment and scalability of software applications.

To ensure consistent execution on both personal computers and high-performance computing systems (HPCs), the TX-Bridge code was deployed within a Docker container. This container encompasses the entirety of the TX-Bridge code, which can be accessed at [https://github.com/andycarter-pe/tx-bridge/tree/hpc\\_run/src](https://github.com/andycarter-pe/tx-bridge/tree/hpc_run/src) . It is constructed upon a Linux version 11 / Debian operating system foundation. This Docker container is located at <https://hub.docker.com/r/civileng127/tx-bridge>

#### 4.2.3.3. TX-Bridge Execution

Once the input data has been properly prepared, the paths to the statewide datasets are specified within the "global configuration" INI file, while parameters unique to a particular run are outlined in the "local input configuration" JSON file. To initiate the TX-Bridge process, deploy the 'TX-Bridge' Docker container and execute the subsequent Python command:

```
python /tx-bridge/src/tx_bridge_local.py -i  
path/to/config_global.ini -g path/to/local/config.json
```

#### 4.2.4. TX-Bridge Output

An example of output generated from TX-Bridge is provided at [https://web.corral.tacc.utexas.edu/nfiedata/acarter/tx-bridge-sample-output/400\\_12040202\\_018/](https://web.corral.tacc.utexas.edu/nfiedata/acarter/tx-bridge-sample-output/400_12040202_018/)

Each successfully executed TX-Bridge run will generate nine (9) output folders. These folders are:

- 00 input shapefile** – Shapefile of the requested area of interest
- 01 las from copc** – The cloud optimized point cloud is cut into processing tiles for extracting bridge deck information
- 02 shapefile of hulls** – Bridge deck points are clustered into polygonal areas noted as “hulls”. This folder contains a polygon shapefile of these ‘hulls’
- 03 osm trans lines** – OpenStreetMap transportation line shapefile roughly within the limits of the area-of-interest.
- 04 major axis lines** – Shapefile of the ‘major-axis-line’ denoting where the cross section of the bridge was cut
- 05 bridge deck dems** – Raster representations DEMs of the bridge deck within each ‘bridge hull’ polygon. Note that the number of this file is from the index of the ‘bridge hull’ shapefile in folder 02.
- 06 flipped major axis**– Intermediate calculation to flip a bridge to be ‘left-to-right’ looking downstream where a bridge crosses a stream.

**07 major axis names**– Intermediate calculation where the cut line from folder 04 is assigned a name from the OpenStreetMap layers.

**08 cross sections** – This folder represents the ultimate output from TX-Bridge. The bridges in a requested area for a given collection are located in the ‘08\_08\_mjr\_axis\_xs\_w\_feature\_id\_nbi\_low\_hull\_rating.geojson’ file. These files match the taxonomy of bridge attributes described in Section 2.9 and Appendix A of Technical Memorandum 5B, Evaluate Streamflow Measurement at TxDOT Bridges (dated 03/31/2023 and revised on 04/10/2023).

Folder 08 also contains a KMZ file most of the computed data for this run can be reviewed in Google Earth. A sample file is located at:

[https://web.corral.tacc.utexas.edu/nfiedata/acarter/tx-bridge-sample-output/400\\_12040202\\_018/08\\_cross\\_sections/run\\_400\\_HUC\\_12040202\\_collecti on\\_018\\_018\\_20230914.kmz](https://web.corral.tacc.utexas.edu/nfiedata/acarter/tx-bridge-sample-output/400_12040202_018/08_cross_sections/run_400_HUC_12040202_collecti on_018_018_20230914.kmz)

The KMZ file shown in Figure 4.10 illustrates the area-of-interest limits of the request. The national water model and Fathom 3m hydrofabrics are also provided. Each bridge that was extracted is represented as a point.

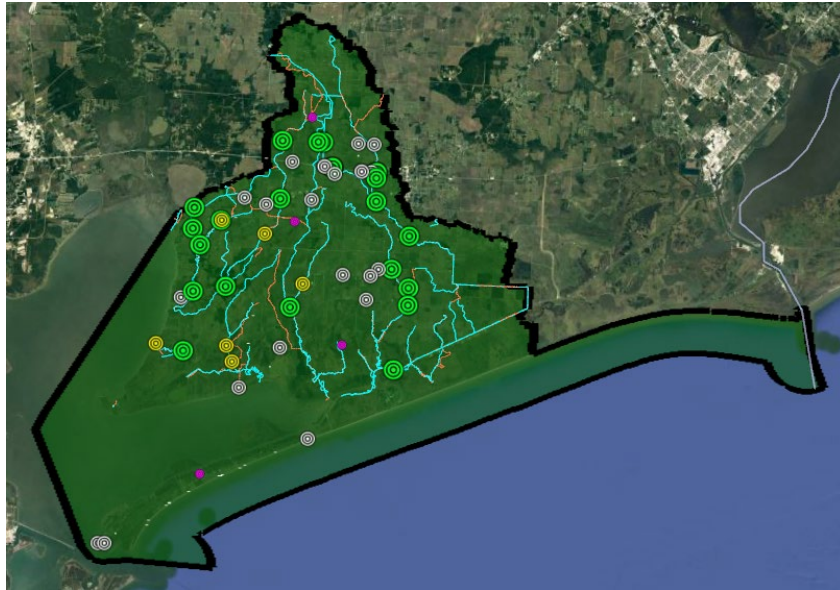


*Figure 4.10 Sample KMZ of Tx-Bridge Output*

Zooming into a point, reveals the ‘bridge hull’ and ‘major axis line’ for that bridge (Figure 4.11)

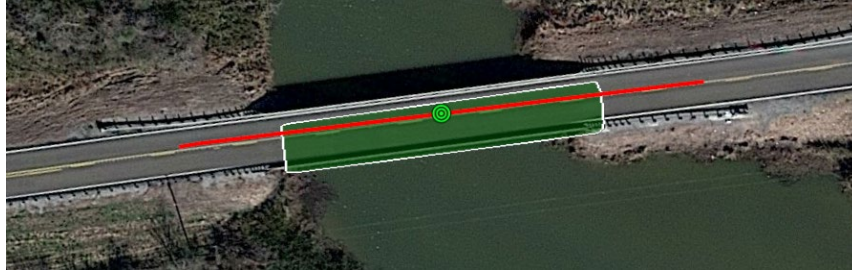


Figure 4.11 Major Axis Line and Bridge Hull for Bridge

Clicking on a point bridge point reveals the extracted cross section for that given bridge (Figure 4.12)

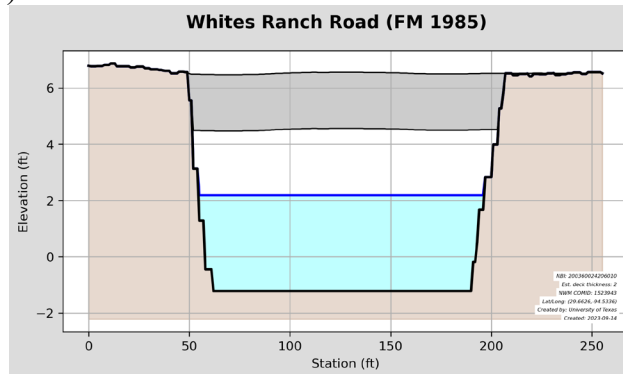


Figure 4.12 Extracted bridge Cross Section.

#### 4.2.5. Statewide Database – TX-Bridge

Using the High-Performance Computing (HPC) resources provided by the Texas Advanced Computing Center (TACC), a total of 495 jobs, each involving a specific LiDAR collection within a particular HUC-8 watershed, were submitted. The geospatial bridge data generated for these executed jobs, formatted as GeoJSON files, were consolidated into a unified database (Figure 4.13). This comprehensive database encompasses a total of 37,488 extracted bridges. With a size of approximately 497 megabytes (MB), the database can be accessed at the following link: <https://web.corral.tacc.utexas.edu/nfiedata/acarter/tx-bridge-db-20230919/>.

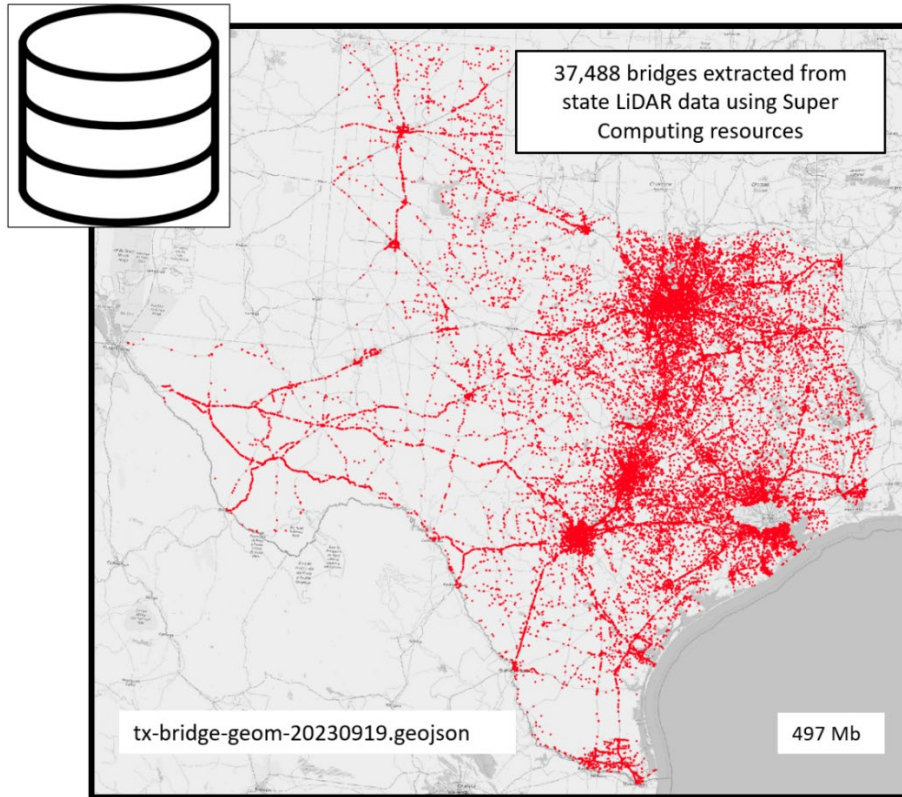


Figure 4.13 TX-Bridge Statewide database (2023.09.19)

As of the time of writing of this report, there are a few areas where data could not be processed:

- 1) The Jack and Archer Counties LiDAR, acquired in January of 2015, does not have any points classified as 'bridge'
- 2) The 'Upper Clear Fork Brazos River' LiDAR around the Abilene has errors in the LiDAR data that need to be reconciled to complete processing.
- 3) The 'Upper Coast LiDAR' over the urban core of Houston has a level of complexity that is difficult for the current TX-Bridge routines to process.

Besides the processing challenges mentioned above, it's important to highlight that the TX-Bridge routines do not address intricate interchange areas. In the database, an attribute called 'bad\_hull' has been introduced to signal instances where geometric complexity was encountered and possibly left unaddressed. A value of 1 (True) in this attribute suggests that additional investigation may be warranted. Approximately 1.6% (616 out of 37,488) of the bridges are marked with this value.

## 4.2.6. Flood Forecaster for TX-Bridge

Through the National Water Model (NWM), the National Water Center computes and broadcasts the predicted flow rates from over 2.7 million stream segments with the continental United States (CONUS). If a bridge extracted by TX-Bridge crosses over one of the NWM streams, then it is possible to determine the predictive water surface elevation at each one of these bridge crossings.

### 4.2.6.1. NOMADS Forecast Server

The NOMADS server, an acronym for the National Oceanic and Atmospheric Administration Operational Model Archive and Distribution System, is an online platform offered by the NOAA (National Oceanic and Atmospheric Administration). It serves as a repository for a wide range of weather and climate model data. You can access data from the National Water Model for the past few days at a URL like this:

<https://nomads.ncep.noaa.gov/pub/data/nccf/com/nwm/v3.0/> Inside this directory, the NWM provides 'short-range' data, which includes forecasts for the upcoming eighteen (18) hours. An example link for this is: [https://nomads.ncep.noaa.gov/pub/data/nccf/com/nwm/v3.0/nwm.20231028/short\\_range/](https://nomads.ncep.noaa.gov/pub/data/nccf/com/nwm/v3.0/nwm.20231028/short_range/). It's important to note that the date in this link changes daily.

Inside the 'short\_range' folder, you'll find files with a structure like 'nwm.t11z.short\_range.channel\_rt.f001.conus.nc'. These files contain predictions for the flow rates of each of the 2.7 million stream reaches in the CONUS. Since this file was retrieved from the '20231028' folder, it specifically represents a prediction made at 11:00 UTC (Coordinated Universal Time). UTC is sometimes referred to as "Zulu time" in aviation and military contexts. The 'f001' designation indicates that this file represents the prediction for one (1) hour in the future, which corresponds to 12:00 UTC on October 10, 2023. The short-range forecast typically comprises eighteen different files numbered 'f001' to 'f018,' representing forecasts from +1 to +18 hours from the time when the forecast was published. NOMADS updates its forecasts, which include eighteen new forecasted hours, approximately every hour, as illustrated in Figure 4.14.

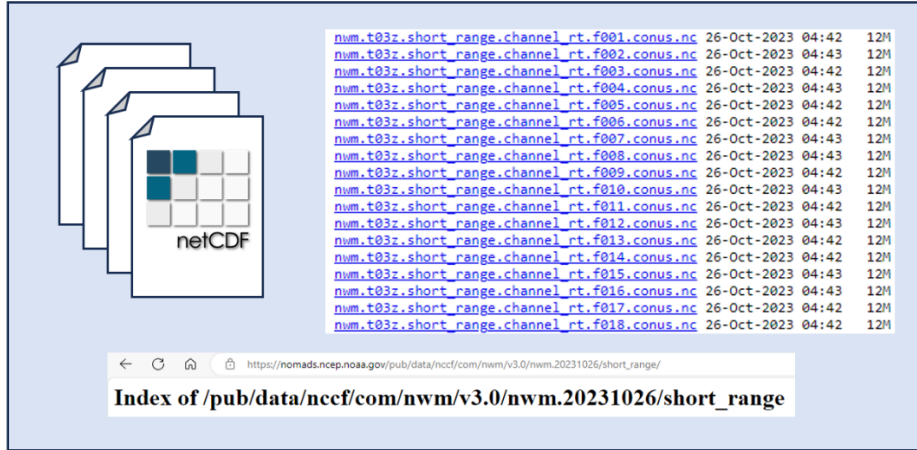


Figure 4.14 NOMADS 'channel\_rt' streamflow forecast files

To forecast the water surface elevations at thousands of points across the state of Texas, a service is required that harvests and compiles for all eighteen (18) forecasts on an hourly basis.

#### 4.2.6.2. TX-Bridge Flood Forecast Points

The database of TX-Bridges identified over 37,000 bridges. Some of these bridges are simply 'on-grade' bridges that are elevated to cross over another roadway. Others may be built over creeks but are not over streams that are ordained as reaches identified in the National Water Model. Intersecting the geometric bridge database with the National Water Model hydrofabric showed that approximately 19,010 (~50%) of the identified bridges were over a stream within the NWM, (Figure 4.15).

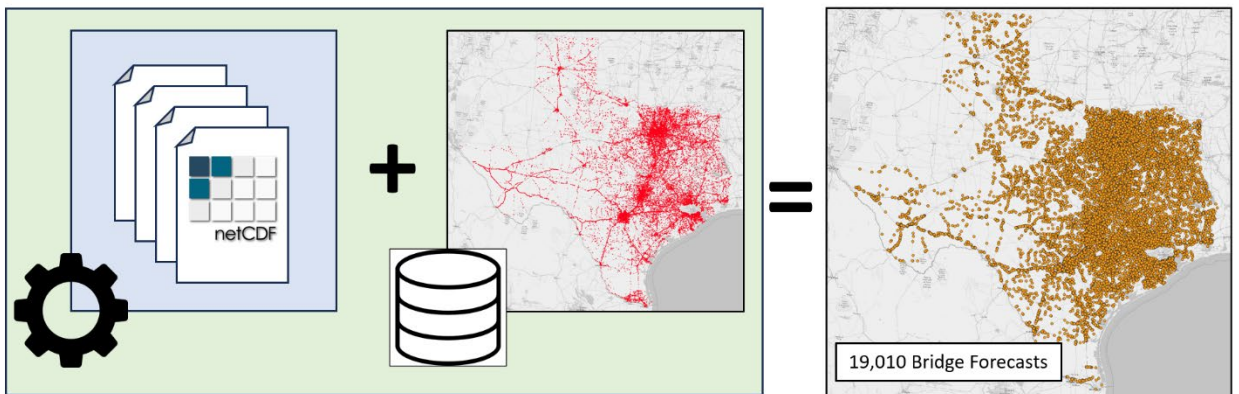


Figure 4.15 Bridge Forecast Points

Upon the release of a 'short-range' stream forecast by NOMADS, an automated computer service will generate a GeoJSON file containing data for the 19,010 bridges. It will then proceed to calculate the water depth, using the synthetic

rating curve specific to each bridge, for every hour within the eighteen-hour forecast.

#### 4.2.6.3. Flood Forecast Web Interface

By utilizing the dynamically refreshing GeoJSON forecast points, it is feasible to construct a web server capable of receiving and visualizing these data. A preliminary interactive map prototype was developed using Leaflet. In this interface, symbology was chosen to represent the distance, in feet, between the determined water surface elevation and the lowest chord of the respective bridge (Figure 4.16).

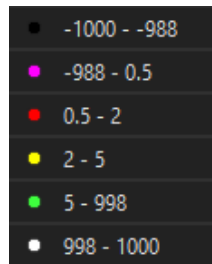


Figure 4.16 Forecast Point Color Coding

The forecast point coloring scheme is: (1) White points indicate no flow at the specified bridge location; (2) A black point signifies that the National Water Model is not providing a flow rate for the corresponding National Water Model reach; (3) A green point represents a predicted flow exceeding 5 feet from the bridge's lowest chord; (4) Yellow serves as the initial warning color, indicating water levels between 2 and 5 feet from the bridge's minimum low chord; (5) Red signifies a range of 0.5 to 2 feet from the bridge; (6) Finally, purple indicates that the predicted water surface elevation is at a minimum, potentially affecting the bridge's bearing pads or worse.

The interface shown in Figure 4.17 includes a time slider that enables users to alter the colorations indicating the forecast for hours +1 to +18. The forecast's issuance date is displayed as well. While the National Weather Service provides the forecast in UTC, it was decided to present it in a more user-friendly format, including local time, the day of the week, and a twelve-hour clock. Additionally, a checkbox was introduced to filter and display only bridges with a warning level of yellow or higher.

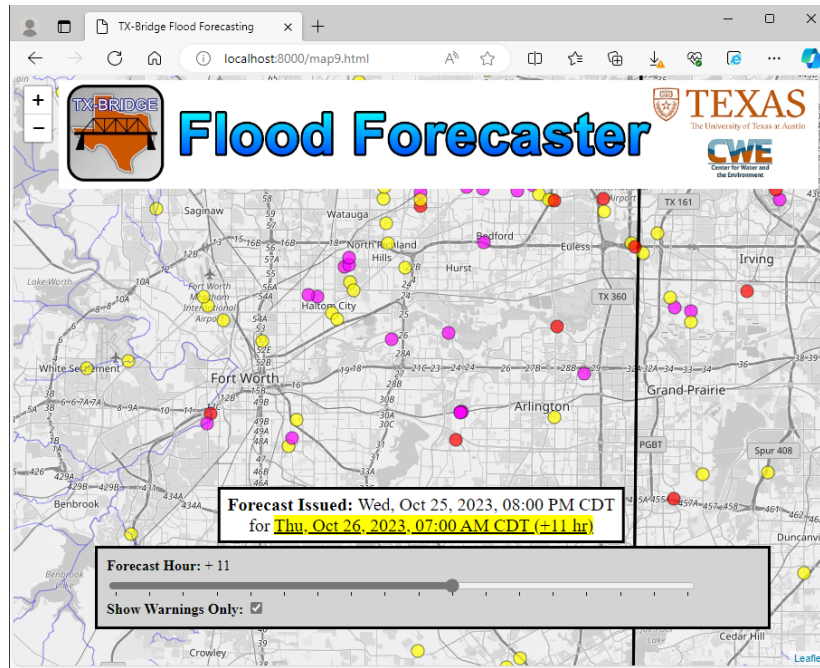


Figure 4.17 TX-Bridge Flood Forecasting Web Mock-up showing only warnings

#### 4.2.6.4. Bridge Cross Section Forecasting - Web Interface

Combining the NOMADS forecast with the TX-Bridge geometric database, it is possible to create a cross section of the bridge that shows (1) the anticipated warning level relative to the minimum low chord, (2) the projected water surface elevation and (3) the expected time of flooding (Figure 4.18).

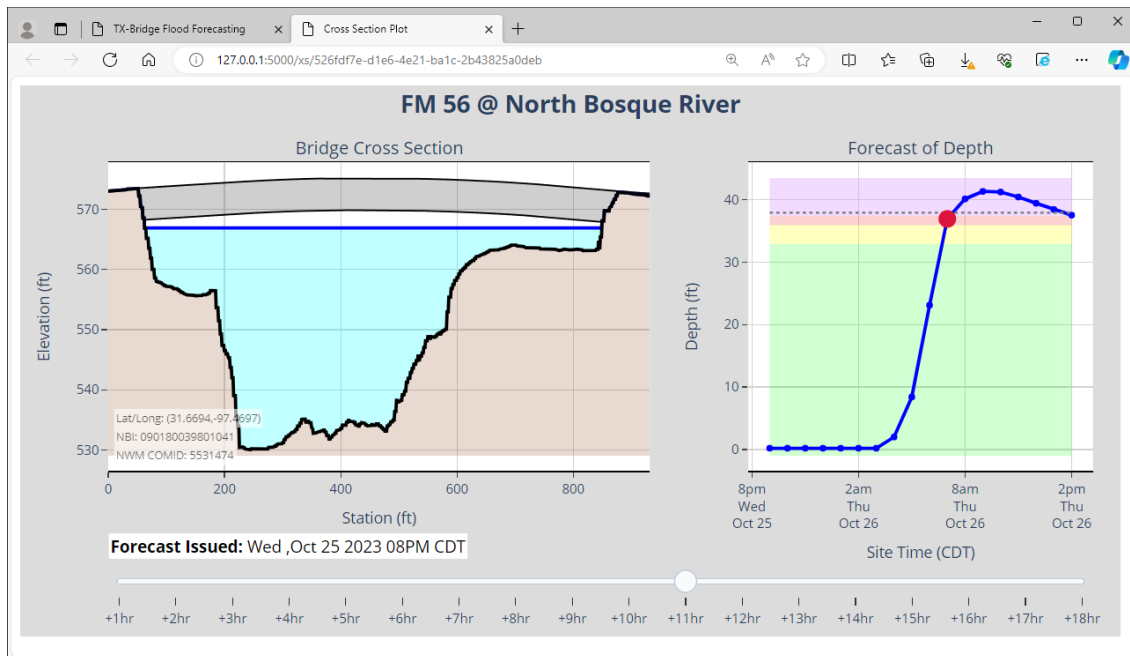


Figure 4.18 Realtime Cross Section Plot

#### 4.2.6.5. Flood Forecasting Interface

The forecasting point map and the cross-section plots both utilize the same input datasets and data streams. Through the inclusion of the ‘pop-up’ on each point, these services can be connected. Additionally, for context, each bridge forecast point can be linked to a ‘Google Street View’ link (Figure 4.19).

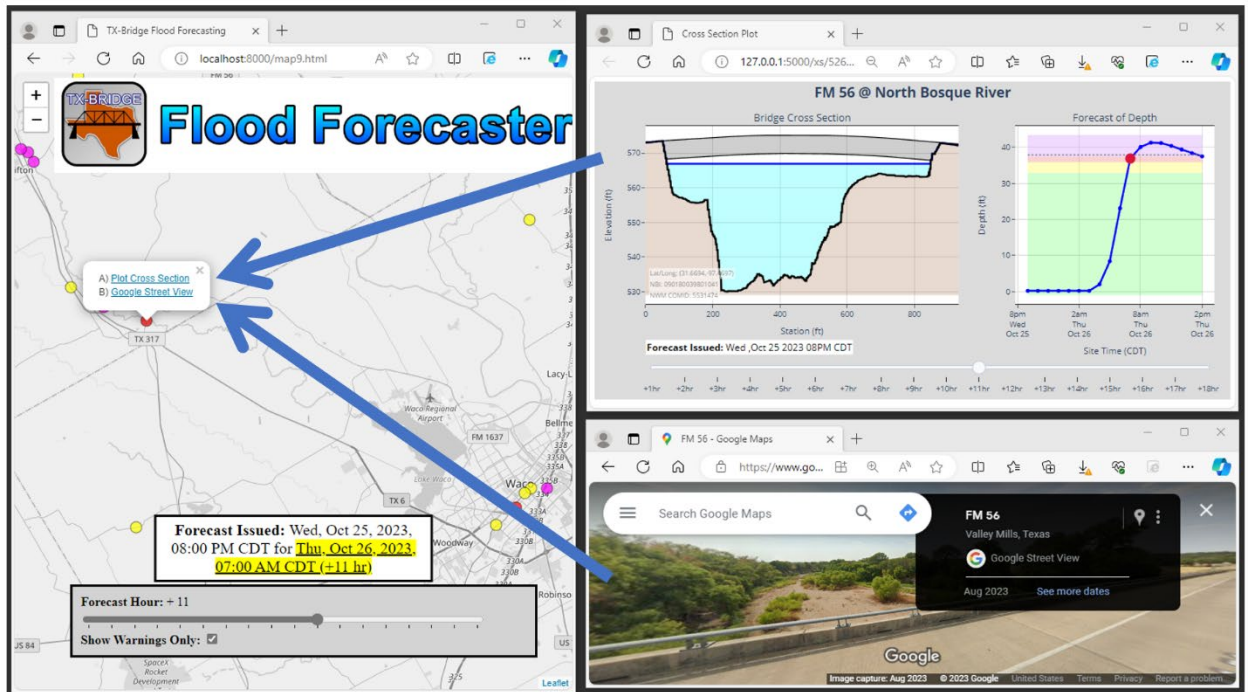


Figure 4.19 TX-Bridge Flood Forecaster Web Service

#### 4.2.6.6. Bridge Flood Forecasting Limitations

The current “TX-Bridge Flood Forecaster” is built to utilize flows broadcast from the National Water Model’s hydrologic simulations.

In the current configuration rating curves at each bridge were synthetically determined from “height above nearest drainage” (HAND) hydraulic calculations on the 3-meter resolution terrain produced by Fathom across the state of Texas. Flood Inundation Mapping version 3 (FIM 3) software and parameterization set by the NWS( <https://github.com/NOAA-OWP/inundation-mapping/tree/dev-fim3> ) were used to generate these rating curves.

Both the hydrologic and hydraulic approaches impact the accuracy of the predictions shown in the “TX-Bridge Flood Forecaster” service. Subsequent sections explore items that may contribute to the predictions’ inaccuracies.

The National Water Model's hydrologic forecasts are based on spatial and temporal forecasts of precipitation patterns. If rain falls with the wrong intensity or lands at the wrong location than what is predicted, then the forecasted flows will vary from what is actually experienced.

The hydrologic model within the National Water Model is notably less complex compared to the traditional hydrologic modeling techniques employed in studies like flood insurance mapping. The NWM approach employs basic routing schemes that frequently underestimate the attenuation and time delays within a river network. Furthermore, it encounters challenges in accurately incorporating the impact of storage in reservoirs and detention facilities. Preliminary assessments indicate that this results in an overestimation of runoff rates and leads to the occurrence of peak flows at an earlier time than expected.

In the FIM3 version of rating curve determinations, Manning's roughness in the Manning's equation is calculated based on the Strahler stream order. For instance, for headwater streams with a stream order of 1, the Manning's roughness value is set at 0.125. However, it is believed that within Texas rivers, this value may be an overestimation. Overestimating the Manning's roughness value can result in an overestimation of water depth for all flow conditions.

In the case of hydrofabric determined from Fathom 3m terrain data, some river segments exhibit flat or negative channel slopes. In such situations, the FIM3 code establishes a minimum slope, which is specific to that particular segment and does not consider the overall slope of the entire river. Consequently, the default slope can occasionally lead to an overestimation of flood depth as a function of discharge.

Rating curves are established HAND calculations without accounting for backwater effects. The presence of downstream bridges can impede flow and lead to an underestimated water surface elevation at a given discharge. Bridge rating curves are specific to their respective locations, and the tool does not account for backwater caused by larger rivers downstream, which might not be reflected in the TX-Bridge Flood Forecaster.

#### **4.2.6.7. Recommended Bridge Flooding Forecast Improvements**

Enhancing the stream gauge network through installation and densification would boost the precision of flood level predictions for bridges situated both upstream and downstream of the gauge. Moreover, synthetic rating curves derived from engineering-scale models could replace those determined using the HAND method, further augmenting the accuracy of flood forecasts at these bridges.

### 4.3. Bridge Warning Service in KISTERS Datasphere

The Bridge Warning Service is an infrastructure monitoring tool designed to enhance the safety and reliability of bridges in potential flood scenarios. By integrating diverse data sources, it provides accurate and timely warnings, enabling authorities to take necessary precautions.

A primary input for this system is the National Water Model (NWM) outputs obtained from the nomad forecast server. These outputs are essential for understanding water flow patterns and potential flood risks. To make this data actionable, the NWM outputs are converted into stage data. This conversion process utilizes synthetic rating curves, derived from 'height above nearest drainage' (HAND) hydraulic calculations. Each calculation corresponds to a streamline in the hydrofabric, which originates from the Fathom 3-meter terrain. This method ensures the accuracy and relevance of the stage data concerning the region's specific topographical and hydrological attributes.

Additionally, the system incorporates bridge inventory data from the TX-Bridge product. This data provides specifics on bridge geometry, emphasizing the bridge's lowest chord. Knowledge of the lowest chord is vital, as it indicates the height at which rising water levels could compromise the bridge's structural safety.

Upon processing these inputs, the Bridge Warning System produces five Web Map Service (WMS) layers. These layers are accessible without authentication, facilitating ease of access for stakeholders.

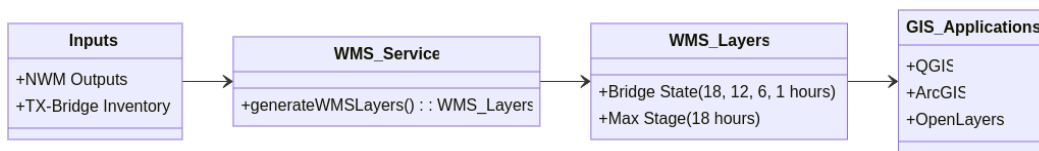


Figure 4.20: Flow diagram of the architecture of the WMS service

The following layers are available in the service:

- bridges-in-01-hrs
- bridges-in-06-hrs
- bridges-in-12-hrs
- bridges-in-18-hrs
- bridges-18hrs-max

The layers offer insights into the projected state of the bridge for the next 1, 6, 12, 18 hours. An additional layer provides data on the anticipated maximum stage over the next 18 hours.

The system's integration into a standardized WMS service is noteworthy. This service transforms the data into a format compatible with any Geographic Information System (GIS) application. The WMS service layer's primary advantage is its standardized interface, ensuring consistent data integration across various GIS platforms.

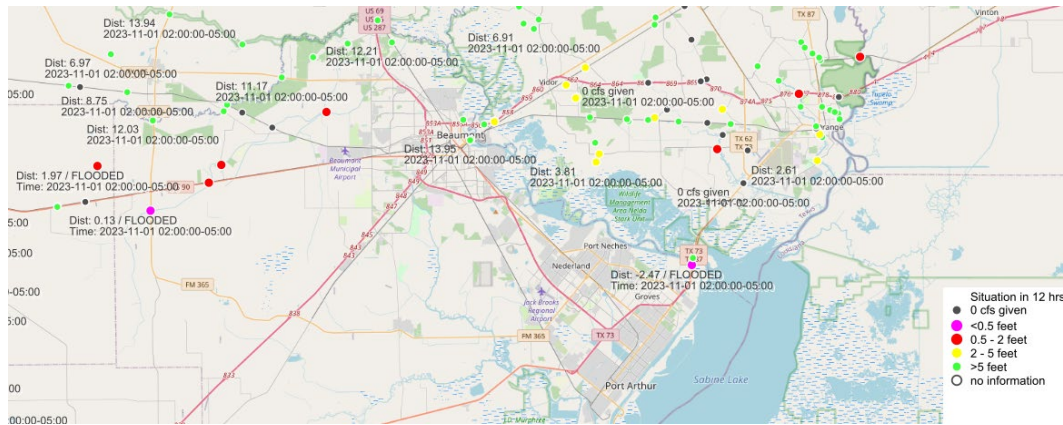


Figure 4.21: Bridge Warning WMS layers displayed in QGIS

The service operates on the KISTERS' Datasphere backend, in order to ensure high availability and scalability. The robust cloud-based backend guarantees that the Bridge Warning System remains reliable and can efficiently manage extensive data volumes and user requests.

The WMS service is available under the following URL, no authentication is required: <https://txdot.datasphere.online/bridges/mapserv?map=txdot-bridges>

# Chapter 5. Road Flooding

## 5.1. Introduction

---

There are two measures of road flooding in the FAST maps shown in Figure 3.1 – a flooded roads depth map, and a map of flood impact on the road transportation system in which the lengths of the various flooded road segments are summarized. This requires the capacity to measure road flooding at two spatial scales – at the scale of an individual street or road segment and at the scale of a watershed, Maintenance Section or TxDOT District.

A convenient way of thinking about the depth of road flooding is to use the relationship:

$$\text{Road Flood Depth} = \text{Water Surface Elevation} - \text{Road Surface Elevation}$$

This rather simple relationship requires two maps – a map of water surface elevation, and a map of road surface elevation. Maps of water surface elevation are standard outputs of hydraulic engineering flood models, such as HEC-RAS. For a long time, the research team was confronted with a very significant challenge – TxDOT has not up to this time recorded the elevation of its road and bridge assets.

The TxDOT Roadway Inventory, the standard GIS road coverage of Texas used at TxDOT is a set of line features joining point vertices which have coordinates (x,y,m) where (x,y) refers to the geographic location, and m refers to distance along the line measures as DFO – distance from the origin in miles. What is needed instead is a 3D GIS road coverage in (x,y,z), where z represents elevation above geodetic datum. A simple way to create such a 3D road coverage is to overlay the TxDOT Roadway Inventory on a digital elevation model. However, that approach has several disadvantages, most particularly that bare-earth digital elevation models have no bridges in them so the road lies along the stream bottom at each bridge location. Another solution was needed.

## 5.2. Road Elevation Model

---

The Ecopia corporation<sup>12</sup> of Toronto, Canada, specializes in the interpretation of aerial imagery into land cover classes using Artificial Intelligence. One of these land cover classes is roads. TxDOT RTI supported the purchase of the Ecopia roads coverage for the 11-county Austin District in an amendment to the original

---

<sup>12</sup> <https://www.ecopiatech.com/>

agreement for this research project. The Ecopia data consisted of road coverage polygons and centerlines for 37,879 miles of roads in the Austin District.

A Road Elevation Model for the TxDOT Austin District has been created using the Ecopia polygon and centerline data. These have been combined with the Texas LIDAR data collections at the Oak Ridge National Laboratory and a selection has been made of LIDAR points that lie on the road polygons. This collection of some 3.8 billion points covers 38,000 miles of the road system in the Austin District.

The 10,100 LIDAR tiles containing 1.5 TB of LIDAR data are illustrated in Figure 5.1. The end result after the selection of the most recent LIDAR points on the road surface was made was a set of LIDAR files, one for each Maintenance Section in the Austin District, collectively containing 19 GB of LIDAR data, which is 1.3% of the original volume of LIDAR data covering the whole Austin District. The Road Elevation Model thus created is a comprehensive and highly detailed description of the road surface elevation of the roadway system.

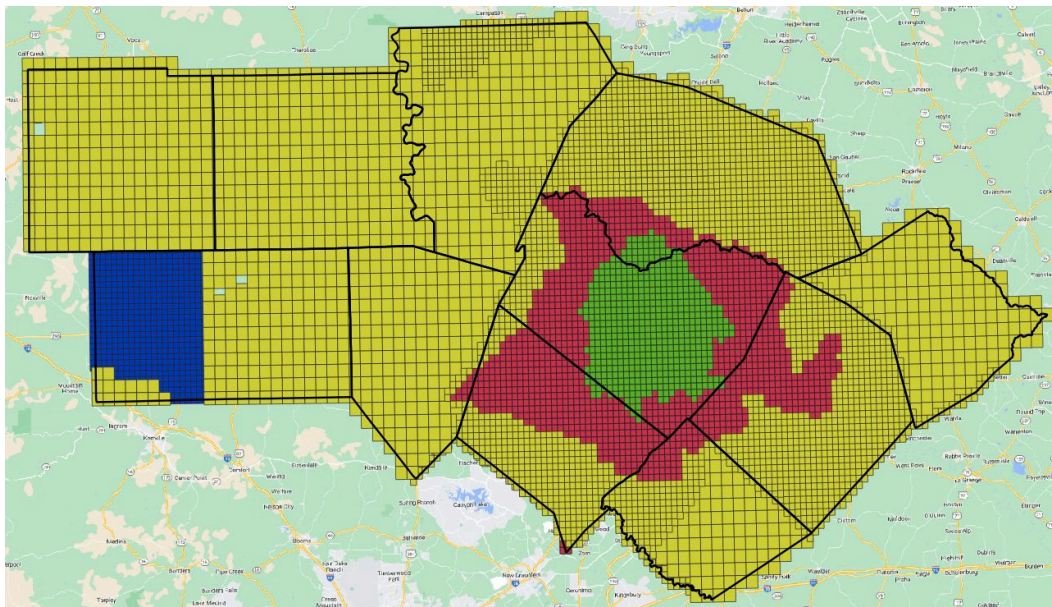


*Figure 5.1 LIDAR tiles covering the TxDOT Austin District*

The use of the Ecopia road coverage to act as the filter for extraction of LIDAR points involves a significant expense for the purchase of the Ecopia data. What freely available road line data could instead be used for this purpose? Two alternatives are examined here:

- TxDOT Roadway Inventory

- Open Street Maps

### 5.2.1. TxDOT Roadway Inventory

In the Austin District, the TxDOT Roadway Inventory shown in Figure 5.2 has a total length of 18,173 miles of roads, of which 3962 miles are On-System, meaning they are maintained by TxDOT, and the remainder are Off-System roads maintained by local cities and counties.

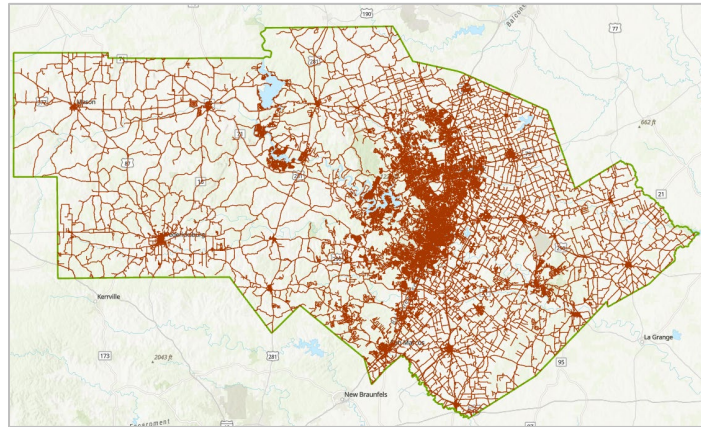


Figure 5.2. TxDOT Roadway Inventory roads for the Austin District (18,173 miles)

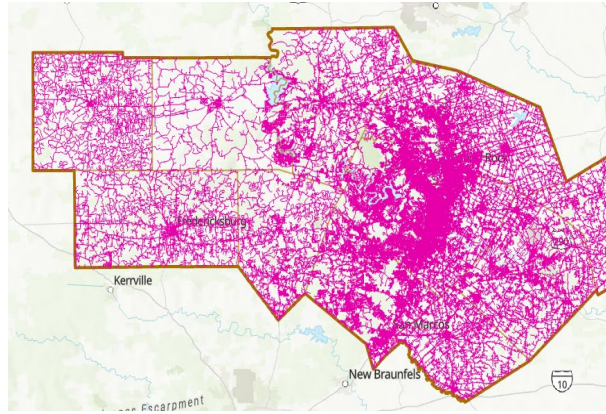
The TxDOT Roadway Inventory lines are of type Polyline (x,y,m), where m is the Distance from Origin measured in miles. This line geometry and a limited set of tabular attributes constitute the Texas part of ARNOLD (All Road Network of Linear Referenced Data) which is used by the states to report the condition of its road system to the Federal Highway Administration.

### 5.2.2. Open Street Map

Open Street Map is a line dataset in type Polyline (x,y) contributed by volunteers, which for the Austin District covers 41,095 miles of roads, as shown in Figure 5.3. However, many of these roads are classified as “service roads” for driveways and private road access. If the service roads are removed, the length of Open Street Map roads in the Austin District is 25,801 miles. From visual inspection of the Open Street Maps line coverage, it is evident that there is a discrepancy in the density of road coverage in Llano County, which has a less dense road coverage than for surrounding counties.



Open Street Map Service  
Roads highlighted in blue



Open Street Map roads in the Austin District

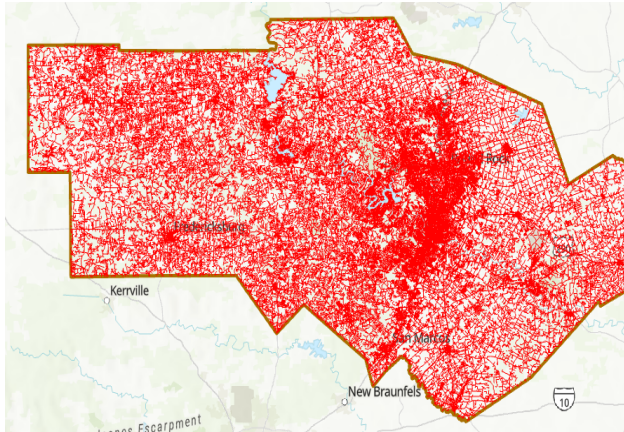
Figure 5.3. Open Street Map lines in the Austin District (41,095 miles)

### 5.2.3. Ecopia

The Ecopia line coverage has 37,879 miles of road coverage in the Austin District and it differs from the TxDOT Roadway Inventory and Open Street Map in providing both line and polygon coverage of the road system, as shown in Figure 5.4. These data are created by a commercial firm Ecopia<sup>13</sup> based in Toronto, Canada, using Artificial Intelligence analysis of Hexagon 6” aerial imagery into nearly 20 land cover classes (Figure 5.5), of which the road system is one land cover class (Figure 5.6).



Road centerlines and  
polygons in the Ecopia  
coverage



Ecopia roads in the Austin District

Figure 5.4. Ecopia road coverage of the Austin District (37,879 miles)

<sup>13</sup> <https://www.ecopiatech.com/>

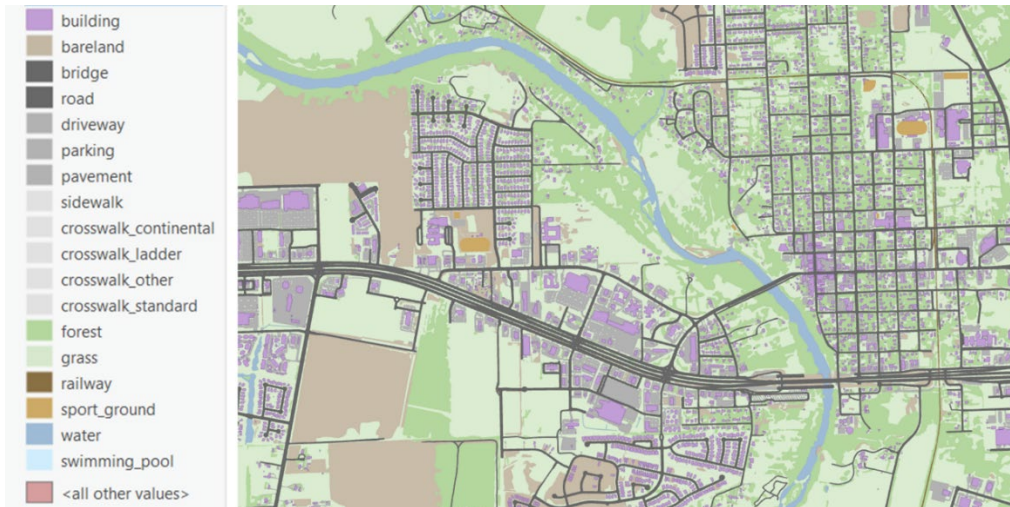


*Figure 5.5. Ecopia classification of land cover classes*



*Figure 5.6. Ecopia classification distinguishes the public road system from driveways, parking lots and buildings*

An early assessment of the validity of road width was made for 17 bridges in the Bastrop area to compare Ecopia road widths going over bridges with the NBI attribute width curb to curb, Figure 5.7 shows these widths are comparable with one another. Later, visual comparison of the Ecopia road polygons and Hexagon imagery confirmed that Ecopia road widths are consistent with aerial imagery.

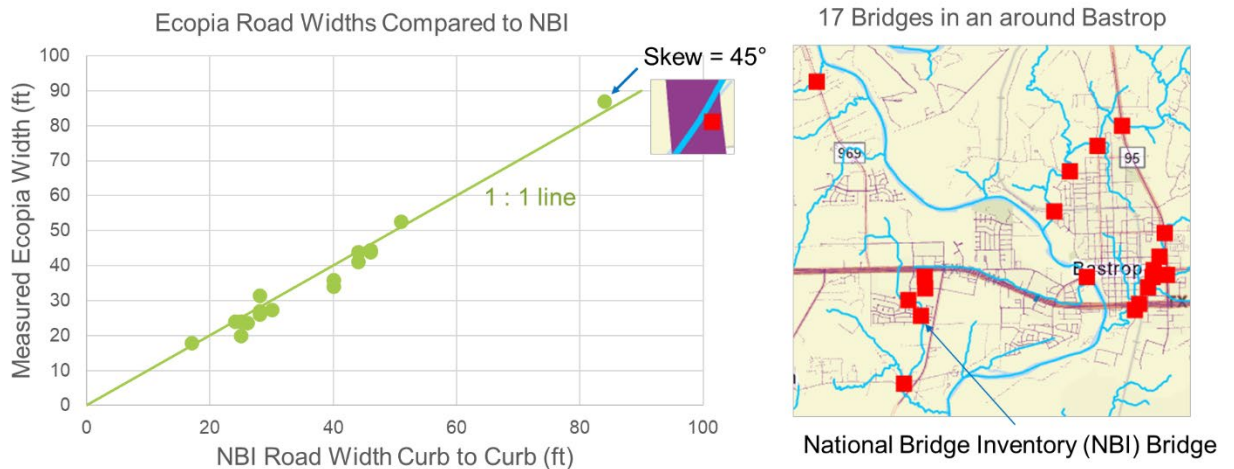


Figure 5.7. Comparison of NBI and Ecopia Road Widths

### 5.2.4. Other Alternatives

Over a period of about a year since May 2022 when the Ecopia coverage was first identified as a possible dataset for the Austin District, a search was made for other alternatives than the ones listed above. What distinguishes Ecopia from other companies such as Hexagon, EagleView, Nearmap and Vexcel working in large scale imagery is that Ecopia buys imagery from other companies and focuses on interpreting it, while the main focus of other imagery companies is on image acquisition.

One alternative is to use the ESRI Deep Learning Model for Road Extraction.<sup>14</sup> This is a pre-trained Artificial Intelligence routine that is applied to aerial images and extracts roads from them. When this alternative was examined, it turned out that while a set of pixels on the road surface are extracted, this covers only part of the roadway pavement, and the main goal of the Road Extraction Deep Learning model is to find the roadway centerline, not the extent of the pavement coverage. As shown in Figure 5.8, a disadvantage of this Deep Learning Model approach is that besides finding actual roads, it identifies linear bare areas in fields as roads, and significant clean-up work would be needed to eliminate these false road data. This shows that there is a significant advantage in classifying the land cover of the whole landscape, as Ecopia does, so that you have to say what everything is, rather than just what a road is.

<sup>14</sup> <https://www.arcgis.com/home/item.html?id=b3696a0118b340c6befb96932f67b29f>



Figure 5.8. Spurious road features in a field identified by the ESRI Road Extraction Deep Learning model.

### 5.3. Road Elevation Model using the TxDOT Roadway Inventory

The TxDOT Roadway Inventory has an attribute RB\_WID, Road Bed Width, that when used to buffer the roadway line can produce a road polygon coverage. For Travis County, this attribute is populated on all the On-System roads (830 miles) and on 40 miles of Off-System roads, for a total of 870 miles of roads. The same process used to create the Ecopia-based Road Elevation Model was applied successfully to this buffered version of the TxDOT Roadway Inventory with the results shown below. A comparison in Figure 5.9 of the Pennybacker bridge on Loop 360 over the Colorado River in Austin, Texas, shows that both approaches give similar results.



Buffered TxDOT Roadway Inventory Road Elevation Model



Ecopia Road Elevation Model

Figure 5.9. Road Elevation Models for the Pennybacker bridge

A similar comparison made at the Highway 183 and Loop 1 interchange shown in Figure 5.10 suggests that some of the roads are omitted from the TxDOT Roadway Inventory compared to the Ecopia coverage.

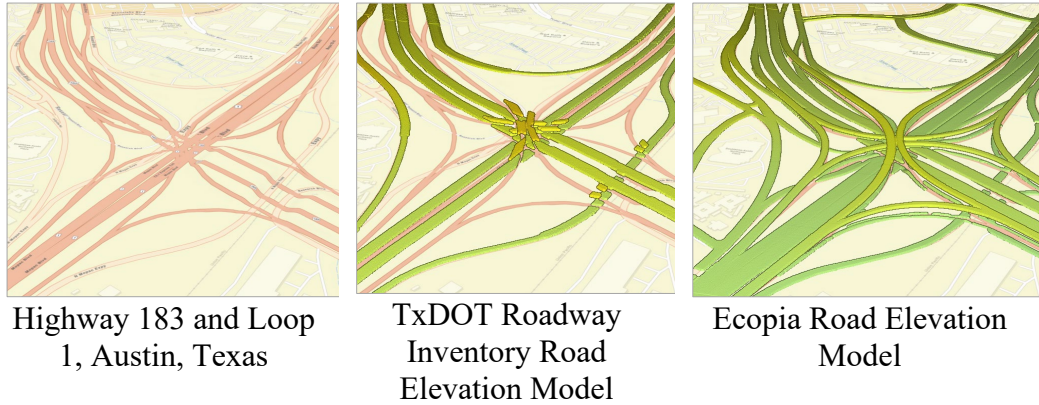


*Figure 5.10. Comparison of Road Elevation Models at Highway 183 and Loop 1, Austin, Texas.*

An assumption in using the TxDOT Roadway Inventory as the road line for creating the buffered coverage for the road polygon is that the road line is actually at the center of the road. In some instances, this is not the case, as illustrated in Figure 5.11. The Ecopia and Open Street map lines are generally close together but there is some discrepancy between the locations of these lines and those of the TxDOT Roadway Inventory. For the Austin District as a whole, an intersection of the TxDOT Roadway Inventory lines and the Ecopia polygons shows that 90% of the TxDOT Roadway Inventory lines overlap the Ecopia polygons. However, 10% of the TxDOT Roadway Inventory lines do not overlap the Ecopia polygons and may be off the road surface itself. The On-System road lines are well located in the TxDOT Roadway Inventory. It is the Off-System lines that have a more varied location compared to the pavement surface.

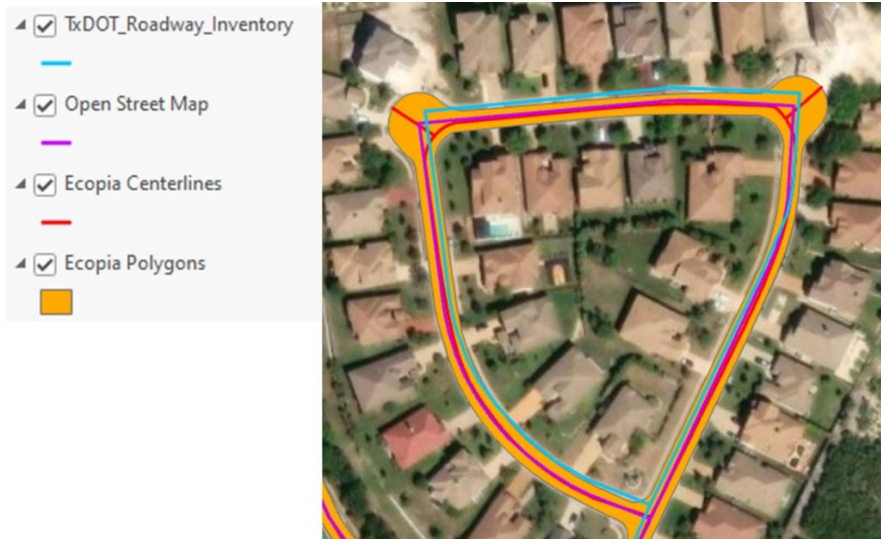


Figure 5.11. Comparison of the location of road lines from the TxDOT Roadway Inventory, Open Street Map and Ecopia, overlaid on the Ecopia road polygons.

The key limitation of using the TxDOT Roadway Inventory to create a Road Elevation Model is the lack of coverage of attribution of the Road Bed Width. This attribute is unpopulated in nearly all the Off-System roads, so the end result is that 870 miles of Road Elevation Model can be built by using the TxDOT Roadway Inventory, compared to 7600 miles using the Ecopia coverage, as shown in Figure 5.12.

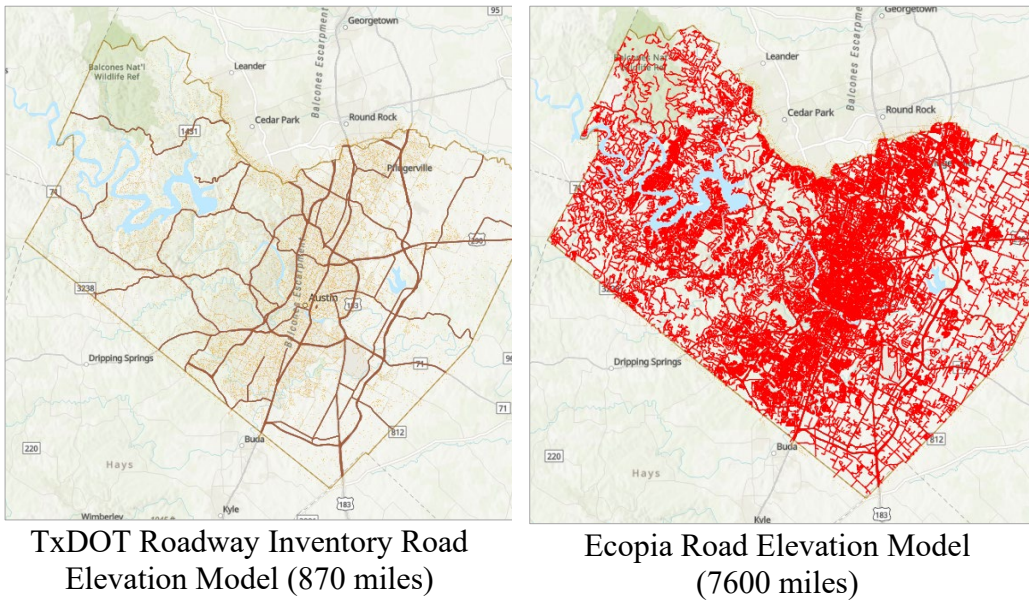


Figure 5.12. Coverage of the TxDOT Roadway Inventory and Ecopia Road Elevation models for Travis County

## 5.4. Road Elevation Model using Open Street Map

A second alternative to using the Ecopia coverage is to use Open Street Map, which has a coverage of the Austin District equivalent to that provided by Ecopia, except in Llano County. This requires some method of inferring the roadway width from the class of road line in the coverage. One way to do that is to use the Functional Classification attribute in the TxDOT Roadway Inventory to distinguish its road bed width values and then assign comparable values to the equivalent road class in Open Street Map. As shown in Table 5.1, both systems have a roughly equivalent number of road categories.

| Level | TxDOT Roadway Inventory      | Open Street Map |
|-------|------------------------------|-----------------|
| 1     | Interstate                   | Motorway        |
| 2     | Other Freeway and Expressway | Trunk           |
| 3     | Other Principal Arterial     | Primary         |
| 4     | Minor Arterial               | Secondary       |
| 5     | Major Collector              | Tertiary        |
| 6     | Minor Collector              | Residential     |
| 7     | Local                        | Unclassified    |
| 8     |                              | Service         |

**Table 5.1. Classification of roads into functional levels.**

The minimum, median and maximum road bed widths summarized by Functional Classification for the state-wide TxDOT Roadway Inventory are shown in Figure 5.13. For categories 1-4 the median road width is 42 ft, and it drops to 26 ft for categories 5-7. It is apparent from the chart, however, that there is a significant variation in road bed width even within one classification category, larger than the variation of the median road bed width from one category to another. The Open Street Map lines for the Austin District were buffered by one half of the median road width, and areal coverage of the resulting road system was compared to that of the Ecopia coverage. Of the total area of the Open Street Map road coverage thus created, 61% of the Open Street Map road area overlapped with the Ecopia road polygon coverage, while the remaining 39% did not overlap.

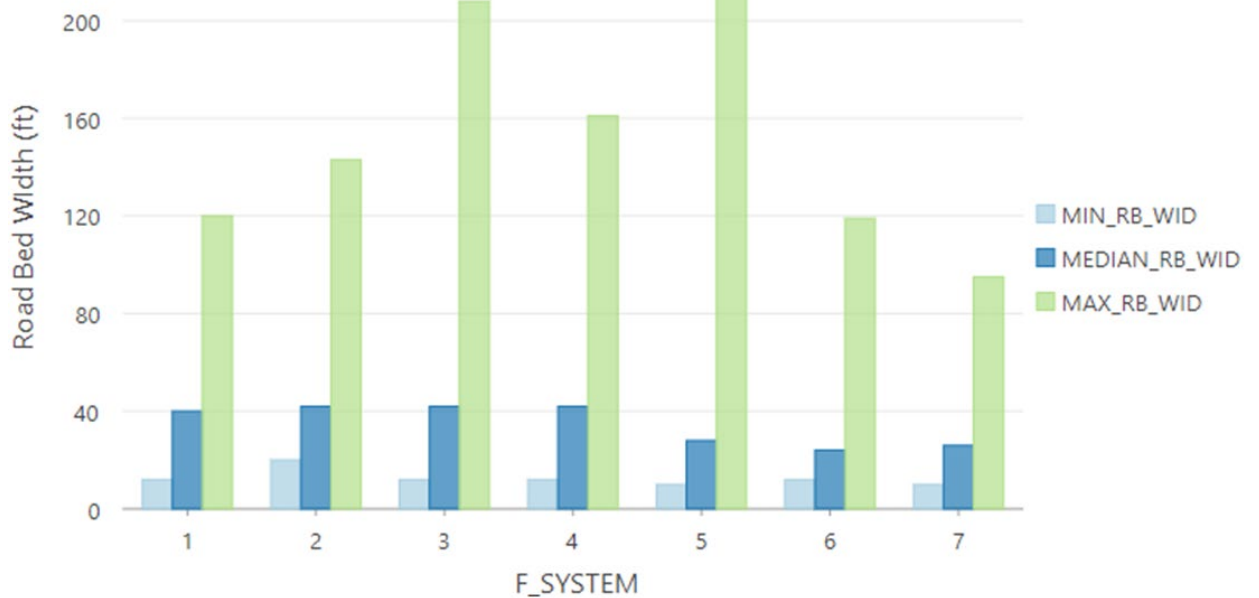


Figure 5.13. Minimum, Median and Maximum Road Bed Width for the TxDOT Roadway Inventory

Figure 5.13 shows Open Street Map lines buffered by half of the estimated road width to form a road surface on Anderson Lane at Shoal Creek. This is compared to the Ecopia road polygon surface. It is clear that the success of a road centerline buffering scheme depends on whether a single road centerline is used or two road lane lines.

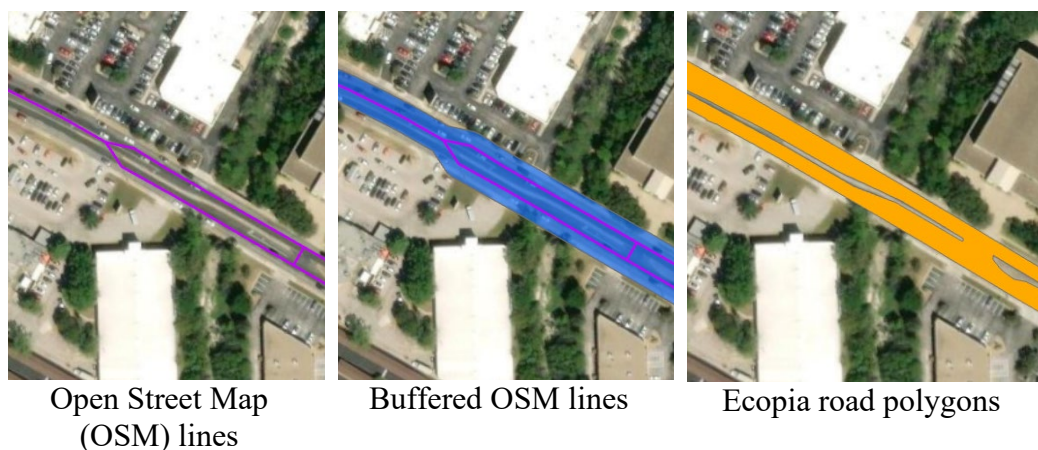


Figure 5.14. Comparison of road widths on Anderson Lane at Shoal Creek in Austin, Texas.

It is apparent that no matter what choice was made as to the road bed width to assign to each roadway category in Open Street Map, there would be many roads

with erroneous road bed widths. If a Road Elevation Model constructed this way is then connected to bridge coverages where the actual width of the bridge is known from LIDAR point cloud classification, then these errors will be obvious. Hence, a road elevation model for the Austin District was not constructed using this approach.

## 5.5. Integration with Bridge Information

In parallel with the development of the Road Elevation Model, the Streamflow research team has also been working on extracting bridge characteristics from the state-wide coverage of Texas LIDAR data. This has produced information for 37,488 bridges, as shown in Figure 5.15.

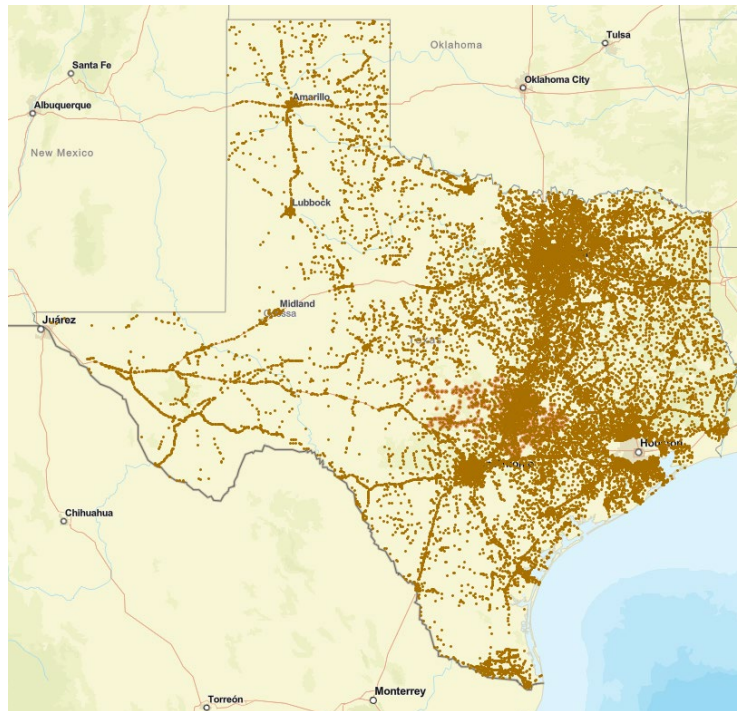


Figure 5.15. Geospatial data for bridges extracted from LIDAR data using Tx-Bridge

Of these bridges, 27,688 have NBI bridge numbers so their characteristics can be compared to the information about bridge dimensions stored in the National Bridge Inventory. An example of these two LIDAR data sources is shown in Figure 5.16 for the bridge over Shoal Creek at Anderson Lane in Austin, Texas. The blue elevation points are drawn directly from the TxGIO LIDAR coverage for the bridge feature, and the orange points are from the Road Elevation Model

for Anderson Lane, as shown in a series of ArcGIS Tutorials<sup>15</sup> developed for showing the Road Elevation Model in the Shoal Creek watershed. The linear gaps in the center of the Ecopia roadway coverage arise from the presence of the roadway median at that location which is omitted from the Ecopia road polygon coverage for the road surface itself. The small holes on the road surface itself are due to the location of cars when the LIDAR data were collected. The purple template for the bridge extent is created from NBI data as shown in Figure 5.17.

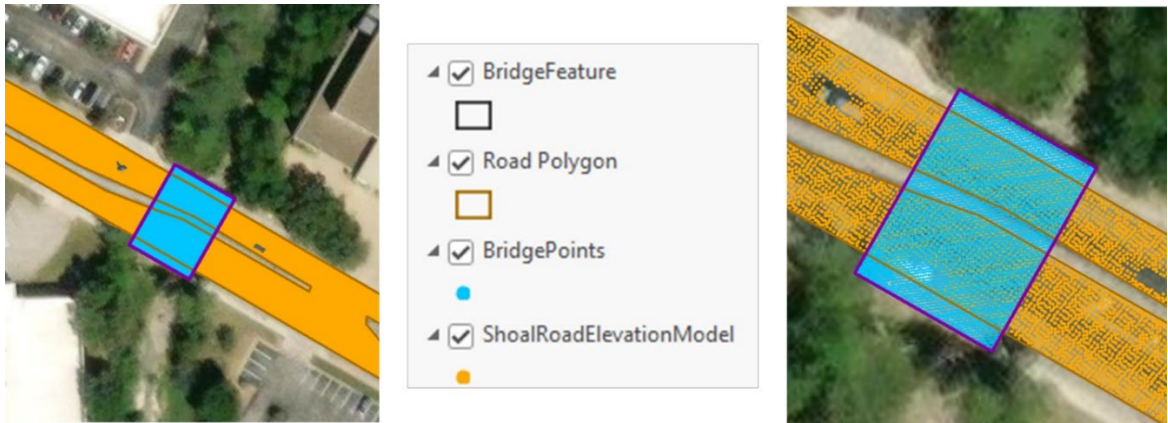


Figure 5.16. Road and Bridge Elevation Points on Anderson Lane at Shoal Creek

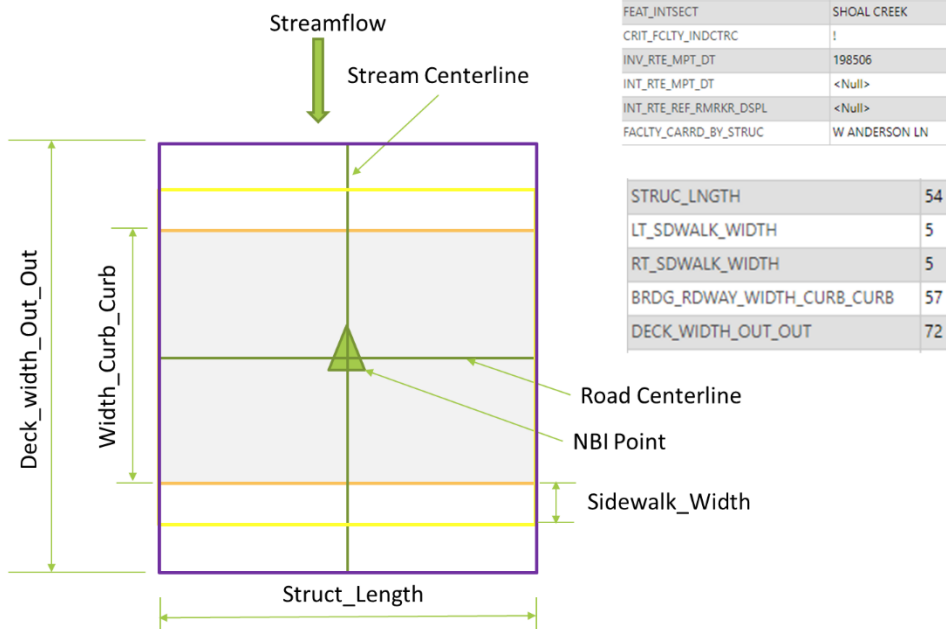


Figure 5.17. Bridge Deck Template Created with Data from the National Bridge Inventory

<sup>15</sup> <https://www.caee.utexas.edu/prof/maidment/RoadElevationModel.htm>

These three independent sources of data all fit together very well at this location:

- The Road Elevation Model points for the road surface
- The LIDAR points for the bridge surface extracted directly from TxGIO LIDAR data
- A geometric template for the bridge dimensions created from AssetWise and NBI bridge data.

This is the type of road and bridge coverage that should be sought as the Road and Bridge LIDAR data are brought together into an integrated 3D Road Transportation Model.

## 5.6. Assessment of Road Elevation Modeling Approaches

---

Three possible methods of constructing a 3D geospatial representation of the public road system in the Austin District have been assessed: TxDOT Roadway Inventory, Open Street Maps and Ecopia roads. The conclusions are:

**(1) TxDOT Roadway Inventory** – A reasonable 3D road coverage can be created from the TxDOT Roadway Inventory for On-System roads by buffering the road line with the road bed width and collecting the LIDAR points that fall on this surface. This assumes that the geospatial coverage of the TxDOT road lines is located exactly at the center of the actual road surface. However, this method is viable only for On-System roads which constitute about 10% of the public road system. Road bed widths are attributed for very few Off-System roads.

**Assessment:** This option is not viable because of inadequate coverage of the extent of the public road system.

**(2) Open Street Map** – The spatial coverage of Open Street Map is much more extensive than for the TxDOT Roadway Inventory and appears to be a good representation of the public road system except in Llano County where the coverage is visibly less dense than for adjacent counties. The road bed width is not attributed on the Open Street Map road lines. There is no reliable way of assigning road bed width as a function of class of roads. The best that can be achieved is a rough estimate based on median road bed widths documented in the TxDOT Roadway Inventory.

**Assessment:** This option is viable but not preferred because it requires buffering with uncertain roadway widths.

**(3) Ecopia** –The polygon coverage of the road extent was derived by AI interpretation of the 6” Hexagon aerial imagery licensed for use by TxDOT. Public roads are one of about 20 land cover classes interpreted across the whole landscape. The Ecopia coverage is a very good but not perfect representation of the extent of the road pavement surface.

**Assessment:** This option is viable and is the preferred option because it is based on explicit mapping of the road surface. The derived LIDAR point cloud is a publicly sharable dataset.

## 5.7. Flood Mapping Tutorials

A series of three ArcGIS tutorials have been created to show the technical details as to how the depth of road flooding on individual streets and an inventory of flooded roads over a watershed can be created. These tutorials can be accessed at: <https://www.cae.utexas.edu/prof/maidment/RoadElevationModel.htm> which also provides access to the Road Elevation Model of the TxDOT Austin District comprising 3.8 billion LIDAR points covering nearly 38,000 miles of roads in the District.

The first tutorial (Figure 5.18) starts with a Road Elevation Model for Travis County comprising 690 million LIDAR points and shows how to select the 24 million points that lie within the boundary of the Shoal Creek watershed. The road system comprises just 1.6% of the total area of the landscape so carrying all the points that lie on it is feasible and the file sizes are reasonable.



Figure 5.18 First tutorial – road elevation points in a watershed

The second tutorial (Figure 5.19) uses the relationship

$$\text{Road Flood Depth} = \text{Water Surface Elevation} - \text{Road Surface Elevation}$$

Where the water surface elevation is taken from a City of Austin HEC-RAS model for Shoal Creek for a 100-year return period storm, and the water depth at

each LIDAR point on the street surface is calculated. This allows for tracking the precise pattern of inundation mapping along and across the street.

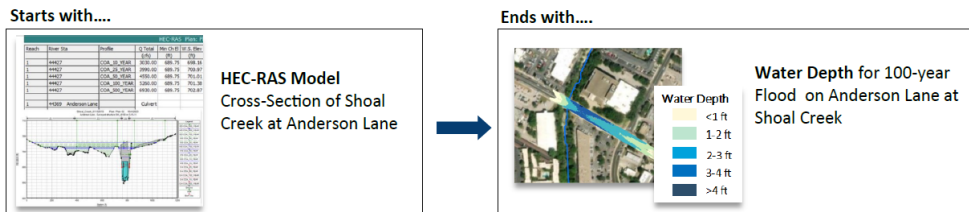


Figure 5.19 Second tutorial -- road inundation mapping at street scale

As shown in Figure 5.20, the resulting flood inundation depth map is very detailed, showing deeper flooding near the gutters and shallower at the center of the street. Also, the maximum flooding depth actually occurs at a low point on the road that is downhill of the bridge as the street slopes downwards from left to right in Figure 5.20. It was found that the actual flood inundation length on such a map depends significantly on where the line is drawn that measures it – the inundation depth along the stream centerline is shorter than along the edges of the street. A more reliable way of calculating the length of flooded street is to compute the inundated street area and divide that by the width of the street. Figure 5.20 also illustrates the statistical distribution of flood depths within this inundated area, that vary from zero to more than 4 feet of water, and average 2.3 feet of water depth.

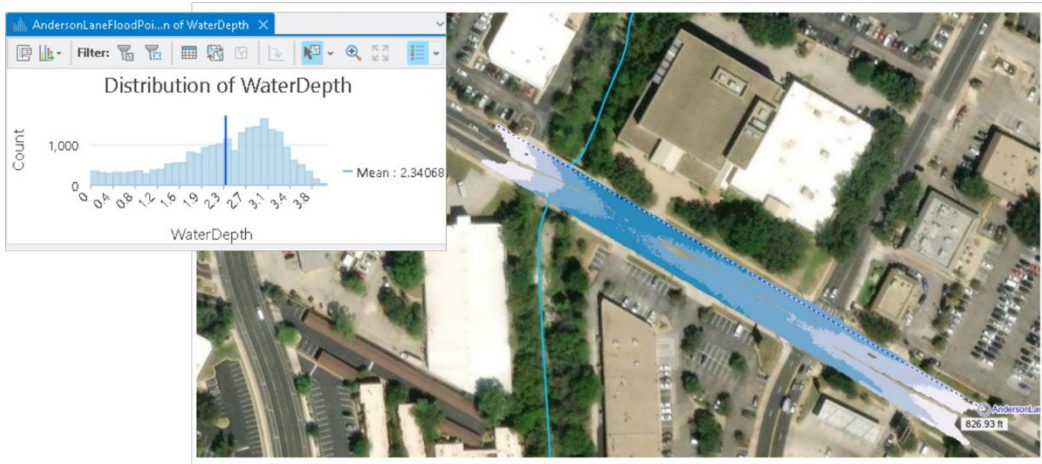


Figure 5.20 100-year flood depth map for Anderson Lane at Shoal Creek developed using water depth at LIDAR points.

The third tutorial (Figure 5.21) applies the same principle as in the second tutorial except that this time the whole Water Surface Elevation grid from the HEC-RAS model is used and the Road Surface Elevation is converted into a 1m DEM and subtracted from the water surface elevation to get the flooded depth in each road

segment. This tutorial shows how to apply the GIS method of linear referencing to overlay the flood inundation areas with the TxDOT Roadway Inventory and thus to create a listing of the lengths of the road segments flooded indexed by road name and by the Functional Classification of the road as given in Table 5.1.

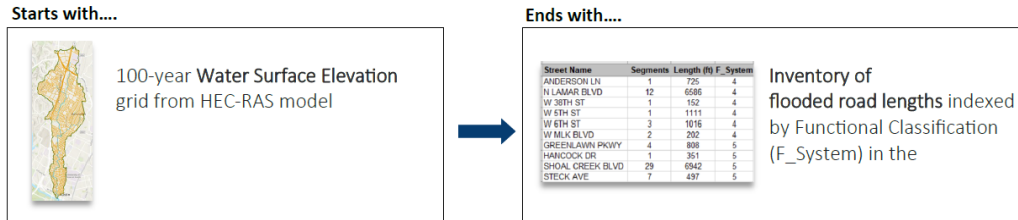


Figure 5.21 Third tutorial – flood impact at the watershed scale.

The inventory of flooded roads along Shoal Creek is shown in more detail in Figure 5.22. It can be seen that there are major impacts on Lamar Blvd, with 16 segments flooded for a total length of 6241 ft, and Shoal Creek Blvd with 13 segments flooded for a total length of 4124 feet. North Lamar Blvd is classified as Level 4 (Minor Arterial) and Shoal Creek as Level 5 (Major Collector) in the TxDOT Roadway Inventory functional classification.

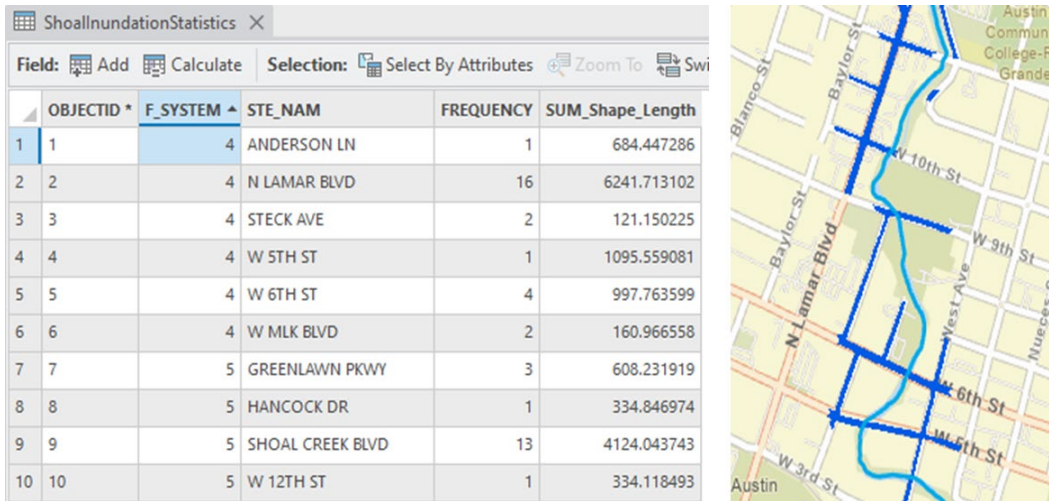


Figure 5.22 Inventory of roads impacted by a 100-year flood on Shoal Creek.

The end result is a rather remarkable connection between the 3D Road Elevation Model in (x,y,z) with the TxDOT Roadway Inventory in (x,y,m), as shown in Figure 5.23. The complementarity and synergy of these two ways of viewing the road system of Texas have much potential for future applications besides this flood project.

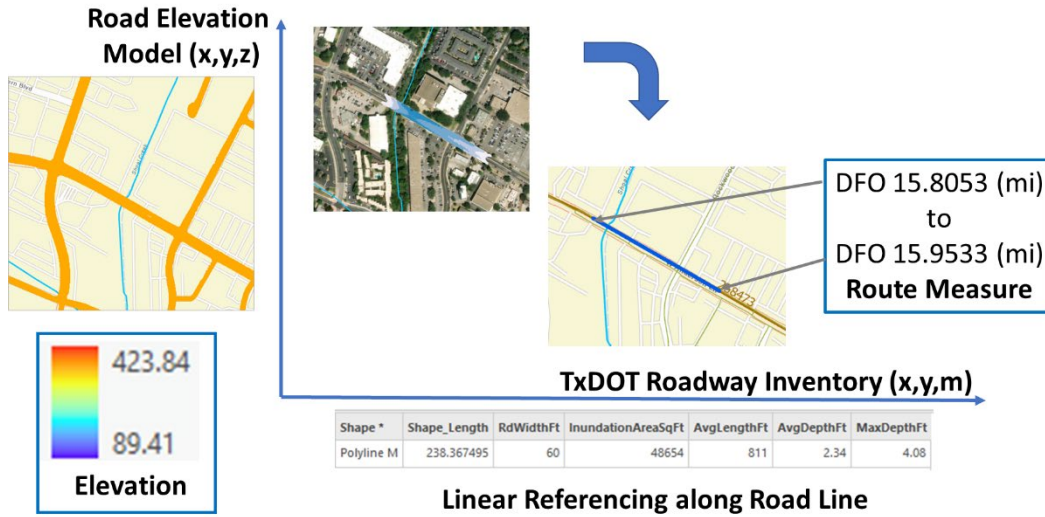


Figure 5.23 Connecting the road representation in  $(x,y,z)$  with that in  $(x,y,m)$

## 5.8. Base Level Engineering Modeling in Texas

The methodology for road flood computation described in the three tutorials was developed using HEC-RAS design flood models contained in the City of Austin FloodPro system.<sup>16</sup> In order to generalize this methodology across Texas, an equivalent source of hydraulic engineering modeling is required. Fortunately, this is supplied by the Base Level Engineering (BLE) modeling program being sponsored by the Texas Water Development Board and FEMA, and being maintained by the Interagency Flood Risk Management<sup>17</sup> program operated by the US Geological Survey in Fort Worth.

The BLE program engages consulting engineering firms to construct HEC-RAS hydraulic engineering models for all the HUC8 watershed units in Texas. As shown in Figure 5.24, this work has either been completed or is programmed to be so in FY 2024. All of the BLE studies done early in the program used 1D HEC-RAS models but the majority are now being completed using 2D HEC-RAS models.

<sup>16</sup> <https://www.austintexas.gov/page/floodpro>

<sup>17</sup> <https://webapps.usgs.gov/infrm/estBFE/>

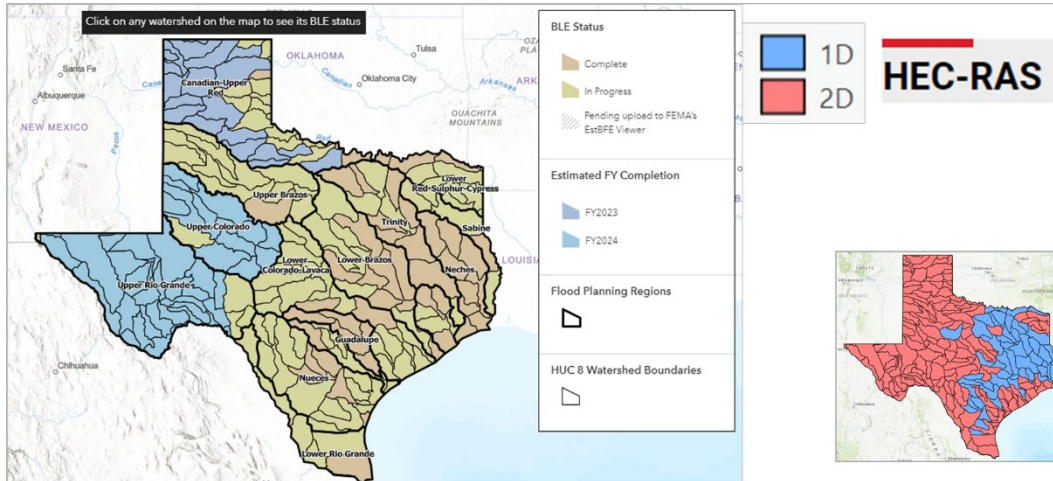


Figure 5.24 Base Level Engineering modeling in Texas.

In order for the flood inundation mapping created in BLE models to be used in real-time forecasting, it has to be indexed against the National Water Model Hydrofabric, which is a GIS description stream reaches and their associated local catchments developed by the National Water Center. That process is accomplished for 1-D HEC-RAS models using a procedure called RAS2FIM<sup>18</sup>, developed initially within this research program, and later extended as part of the flood inundation mapping program at the National Water Center. An equivalent procedure for 2D HEC-RAS models has not yet been developed.

As a standard approach, the BLE models, are developed on bare-earth digital elevation models that have no bridges in them. This means that the resulting inundation mapping is always flooded at bridge locations as shown in Figure 3.5. The TWDB and TxDOT have together sponsored a project for automatically inserting bridge information into the BLE models and those projects are being supported by bridge information compiled in this project using the Tx-Bridge procedure described in Chapter 4. It has been found that this bridge insertion is a good deal more readily done for 2-D HEC-RAS than for 1-D HEC-RAS because in 1-D HEC-RAS models the placement of the bridge with respect to the cross-section lines on the stream is critical. Cross-section lines are not used in 2-D HEC-RAS models. Once the bridges are inserted, the Base Level Engineering models are then capable of being run as detailed hydraulic engineering models that correctly represent the backwater effect of bridge structures.

<sup>18</sup><https://github.com/NOAA-OWP/ras2fim>

## 5.9. Bridge-Class Culverts

Besides the 25,000 span bridges, there are also about 20,000 bridge class culverts contained in the National Bridge Inventory (NBI). These are generally large multiple concrete box culvert structures which are imbedded within the road embankment and are designed to function even when submerged. To be recorded in the NBI, the culvert structure must exceed 20 ft in length measured along the roadway centerline. While some information is recorded in the NBI about these culvert structures, such as the number of culvert openings, it is within the TxDOT AssetWise system that the critical information about bridge-class culverts is to be found. An example of such a bridge-class culvert is shown in Figure 5.25.

| NBI 062: Culverts                   |                  |                   |   |
|-------------------------------------|------------------|-------------------|---|
| A                                   | B                | C                 |   |
| Parent Asset                        | Asset Name       | NBI 062: Culverts | TxDOT_SI&A_Bridge_Description   |
| District 14 - Austin > BASTROP - 11 | 4501100214260581 | 7                 | 3 - 6' x 4' Concrete Multiple Box Culvert at 45 Degree Right Forward Skew |
| District 14 - Austin > BASTROP - 11 | 4501100214260582 | 7                 | 4 - 6' x 7' Concrete Multiple Box Culvert                                 |
| District 14 - Austin > BASTROP - 11 | 4501100214260583 | 7                 | 4 - 10' x 8' x 36.5' Co   |
| District 14 - Austin > BASTROP - 11 | 4501100214260584 | 7                 | 4 Barrel 10' x 8' x 36  |
| District 14 - Austin > BASTROP - 11 | 4501100214260585 | 7                 | 3 - 6' x 5' Concrete h  |
| District 14 - Austin > BASTROP - 11 | 4501100214260586 | 7                 | 4 - 6' x 5' Concrete h  |
| District 14 - Austin > BASTROP - 11 | 4501100214260587 | 7                 | 6 - 7' x 6' Concrete h  |
| District 14 - Austin > BASTROP - 11 | 4501100214260588 | 7                 | 3 - 10' x 10' Concrete  |
| District 14 - Austin > BASTROP - 11 | 4501100214260589 | 7                 | 4 - 8' x 6' Concrete h  |
| District 14 - Austin > BASTROP - 11 | 4501100214260590 | 7                 | 5 - 8' x 4' Concrete h  |
| District 14 - Austin > BASTROP - 11 | 4501100214260591 | 7                 | 3 - 10' x 8' Concrete   |
| District 14 - Austin > BASTROP - 11 | 4501100214260592 | 7                 | 3 - 8' x 4' Concrete  |
| District 14 - Austin > BASTROP - 11 | 4501100214260593 | 7                 | 6 - 5' x 4' Concrete f  |
| District 14 - Austin > BASTROP - 11 | 4501100214260594 | 7                 | 4 - 6' x 4' Concrete h  |
| District 14 - Austin > BASTROP - 11 | 4501100214260595 | 7                 | 7 - 8' x 7' Concrete h  |
| District 14 - Austin > BASTROP - 11 | 4501100214260596 | 7                 | 3 - 10' x 11' Concrete  |
| District 14 - Austin > BASTROP - 11 | 4501100214260597 | 7                 | 3 - 8' x 8' Concrete h  |
| District 14 - Austin > BASTROP - 11 | 4501100214260598 | 7                 | 4 - 6' x 5' Concrete h  |
| District 14 - Austin > BASTROP - 11 | 4501100214260599 | 7                 | 2 Barrel 10' x 4' x 75  |
| District 14 - Austin > BASTROP - 11 | 4501100214260600 | 7                 | 4 Barrel 8' x 6' x 69   |
| District 14 - Austin > BASTROP - 11 | 4501100214260601 | 7                 | 3 Barrel 7' x 6' x 297  |
| District 14 - Austin > BASTROP - 11 | 4501100214260602 | 7                 | 4 Barrel 10' x 9' x 89  |
| District 14 - Austin > BASTROP - 11 | 4501100214260603 | 7                 | 4 Barrel 6' x 4' x 78.1   |
| District 14 - Austin > BASTROP - 11 | 4501100214260604 | 7                 | 4 Barrel 6' x 6' x 88.2   |
| District 14 - Austin > BASTROP - 11 | 4501100214260605 | 7                 | 2 Barrel 10' x 10' x 1  |
| District 14 - Austin > BASTROP - 11 | 4501100214260606 | 7                 | 2 - 10' x 8' Concrete Multiple Box Culvert                                |
| District 14 - Austin > BASTROP - 11 | 4501100214260607 | 7                 | 3 - 6' x 6' Concrete Multiple Box Culvert                                 |
| District 14 - Austin > BASTROP - 11 | 4501100214260608 | 7                 | 3 - 7' x 5' x 60' Concrete Multiple Box Culvert at Variable Degree Skew   |
| District 14 - Austin > BASTROP - 11 | 4501100214260609 | 7                 | 3 - 10' x 10' x 37.3' Concrete Multiple Box Culvert                       |
| District 14 - Austin > BASTROP - 11 | 4501100214260610 | 7                 | 3 - 8' x 5' Concrete Multiple Box Culvert                                 |
| District 14 - Austin > BASTROP - 11 | 4501100214260611 | 7                 | 4 Barrel 8' x 6' x 81.3' Precast Concrete Box Culvert                     |

|                                 |                                     |
|---------------------------------|-------------------------------------|
| OBJECTID                        | 938                                 |
| Parent Asset Maintenance        | District 14 - Austin > TRAVIS - 227 |
| Asset Name Bridge Number        | 142270800174006                     |
| NBI 062: Culverts               | 6 (Culvert condition 1-9)           |
| TxDOT_SI&A_Bridge_Description   | 5 - 10' x 6' x 72' MBC              |
| Fill Height (On top of culvert) | 18                                  |

Figure 5.25 Description of a bridge-class culvert in the TxDOT AssetWise system

This example is a bridge-class structure with five concrete box culverts, each 10 feet wide by six feet high and 72 feet long on which there is 18 inches of fill beneath the road surface. This structure is rendered in 3D in Figure 5.26 where it is fitted into the stream cross-section at the correct elevation beneath the Road Elevation Model. This location is on Shoal Creek at Anderson Lane, the same location as for Tutorial 2 described previously in this chapter.

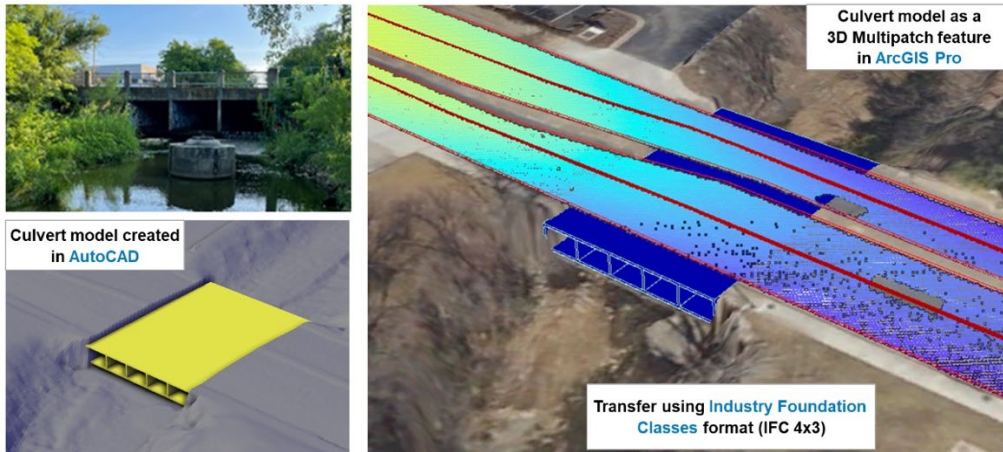


Figure 5.26 3D Bridge-class culvert positioned beneath the Road Elevation Model for Anderson Lane at Shoal Creek in Austin, Texas.

## 5.10. Low-Water Crossings

There is also a need to describe culverts of less than 20 feet in length, and to describe Low-Water Crossings that may have only a small underflow pipe capacity to convey normal water flow in the stream. The research team developed a Rapid Field Assessment for Culvert Crossings<sup>19</sup> and applied it to 20 Low-Water Crossings in the Austin District. This involves going to a low-water crossing and using GPS surveying to record location and elevation for the road edge, pipe inverts, and flood gage base, as shown in Figure 5.27.

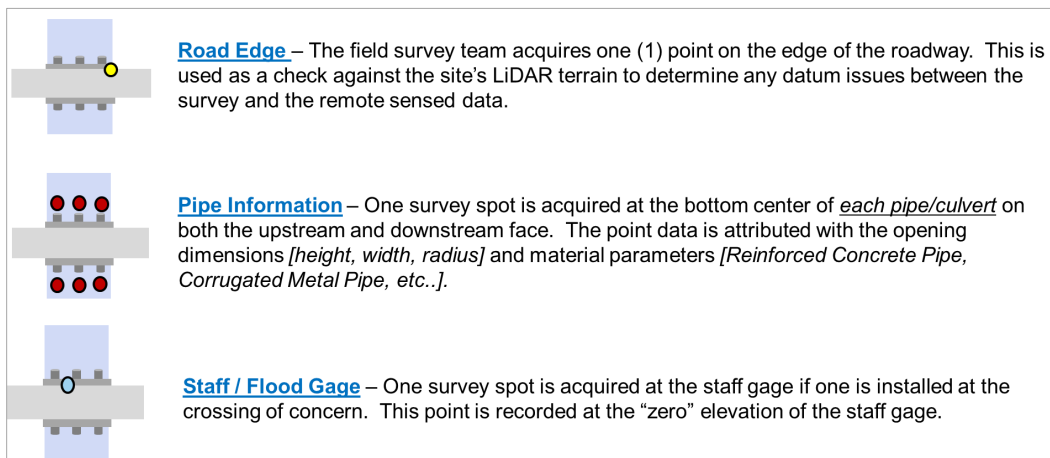


Figure 5.27 Survey information acquired in the rapid field assessment for culverts

Additional information to be collected includes photographs, descriptions of pipe materials and measurement of the culvert pipes. This is automatically recorded in an ArcGIS database for referral later. A web-based StoryMap “Rapid Assessment Survey for Culvert Crossings – Central Texas” is available for seeing the results of application of this procedure in the Austin District<sup>20</sup>.

One of the low water crossings surveyed with this procedure is on Onion Creek at FM 150 in Hays County, as shown in Figure 5.28. This low-water crossing has a nearby USGS gauge, Onion Creek at Driftwood, which shows that the crossing has been flooded at a depth of more than 20 ft seven times since the gauge was installed in 1974! Careful study of the road elevation at this location revealed that a 3m digital elevation model underestimated the actual elevation of the road because 3m cells are large enough that some of the LIDAR points they contain fall off the road surface into the lower areas on the road verge. The road surface elevation is correct when formed from LIDAR points on the road surface or from a 1m DEM derived from those points.

Low-Water Crossings like this one need to have a culvert rating program such as the FHWA HY8<sup>21</sup> program run on them to determine the rating curve because of the substantial amount of water passing beneath the road in the culvert pipes compared to the water flowing on the road surface itself, especially as a flood hydrograph recedes.



*Figure 5.28 Low-water crossing on Onion Creek at FM 150*

---

<sup>20</sup> <https://ut-austin.maps.arcgis.com/apps/MapSeries/index.html?appid=30acdecc9e5d4bae8568dc6a0047cab>

<sup>21</sup> <https://www.fhwa.dot.gov/engineering/hydraulics/software/hy8/>

# Chapter 6. Error Analysis and Data Assimilation

## 6.1. Introduction

---

Flood forecasting at the watershed scale is inherently uncertain. Rainfall forecasts are subject to substantial errors in both the timing and magnitude of rainfall. Hydrologic and hydraulic models that translate rainfall into stream discharge are also uncertain, and suffer from parameterization error due to a lack of field data on soil properties, antecedent wetness, and channel geometries. Finally, gage data is sparse and, due to the considerable cost of sensor installation, only a small fraction of stream reaches are monitored. Where available, sensor data are themselves also uncertain due to both intrinsic sensor noise and the uncertain relationship between the observed quantity (e.g., water surface velocity) and the quantity of interest (e.g., discharge). Taken together, these various sources of error substantially complicate the prediction of river stage at TxDOT bridges and roadways. Uncertainties in predicted river stage in turn inhibit effective decision making by emergency operators. Thus, it is essential to characterize and reduce uncertainties in river stage forecasts to the maximum degree possible.

Data assimilation (DA) helps to tame uncertainties in flood forecasts by fusing sensor and model data together to produce estimates of flood stage that are better than either data source in isolation. In this context, data assimilation assists in two primary ways. First, data assimilation enables better forecasting of stream stage and discharge at actionable lead times. By assimilating sensor data into the process model, DA improves estimates of the initial hydraulic state at the start of the forecast window. By starting the flood forecast with improved estimates of initial discharges in the river network, forecasted discharges at the end of the forecast window are also improved. Second, DA improves estimates of flood stage at ungauged locations. By assimilating sensor data into the model, DA allows for improved prediction of flood stage at ungauged sites. This capability to estimate flood stage at unmonitored locations is significant given that the vast majority of TxDOT bridges and low-water crossings are ungauged.

In this section, we characterize the scale of uncertainty in river stage and discharge estimates, develop a data assimilation methodology for improving stage predictions, and then evaluate this data assimilation procedure with respect to both forecasting (i.e., extrapolation in time) and estimation of discharge at ungauged locations (i.e., interpolation in space). Finally, we examine how

information from new stream velocimetry sensors adopted in the streamflow monitoring project can be used to reduce uncertainty in flood predictions at the reach scale.

The outline of this section is as follows. Section 6.2 describes the evaluation of the National Water Model at the river network scale over the State of Texas to quantify the error associated with the model and identify spatial and/or temporal patterns in the estimated error. Section 6.3 describes the state-space Muskingum model used to simulate discharge at the river network scale. Section 6.4 describes the DA methodology, as well as the methodology used to compute error bounds for anticipated discharges and the ultimate probability of road overtopping. Section 6.5 describes the software implementation of the modeling system within Kisters DataSphere. Section 6.6 evaluates the DA procedure with respect to improving flood forecasts. Section 6.7 evaluates the DA procedure with respect to improving flood stage estimates at ungauged locations. In Section 6.8 we present an analysis of the data collected at RQ-30 sites to quantify hysteresis patterns and a theoretical and modeling analysis of this behavior. Conclusions are presented in Section 6.9.

## **6.2. Error analysis at network scale**

---

The National Oceanic and Atmospheric Administration (NOAA) has developed the National Water Model (NWM), a hydrologic model that can predict streamflow and other water-related variables throughout the United States. The model has four configurations (Analysis and Assimilation, Short-range, Medium-range, and Long-range) for the Continental United States (CONUS), Alaska, Hawaii, Puerto River and other US territories. The NWM provides analysis of streamflow, as well as other hydrologic states on the land surface and in the shallow subsurface. The NWM provides streamflow forecasts for short (next 18 hours), medium (next 10 days), and long-term (next 30 days) periods. The NWM's ability to provide streamflow forecasts over these three timescales for over 2.7 million river reaches in the United States has made it a useful tool for flood risk analysis and management purposes for emergency managers, water utilities, and other agencies and institutions.

In this project, the NWM forecasts provide a spatially continuous hydrological prediction over the watersheds in the State of Texas (190,000 miles of streams and rivers in Texas divided into 100,000 individual stream reaches). The availability of these predictions provides important information for issuing warnings and developing flood inundation mapping on roads. However, as with any model, the NWM is expected to have errors, particularly given that the model runs at continental scale simulating various subsurface and surface water

processes, without calibrating those processes and associated parameters locally. It is thus essential that as part of this project we assess the accuracy and performance of the NWM's streamflow forecasts to confidently use them for flood prediction purposes.

To quantify the NWM's performance in Texas, we conducted an error analysis of the hydrological forecast by comparing it with the streamflow measurements available at Texas gages. In particular, the USGS collects observations of stage and streamflow across thousands of gauging stations on rivers in the United States. Based on the available data, we have information at 553 USGS gages distributed throughout Texas (<https://waterdata.usgs.gov/nwis>) at which we performed a comparison of the measured and the forecasted streamflow.

As we are mostly concerned with flood conditions, and the ability of the model to predict them, we defined a discharge threshold to select events of interest and compute the error metrics only for those events. In order to define this threshold based on the historical record, we analyzed the annual maximum streamflow data from the NWM retrospective dataset, which provided us discharge data for 42 years (1979-2020). We defined the minimum annual maximum flow with a return period of 1.02 years from the 42-year dataset as the threshold value for each location to maximize data availability and ensure an adequate amount of data for the error estimation.

We computed the Root Mean Square Error (RMSE) and percent bias for the short-range and retrospective streamflow for the time period between 2020 and 2022. We computed these error metrics at all 553 USGS gages and generated maps to analyze the spatial pattern of the error metrics throughout Texas (Figures 6.1 and 6.2). The average and median RMSE are 10.19 m<sup>3</sup>/s and 3.39 m<sup>3</sup>/s, respectively. The RMSE for the period 2020-2022 (Figure 6.1) shows higher errors in larger cities and the southeast region of Texas, which is more susceptible to extreme weather events.

The percent bias does not show spatial patterns (Figure 6.2) for the analyzed period from 2020 to 2022. *This is an important result as it shows that there is no particular spatial pattern to the errors and thus that there is no evidence that the model is less accurate in one climatic region of Texas compared to another.* The average and median percent bias are 16.57% and -0.55%, respectively. Out of the 553 gage locations, the NWM overestimates discharge in 147 locations and underestimates it in 204 locations. At the remaining 202 gages, the discharge did not exceed the threshold value over the 2020-2022 time period and we excluded them from the analysis. These results indicate that, on average, the NWM

underestimates discharge, at least over the analyzed 2020-2022 time period. This underestimation is often due to an underestimation of the precipitation input.

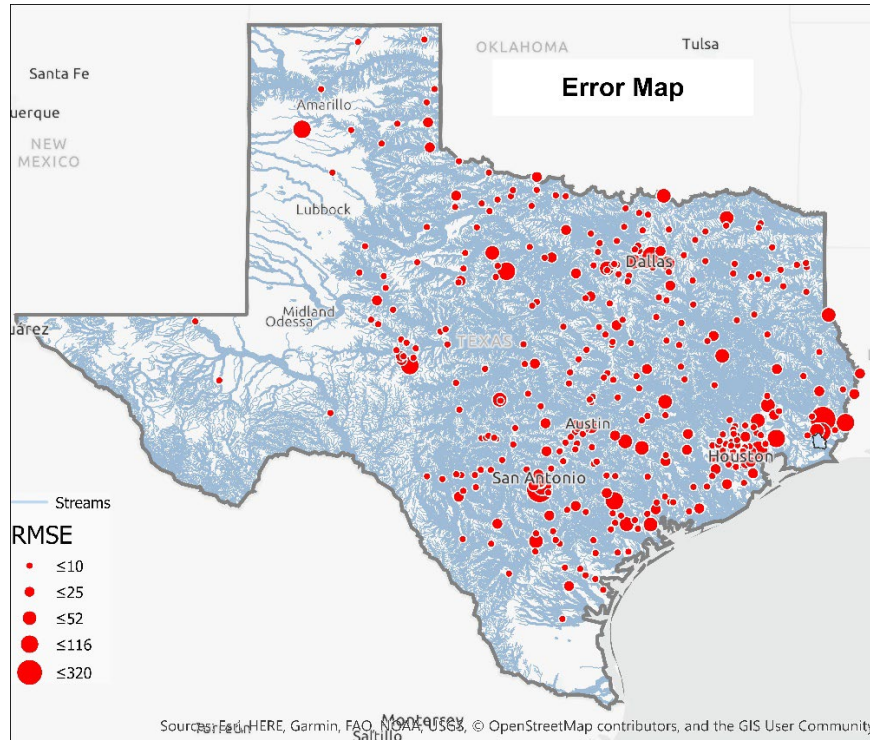


Figure 6.1. RMSE map for Texas for period 2020-2022. Dots represent gage locations. The size of the dot indicates the magnitude of the RMSE (in  $m^3/s$ ).

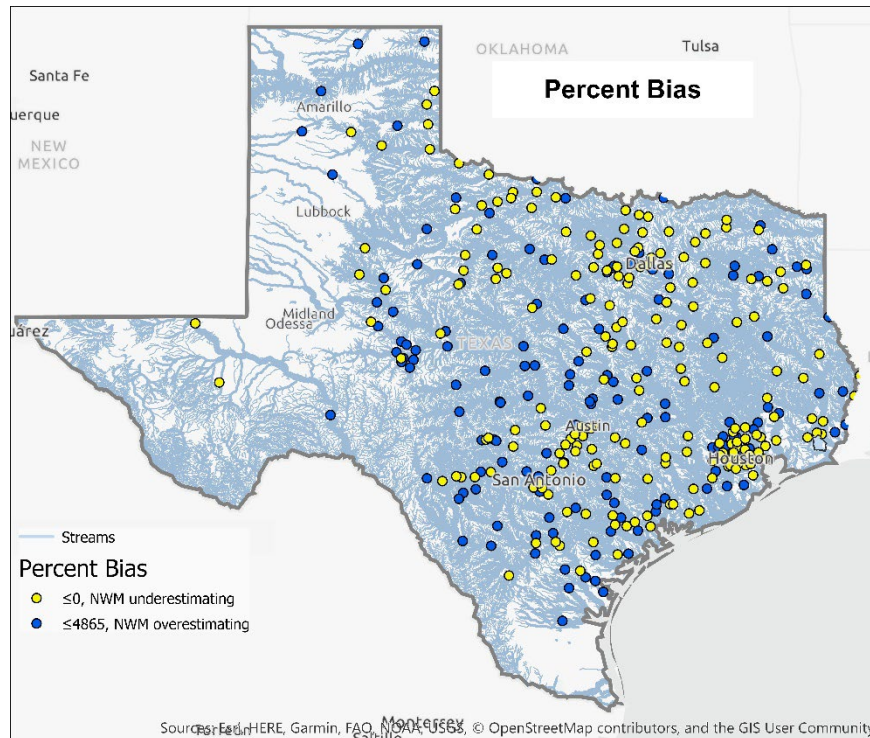


Figure 6.2. Percent Bias map for Texas for period 2020-2022. Dots indicate the location of the gage. The color indicates whether the NWM is underestimating (yellow) or overestimating (blue) with respect to the observed discharge.

We investigated the possible relationship between RMSE and river network properties in terms of mean annual discharge and stream order. When RMSE is plotted with respect to mean annual discharge (Figure 6.3), we find a positive relationship between the two variables, for the 2020-2022 time period analyzed. In particular, we find the following statistically significant relationship between RMSE and mean discharge:

$$\log(\text{RMSE})=0.34*\log(\text{discharge})+0.914 \quad (6.1)$$

which allows us to predict the RMSE expected for a given discharge value.

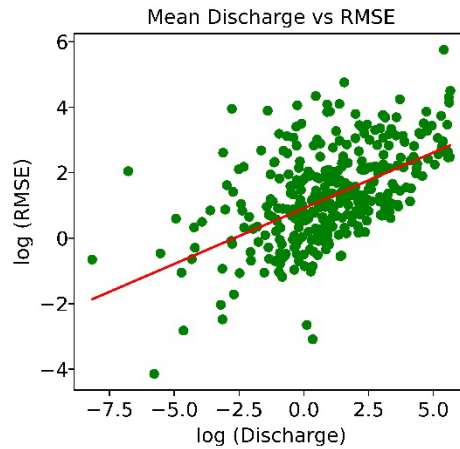


Figure 6.3. RMSE versus mean discharge.

## 6.3. Modeling of discharge in river networks

### 6.3.1. State-space Muskingum-Cunge routing

The NWM employs the Muskingum-Cunge (MC) method for channel routing. MC is a conceptual hydraulic model based on a unidirectional simplification of the physically-based Saint-Venant equations for unsteady open channel flow. The MC method in the NWM is implemented as the following discrete difference equation:

$$\mathbf{Q}_{j+1}^{t+\Delta t} = C_1 \mathbf{Q}_j^{t+\Delta t} + C_2 \mathbf{Q}_j^t + C_3 \mathbf{Q}_{j+1}^t + C_4 \quad (6.2)$$

where  $Q$  represents the estimated flow of a segment at both the upstream ( $j$ ) and downstream ( $j+1$ ) locations, calculated at the previous time step ( $t$ ) and the current time step ( $t + \Delta t$ ).  $C_1$ ,  $C_2$ ,  $C_3$ , and  $C_4$  are parameters. When considering

the topology of a stream network, the routing equation (6.2) for each reach leads to a large system of equations. In a state-space formulation, streamflows at time  $(t + \Delta t)$  are expressed in terms of streamflow ( $Q$ ) and the lateral inflow ( $q$ ) at time  $(t)$  for each reach, as shown in Figure 6.4. The matrices  $A$  and  $B$  are determined by the routing coefficients, taking into account the stream connectivity.

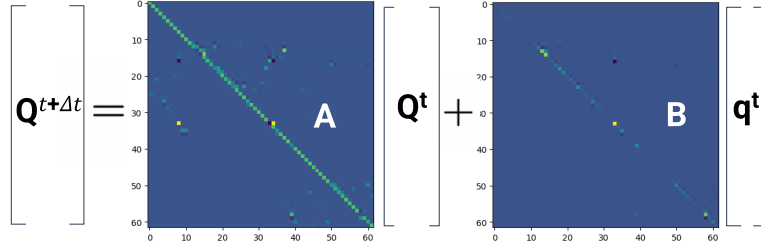


Figure 6.4 Example of state-space representation of the New Year Creek watershed.

## 6.4. Probability of road overtopping

### 6.4.1. Ensemble model for probabilistic forecast with data assimilation

From the discretized state-space MC equation, the model for ensemble member  $i$  can be expressed as:

$$\mathbf{x}_i^{t+\Delta t} = A \mathbf{x}_i^t + B \mathbf{u}_i^t + \mathbf{w}_i^t \quad (6.3)$$

$$\mathbf{y}_i^{t+\Delta t} = C \mathbf{x}_i^{t+\Delta t} + \mathbf{v}_i^{t+\Delta t} \quad (6.4)$$

where  $\mathbf{x}_i^t$  is the state vector of streamflow for each reach for ensemble member  $i$  at time  $t$ ;  $\mathbf{y}_i^t$  is the observed streamflow (obtained from sensor data);  $\mathbf{w}_i^t$  is the process noise;  $\mathbf{v}_i^t$  is measurement noise;  $A$  is the state transition matrix;  $B$  is the input matrix; and  $C$  is the observation matrix. Then, data assimilation using the Kalman Filter is applied to find the optimal linear estimation of the states:

$$\hat{\mathbf{x}}_i^{t+\Delta t} = \mathbf{x}_i^{t+\Delta t} + L_i^{t+\Delta t} \cdot [\mathbf{y}^{t+\Delta t} - C \cdot \mathbf{x}_i^{t+\Delta t}] \quad (6.5)$$

$$L_i^{t+\Delta t} = P_i^t C^T (C P_i^t C^T + V_i^{t+\Delta t})^{-1} \quad (6.6)$$

$$P_i^{t+\Delta t} = A \cdot (P_i^t - L_i^{t+\Delta t} \cdot C P_i^t) \cdot A^T + W_i^{t+\Delta t} \quad (6.7)$$

where  $\hat{\mathbf{x}}_i^{t+\Delta t}$  is the optimal posterior state estimate;  $P_i^{t+\Delta t}$  is the posterior estimation error covariance,  $V_i^{t+\Delta t}$  is the covariance of the measurement noise; and  $W_i^{t+\Delta t}$  is the covariance of the process noise. The measurement errors are estimated at 2.5% of the observed discharge. The standard deviation of process noise is assumed to be the 100% of the input runoff at each time. These errors are assumed to be uncorrelated Gaussian noise between gages. For the forecasting

assessment, data assimilation is only executed at the initial time step to set conditions for all ensemble forecasts. For all other steps, predictions are propagated based on system equation (6.3).

Based on the state-space MC model constructed for each ensemble, a Gaussian mixture model can be derived that explains the entire ensembles probabilistically. The mean and covariance for each ensemble member can be determined as follows:

$$\boldsymbol{\mu}_i^{t+\Delta t} = A\mathbf{x}_i^t + B\mathbf{u}_i^t \quad (6.8)$$

$$\boldsymbol{\Sigma}_i^{t+\Delta t} = A\boldsymbol{\Sigma}_i^t A^T + W_i^t \quad (6.9)$$

Given the k ensemble members, the probability density function (PDF), mean and the covariance of the gaussian mixture model are given by:

$$p(\mathbf{x}) = \sum_i w_i \mathcal{N}(\mathbf{x} | \boldsymbol{\mu}_i^{t+\Delta t}, \boldsymbol{\Sigma}_i^{t+\Delta t}) \quad (6.10)$$

$$\boldsymbol{\mu}^{t+\Delta t} = \sum_i w_i \boldsymbol{\mu}_i^{t+\Delta t} \quad (6.11)$$

$$\boldsymbol{\Sigma}^{t+\Delta t} = \sum_i w_i [\boldsymbol{\Sigma}_i^{t+\Delta t} + \boldsymbol{\mu}_i^{t+\Delta t} \boldsymbol{\mu}_i^{t+\Delta t T}] - \left( \sum_i w_i \boldsymbol{\mu}_i^{t+\Delta t} \right) \left( \sum_i w_i \boldsymbol{\mu}_i^{t+\Delta t} \right)^T \quad (6.12)$$

where  $w_i$  is the weight for the i th ensemble member, with  $0 \leq w_i \leq 1$  and  $\sum_i^k w_i = 1$ .

Then, the probability of road or bridge overtopping is the integral of the PDF up to the overtopping discharge (Q):

$$P_{\text{overtop}} = F(Q) = \int_{-\infty}^Q p(x) dx \quad (6.13)$$

Figure 6.5 illustrates the ensemble hydrological forecasting and the overtopping probability for New Year Creek during the Mother's Day flood event in May 2023. The probabilistic hydrological forecast is derived from seven medium-range ensemble predictions from the NWM. Correspondingly, the probability of overtopping is calculated based on equation (6.12).

In Figure 6.5, Part (a) represents the probabilistic hydrologic forecast produced on "2023-05-07 06h", showing ensemble median, measurements, overtopping discharge, interquartile range, and the 95% confidence interval. Part (b) shows the probability of bridge overtopping derived from the probabilistic forecasts. The actual observed discharge and overtopping probability for future events, as

recorded after the time of forecasting, are represented in dashed lines for comparison with the predictions.

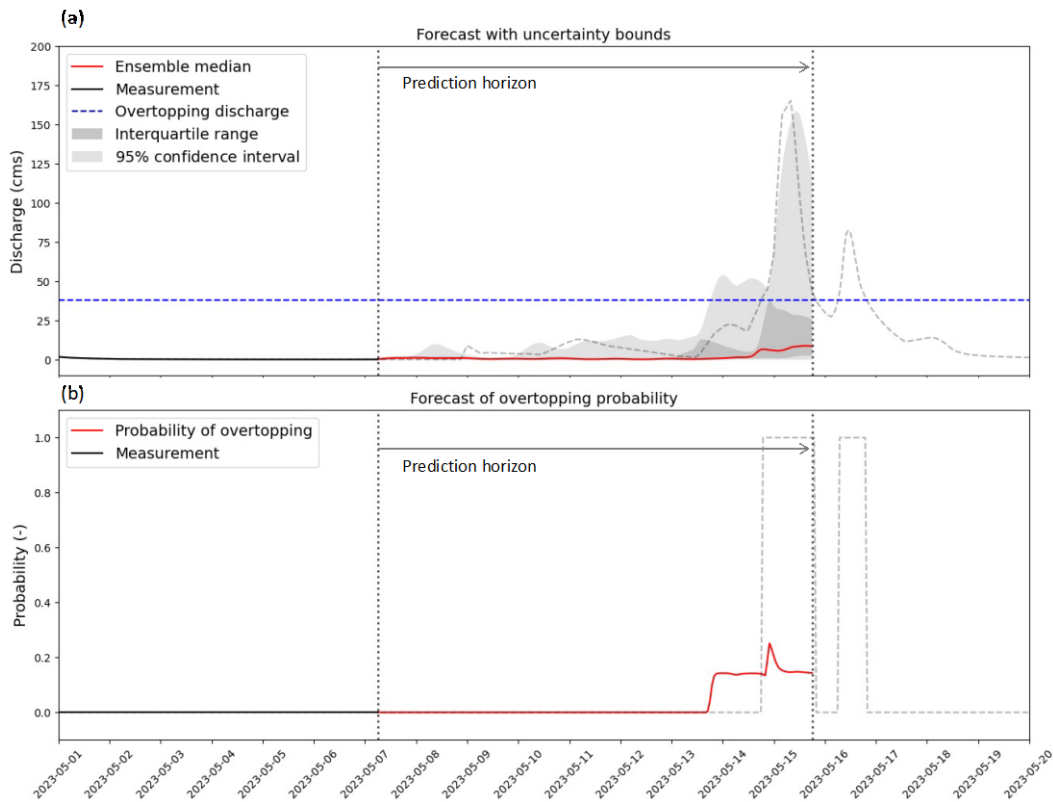


Figure 6.5 Hydrological Forecast and Overtopping Probability Analysis.

## 6.5. Software implementation and web architecture

In order to perform operational Data Assimilation at network scale, KISTERS developed a Real-time Optimization (RTO), which is an optimization model driven by IPOPT (Interior Point Optimizer). The mathematical formulation of the optimization problem, the governing equations of the model library, as well as its numerical schematization can be found in Technical Memo 5A<sup>22</sup>. This approach makes the data assimilation setup highly scalable. Multiple data assimilation setups can be run in parallel, with different setups for different spatial and temporal scale. The data assimilation and forecast timeseries are uploaded to a temporary Amazon Web Services (AWS) bucket. The timeseries are associated with the streamline COMID also used by the National Hydrography Dataset

<sup>22</sup><https://www.caee.utexas.edu/prof/maidment/StreamflowII/Documents/ReportTM5AProject07095.pdf>

(NHD) Plus . This storage space can be accessed by Datasphere, and Datasphere’s Extract, Transform, Load (ETL) can ingest the results. The results are displayed in KISTERS’s Datasphere (Figure 6.6), by selecting the NHD COMID and the time horizon of the assimilation run ( $t_0$ ).

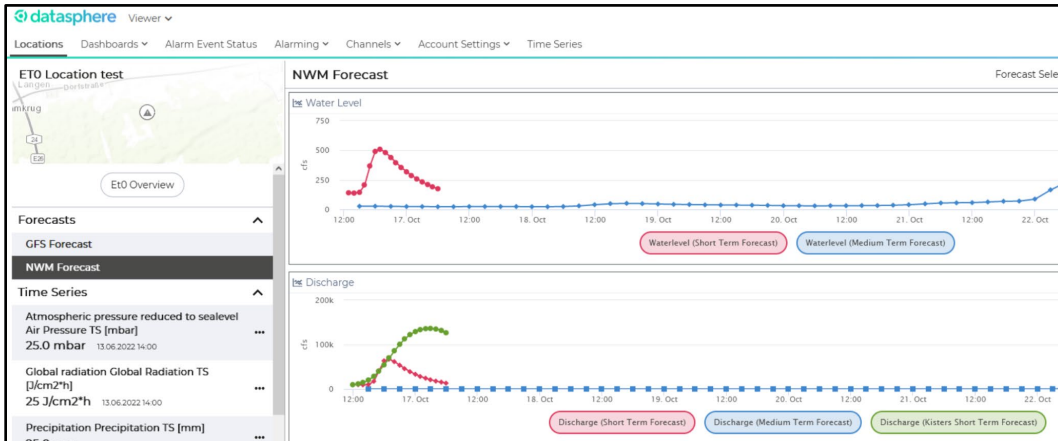
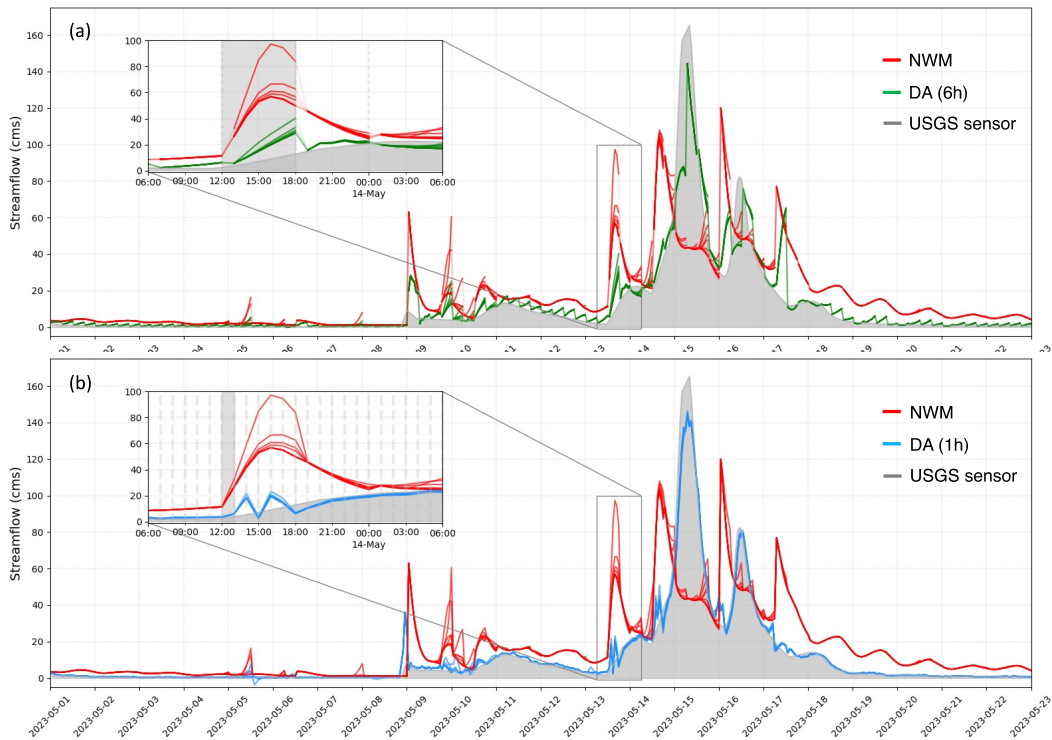


Figure 6.6. Adjusted forecasts displayed in Datasphere.

## 6.6. Data assimilation for improved forecasting

The NWM updates its short-range forecast every hour and its medium-range ensemble forecasts every six hours. Therefore, the forecasts generated at a specific time are not static, but rather dynamic, evolving with each update frequency based on the latest atmospheric forcings. Here, we assess the DA approach operationally by comparing forecasts updated at intervals of 6 hours and 1 hour, respectively, to the NWM. To be specific, the DA with a 6-hour update frequency employs both short and medium-range forecasts, which are generated during the 0/6/12/18 hour cycles. USGS gages are assimilated at a corresponding 6-hour frequency. Subsequently, streamflows for the upcoming 6 hours are predicted by utilizing the state-space MC model in conjunction with the short and medium-range forecasts from the NWM. It is important to note that while predictions can extend up to 18 hours for the short-range and between 8.5 and 10 days for the medium range, any predictions spanning more than 6 hours will be refreshed in the subsequent operational update cycle. Since the NWM updates its short-range forecast every hour, the DA with a 1-hour update frequency directly uses this forecast. For the medium-range forecasts, they are also updated hourly, making use of the forecast generated from the most recent update cycle. Data assimilation from USGS sensor gage is done on an hourly basis.

Data assimilation using Kalman Filtering significantly improves streamflow forecasting. Figure 6.7 illustrates the forecasted streamflow downstream, updated at frequencies of (a) 6 hours and (b) 1 hour, respectively. We effectively utilize the streamflow sensors in New Year Creek. By assimilating discharge data from the RQ-30 sensors at two upstream sites, corrections from the Kalman Filter propagate downstream, enhancing the downstream streamflow forecasts at the FM 1155 site. Furthermore, by incorporating data downstream, the forecast can start from the better characterized initial conditions. Here, the NWM forecast is shown in red, the USGS gage is depicted by a grey area plot, and the DA with 6-hour and 1-hour update frequencies are shown in green and blue, respectively. The shaded intervals in the inset plot indicate the update frequency. While the NWM significantly struggles with inaccuracies in predicting streamflows, both in terms of magnitude and timing, the DA with 6-hour and 1-hour update frequencies shows superior predictive performance. When compared to the NWM, the DA effectively reduces overpredictions and captures the actual streamflow with greater precision. Furthermore, the DA with a 1-hour update frequency enhances this predictive performance even more, as it updates the model and assimilates sensor data more frequently, leading to a better model realization.



**Figure 6.7** Forecasted streamflow with data assimilation, New York Creek at FM 1155 near Chapell Hill, Tx

Table 6.1 presents the predictive performance of each model on New Year Creek at FM 1155 evaluated using metrics such as Root Mean Square Error (RMSE), Nash-Sutcliffe Efficiency (NSE), Kling-Gupta Efficiency (KGE), and the Coefficient of Determination ( $R^2$ ). These data apply at In terms of performance, the DA with 1-hour update frequency shows the highest performance in every metric. Specifically, the DA with 1-hour update frequency reduces the RMSE by 79.2% compared to NWM and 52.7% relative to the DA with 6-hour update frequency. In terms of NSE, KGE, and  $R^2$ , it improves upon the NWM's values by approximately 800%, 167.5%, and 91.5% respectively, and outperforms the 6-hour update frequency by around 20.1%, 11.3%, and 13.2%. This highlights the marked advantage of more frequent data assimilation in predictive accuracy.

**Table 6.1 Performance evaluation for National Water Model, Data Assimilation with 6-hour and 1-hour update frequencies**

|         | RMSE                                | NSE                                | KGE                                 | $R^2$                               |
|---------|-------------------------------------|------------------------------------|-------------------------------------|-------------------------------------|
| NWM     | $21.358 \pm 0.258$                  | $-0.137 \pm 0.013$                 | $0.339 \pm 0.008$                   | $0.505 \pm 0.002$                   |
| DA (6h) | $9.39 \pm 0.052$                    | $0.799 \pm 0.002$                  | $0.815 \pm 0.002$                   | $0.854 \pm 0.002$                   |
| DA (1h) | <b><math>4.439 \pm 0.133</math></b> | <b><math>0.96 \pm 0.003</math></b> | <b><math>0.907 \pm 0.003</math></b> | <b><math>0.967 \pm 0.002</math></b> |

## 6.7. Data assimilation for improved estimation at ungauged bridges and roads

Given the limited number of sensors available for flood monitoring, the significance of improving discharge forecasts at ungauged sites, especially bridges and roads, cannot be overstated. While the NWM employs a nudging technique in data assimilation to enhance discharge forecasts, its major limitation is its exclusive focus on updating gaged sites. Consequently, ungauged sites are left to rely entirely on the NWM's projections. We leveraged the state-space MC model to emulate NWM's discharge predictions and implement the Kalman Filter for more precise data assimilation. Then, we examined the shifts in streamflow forecasts at ungauged sites post-assimilation and assessed the effectiveness of this approach using specific validation points.

The data assimilation was implemented in two watersheds: New Year Creek watershed and Llano watershed in Texas. We obtained the inputs from the analysis-assimilation product from the NWM and used the state-space MC method to reproduce the NWM discharge predictions. We used three USGS gages to assimilate the flows in New Year Creek watershed. In the Llano watershed, we used four gages from the USGS and seven gages from LCRA.

After implementing the data assimilation, we found that the error was reduced at all gage sites of the New Year Creek watershed. In the Llano watershed, we found that the error was reduced in 10 out of 11 gage sites. Table 6.2 and 6.3 show the mean flows, RMSE and percent reduction in RMSE after data assimilation (DA). The reduction in RMSE is similar for all gages in the New Year Creek watershed but the reduction in RMSE is seen to be generally higher for the LCRA gages compared to the USGS gages, the reason being that the USGS data are already assimilated through nudging in the analysis/assimilation product of the NWM.

**Table 6.2 Mean flows, RMSE and percent reduction in RMSE after data assimilation in New Year Creek watershed**

| Station ID | Gages | Observed Mean Flow (cms) | NWM Mean Flow (cms) | After DA (cms) | RMSE NWM | RMSE After DA | % Reduction in Error after DA |
|------------|-------|--------------------------|---------------------|----------------|----------|---------------|-------------------------------|
| 8111090    | USGS  | 2.17                     | 3.53                | 2.16           | 7.24     | 0.07          | 99.08                         |
| 8111085    | USGS  | 2.04                     | 3.18                | 2.03           | 4.43     | 0.04          | 99.11                         |
| 8111110    | USGS  | 10.96                    | 16.98               | 10.97          | 20.85    | 0.02          | 99.90                         |

**Table 6.3 Mean flows, RMSE and percent reduction in RMSE after data assimilation in Llano watershed**

| Station ID | Gages | Observed Mean Flow (cms) | NWM Mean Flow (cms) | After DA (cms) | RMSE NWM | RMSE After DA | % Reduction in Error after DA |
|------------|-------|--------------------------|---------------------|----------------|----------|---------------|-------------------------------|
| 2625       | LCRA  | 0.43                     | 0.04                | 0.00           | 1.33     | 1.29          | 3.02                          |
| 2616       | LCRA  | 1.99                     | 0.42                | 1.27           | 2.28     | 3.78          | -65.59                        |
| 2498       | LCRA  | 1.55                     | 0.42                | 1.55           | 8.39     | 0.03          | 99.66                         |
| 2443       | LCRA  | 0.03                     | 0.13                | 0.01           | 0.83     | 0.12          | 85.24                         |
| 2424       | LCRA  | 1.29                     | 0.11                | 0.04           | 4.75     | 3.88          | 18.49                         |
| 2399       | LCRA  | 10.65                    | 1.98                | 0.07           | 29.54    | 23.08         | 21.88                         |
| 2313       | LCRA  | 0.20                     | 1.10                | 0.16           | 2.82     | 0.06          | 97.92                         |
| 8151500    | USGS  | 0.02                     | 13.93               | 10.65          | 28.23    | 23.07         | 18.29                         |
| 8150800    | USGS  | 3.67                     | 0.52                | 0.42           | 6.10     | 4.45          | 27.07                         |
| 8150700    | USGS  | 0.07                     | 3.87                | 3.67           | 5.80     | 5.21          | 10.25                         |
| 8150000    | USGS  | 0.00                     | 2.10                | 1.98           | 2.13     | 2.05          | 3.94                          |

Figure 6.8 shows the changes in flows in the New Year Creek watershed due to data assimilation; discharge in all the streams is reduced after data are assimilated in the three gages. Similarly, Figure 6.8 shows the changes in flows in the Llano watershed due to data assimilation. Blue lines indicate streams where discharge increased after DA, while red lines indicate streams where discharge decreased after DA.

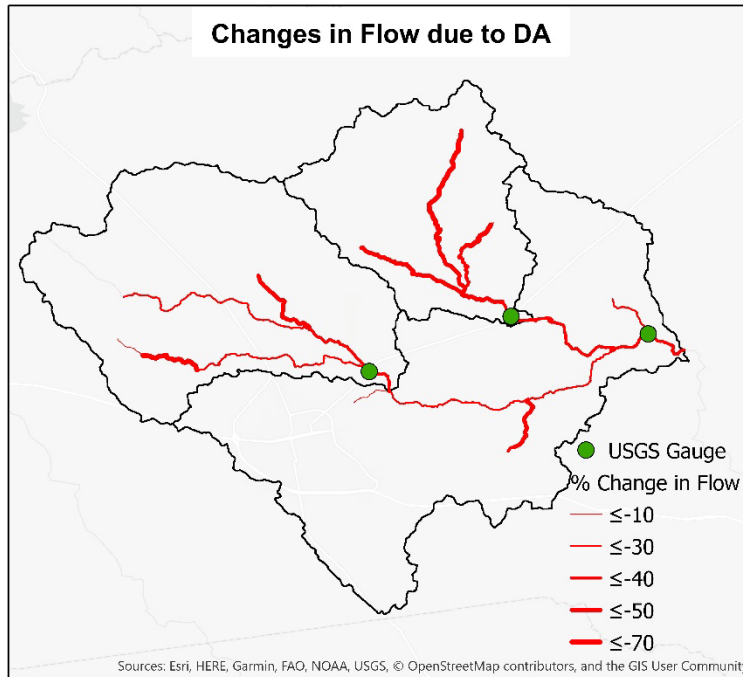


Figure 6.8 Changes in flow due to data assimilation in the New Year Creek watershed.

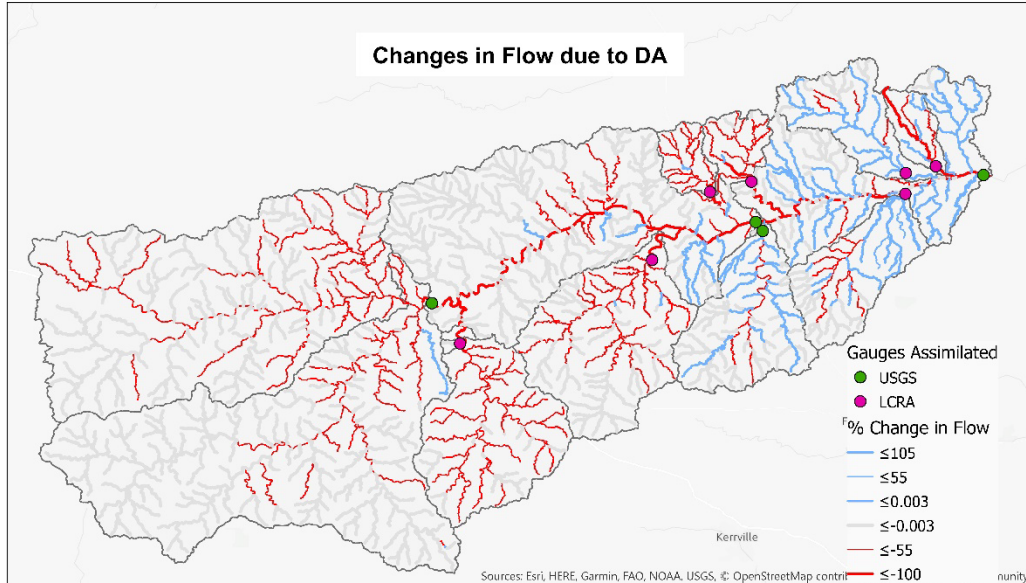


Figure 6.9 Changes in flow due to data assimilation in the Llano watershed

We analyzed the performance of the model at two validation sites - site 08111110, New Year Creek at FM 1155 near Chapel Hill, Tx, for New Year Creek watershed, and site 0851500, Llano River at Llano, for Llano watershed. For this scenario, the DA was implemented in all the remaining gages, excluding the gage

at the validation site. Figure 6.10 below show the performance of the model at the two validation sites.

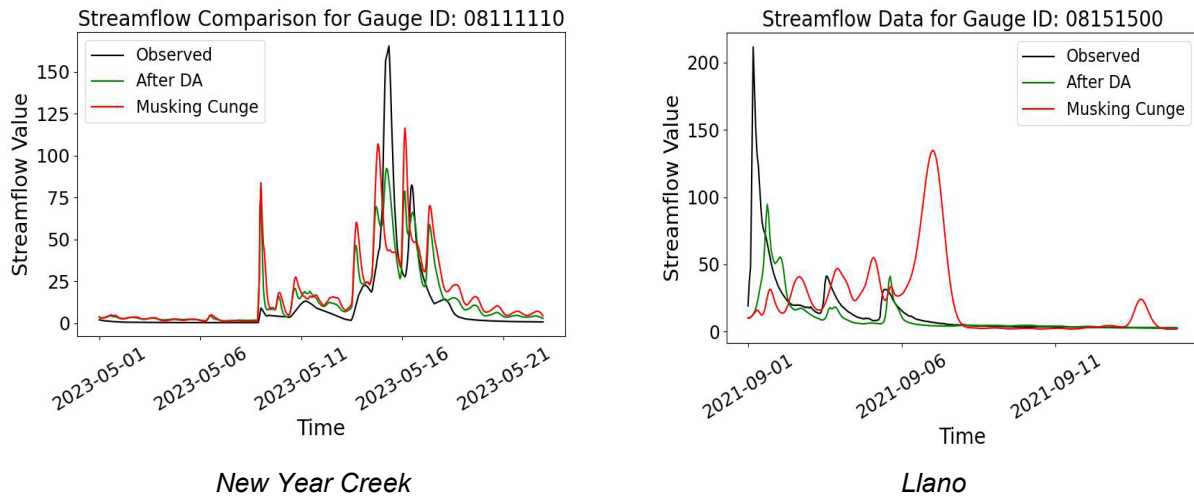


Figure 6.10 Streamflow comparison for validation site at New Year Creek watershed.

Table 6.4 below shows the performance of the model at the validation sites.

**Table 6.4 Performance of the model at validation sites**

| Model         | 08111110 |       | 08151500 |      |
|---------------|----------|-------|----------|------|
|               | RMSE     | KGE   | RMSE     | KGE  |
| Musking Cunge | 38.65    | -0.09 | 22.08    | 0.29 |
| DA            | 20.98    | 0.30  | 14.18    | 0.57 |

It is important to note that at the beginning of the project we had designed the gage placement at HUC10 scale so as to achieve a reasonably uniform gage coverage across all basins. *The DA results on the Llano watershed show that we are able to use DA at HUC8 scale, thus creating a framework for improvement of discharge estimates in other regions of Texas where we have gages installed.*

## 6.8. Analysis and modeling of hysteresis patterns

Flow in open channels exhibits hysteresis behavior, such that depth and discharge differ on the rising and falling limbs of the hydrograph. Typically, the depth-discharge relationship will consist of a loop, rotating either counterclockwise (meaning that the flow velocity is larger on the rising limb) or possibly clockwise (meaning that the flow velocity is larger on the falling limb). Because rating curves do not account for this looping behavior, discharge estimates produced

using traditional methods may not be accurate on the rising limb, leading to inaccuracy in flood forecasts.

Flood wave hysteresis is a well-known phenomenon, but research on stream characteristics influencing its magnitude and variability is limited. We thus decided to take advantage of the observations collected at the RQ-30 sites to analyze patterns of hysteresis over a range of streams and to quantify hysteresis patterns, including the rapid velocity increase prior to a flood event for potential use in flood warning systems.

We focused this analysis in particular on a subset of streams of different characteristics. The availability of high temporal resolution measurements allows the detection of hysteresis patterns, as the example shown in Figure 6.11. As seen, velocity increases rapidly during the rising limb, and decreases slowly during the falling limb. Velocity-to-stage ratio is higher at the start of the flow event.

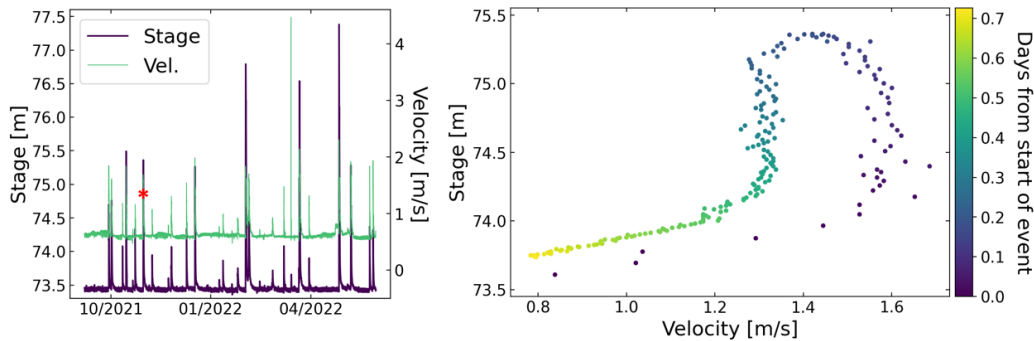


Figure 6.11: Stage and velocity data at a sensor in Carters Creek near College Station, TX.

To quantify the dependence on local stream characteristics, for each stream, we plotted stage-velocity curves for flow events with return periods greater than four weeks, resulting in a diverse set of hysteresis patterns, as it can be seen in the examples shown in Figure 6.12. Hysteresis varies among locations, but at a given location, similar patterns emerge.

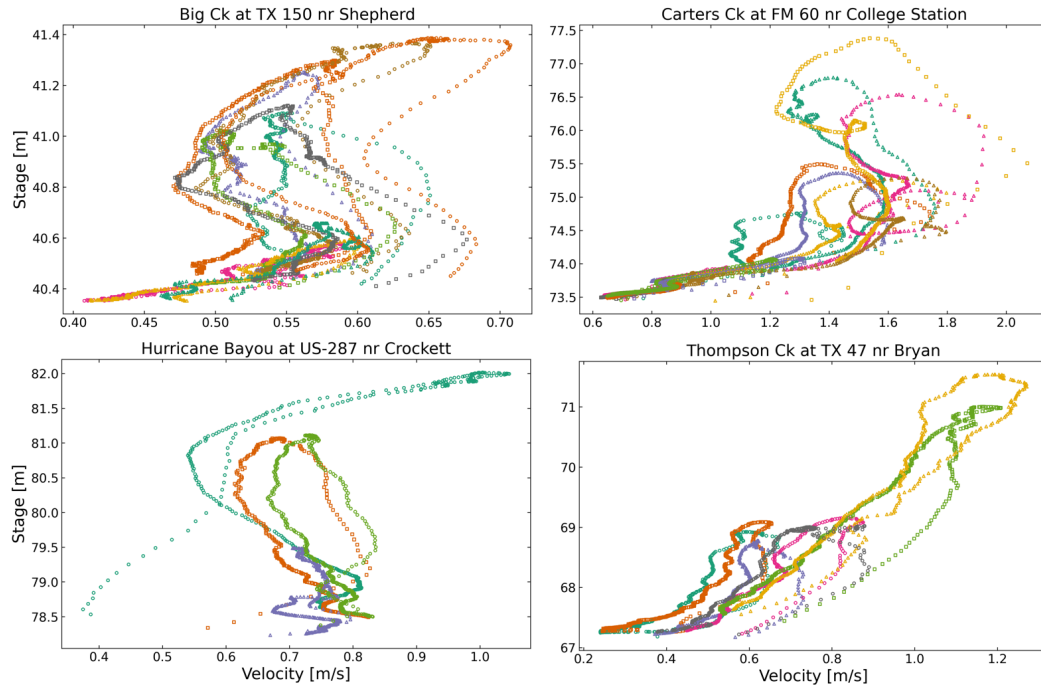


Figure 6.12: Plots of stage vs. velocity for four streams, where each curve is a unique flow event.

Understanding the physical basis of hysteresis provides a pathway for potentially using the pre-emptive velocity rise information as an early flood warning indicator. Moreover, understanding hysteresis behavior can enable more accurate discharge estimates on the rising limb that can in turn be used to improve flood modeling efforts. Traditional discharge estimates based on rating curves assume a one-to-one relationship between depth and discharge, which is inconsistent with real-world open channel flow behavior, and may underestimate discharge particularly on the rising limb. Incorporating hysteresis behavior gives rise to the potential for ‘dynamic rating curves’ that better capture real-world stage-discharge behavior.

The hysteresis behavior arises from the dynamical equations of motion describing unsteady fluid flow, and can be confirmed using simulations of open channel flow using the Saint-Venant equations. Figure 6.13 shows the depth time series and velocity time series of a simulated hydrograph at a single point in a prismatic open channel (top), along with the forces acting on a control volume at that point (bottom). As can be seen from this figure, the velocity peaks roughly 45 minutes before the peak of the depth hydrograph. Considering the momentum component of the Saint-Venant equations, the change of momentum in fluid flow (i.e. acceleration) is influenced by inertial, hydrostatic, gravitational, frictional, and local forces. From Figure 6.13 (bottom), the timing and scale of each of these

forces can be observed. Here, it can be seen that the peak of the velocity hydrograph is largely driven by the hydrostatic force, while the frictional and gravitational forces lag behind the velocity peak. Specifically, the steep gradient in the water surface associated with the advancing front of a flood wave generates a hydrostatic force in the direction of flow, causing the water to accelerate. This acceleration leads to a peak in the velocity hydrograph that precedes that of the depth hydrograph.

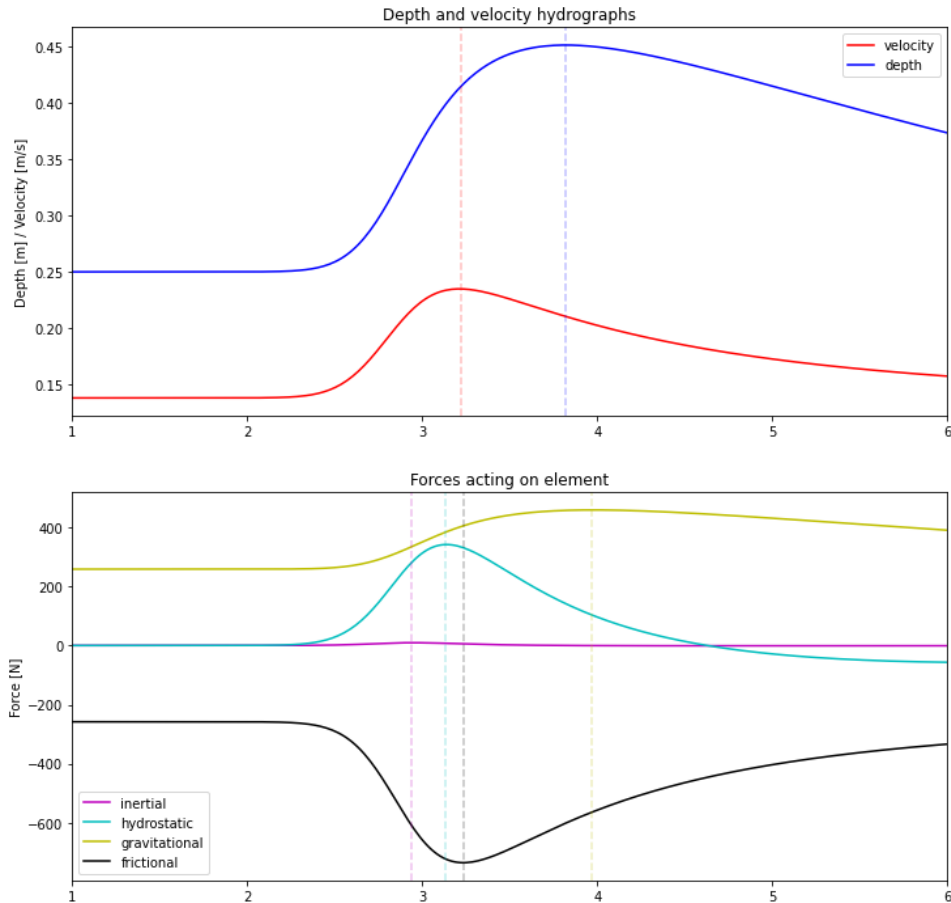


Figure 6.13. (Top): Depth and velocity hydrographs for a flood wave at a single point in a rectangular channel, simulated using the Saint-Venant equations. (Bottom): Forces acting on the control volume, including inertial, hydrostatic, gravitational, and frictional forces.

The RQ-30 gages in the TxDOT streamflow monitoring network use a parameter called the k-factor to translate surface velocity measurements into discharge measurements used for flood forecasting. We theoretically-derived the k-factor used at the gages. This showed promise in improving discharge estimates produced by RQ-30 gages. Because this k-factor can be derived from known values of channel surface roughness—a property that can be estimated directly

from material properties—it can potentially be applied to new gage sites without the need for calibration to manual discharge measurements. By reducing the need for manual calibration, and providing an alternative source of verification for discharge estimates, this methodology has the potential to help expand the number of trusted gage sites in the RQ-30 network.

## 6.9. Conclusions

---

Based on our analysis, we find that the performance of the National Water Model (NWM) varies spatially across the State of Texas. In particular, the NWM was found to have greater errors in areas that experienced higher precipitation, and on average, it underestimated discharge during the time period analyzed. Additionally, the analysis of mean discharge indicated that error increased with mean discharge and the analysis of stream orders indicated that stream order 4 had the lowest RMSE, while stream orders 6 and 7 had the highest RMSE values. Further, the assessment of similarity between the NWM and observed annual peak streamflow distributions showed that the NWM was able to capture the annual peak flow in less than 44% of the locations. Additionally, no spatial bias is observed over the state of Texas, suggesting that the NWM does not preferentially overperforms or underperforms in specific areas.

We developed a scalable and solution architecture utilizing KISTERS' cloud-based services to perform data assimilation runs dynamically, based on the currently available discharge measurements. The dynamic approach to the discharge measurements makes the solution robust and less sensitive to temporary data unavailability. It automatically adapts to the currently available gauges, making fully autonomous updating the models. The data assimilation based on excess rainfall optimization can be deployed at a local, at HUC8 or larger scale if the necessary discharge observations are available.

A comprehensive Data Assimilation (DA) approach called the State-Space Muskingum method has been developed in this project to use observed streamflow data from gauges not employed by the NWS in generating the National Water Model streamflow forecasts to correct those forecasts by comparing them with observed flows at the additional gauges. This method uses the same Muskingum-Cunge flow routing framework as does the NWM, but places this within a Kalman filter statistical framework drawn from Optimal Control theory.

Results have been presented from two data networks – from three gauges in the TxDOT RQ-30 network in the New Year Creek watershed located near Brenham, Texas, and from six gauges in the Lower Colorado River Authority (LCRA)

gauging network in the Llano watershed located west of Austin, Texas. At New Year Creek, both in terms of magnitude and timing of the flows, the DA with 6-hour and 1-hour update frequencies shows superior predictive performance to the National Water Model forecasts taken alone. Furthermore, the DA with a 1-hour update frequency enhances this predictive performance in particular, as it updates the model and assimilates sensor data more frequently, leading to a better model realization.

Similar results were achieved in the Llano basin at a much larger spatial scale (1700 stream reaches compared to about 30 at New Year Creek). It is important to note that at the beginning of the project we had designed the gage placement at HUC10 scale so as to achieve a reasonably uniform gage coverage across all basins. The DA results on the Llano watershed show that we are able to use DA at larger HUC8 scale, thus creating a framework for improvement of discharge estimates in other regions of Texas where we have gages installed. In both the New Year Creek watershed and in the larger Llano basin, the DA method succeeded in consistently adjusting the NWM streamflow forecasts in ungauged reaches as well as in the gauged reaches.

The analysis of RQ-30 stage and discharge data has revealed previously unobserved hysteresis behavior in which the discharge and velocity are larger on the rising limb of the hydrograph. An analysis of hysteresis based on the Saint-Venant equations suggests that the pattern observed at the gauges is real and this finding opens the door to more accurate estimation of discharge through the development of 'dynamic rating curves' that account for this behavior.

## Chapter 7. Conclusions

The overall goal of this project is to improve real-time information that TxDOT can use to manage its operations during flood emergencies. The project has six key accomplishments:

**Stream Gauge Network** -- established and maintained a network of 80 radar stream gauges on TxDOT bridges that measure water surface elevation and velocity and use these to calculate discharge.

**Streamflow Velocimetry** – developed a method for efficiently calibrating the radar gauges by comparing their measurements with those from Acoustic Doppler Current Profilers. This allows for time patterns of interaction between water level and velocity that differ from one site to another.

**Flood Assessment System for TxDOT (FAST)** – this is a set of flood map services, accessed through a readily usable web viewer, that provide flexible map overlays displaying current and forecast flood information on a background of TxDOT roads, bridges and jurisdictional boundaries.

**Bridge Warning Service** – a demonstration bridge warning service has been developed for 19,000 bridges state-wide, and implemented in a prototype operational form as part of FAST.

**Road Elevation Model** – a 3D model of the elevation of the roadway surface of the TxDOT Austin District comprising 3.8 billion LIDAR points covering 38,000 miles of roadway. This is a first for TxDOT and for Texas. This is accompanied by a series of three tutorials that explain how flood water depth is calculated for individual road segments, and summarized using the TxDOT Roadway Inventory for flooding along Shoal Creek in Austin, Texas.

**Forecast Error and Data Assimilation** – this is an assessment of the error in the National Water Model discharge forecasts, and how this error is reduced by using data assimilation to combine the forecast information with observed information at TxDOT and LCRA network gauges.

Each of these accomplishments is now described further.

### Stream Gauge Network

A network of 80 RQ-30 radar stream gauges has been established in data sparse-areas of flood-prone southeast Texas, with about half the gauges on tributaries of inland Brazos and Trinity basins and the other half in coastal basins where flat

terrain makes gauging by traditional USGS methods challenging. The resulting gauging distribution approximately doubles the existing USGS gauging density in the chosen watersheds. The gauges were sited to provide TxDOT with early warning of flood events, to be grouped within watersheds so that the measurements can be used to correct streamflow estimates in adjacent streams using data assimilation, and to be good streamflow measurement locations located on high bridges to protect the gauge equipment during flood events.

The RQ-30 sensors are designed to have a small footprint on a TxDOT bridge, being attached with a bracket bolted to the side of the bridge. They are solar powered and communicate through the cell phone network. The RQ-30 sensor used for this project requires less time to install compared to a traditional USGS gauge. Once bridge attachment permitting is complete, traditional USGS gauges can take up to one week to install while the typical RQ-30 velocimetry gauge could be operational in less than 4 hours, often allowing the opportunity to install two complete gauges in a single day.

The gauges have been regularly visited to check their operation. The radar water surface elevation measurement has been found to be reliable, with 93% of the stage verifications being within +/- 0.05 ft of a wire-weight measurement without adjustment of the radar sensor at the gauge sites. The gauge equipment has functioned successfully with only minor outages at a few sites. There have been challenges with cell-phone communication connectivity at times in some rural areas. Data for all gauges are being publicly reported through the USGS National Water Information System, and are also being ingested into the NWS data system. Progress is being made in setting NWS alert levels at each gauge that signal minor, moderate and major flooding.

### **Streamflow Velocimetry**

The United States Geological Survey (USGS) traditionally employs a method of discharge computation relating continuously measured stage to an associated discharge built using numerous physical discharge measurements, which is labor intensive. A significant research objective of this project is to evaluate the feasibility of methods alternative to the traditional USGS stage-discharge relation, namely the computation of discharge using surface velocimetry. Velocimetry gauges are not widely used by the USGS as a method of discharge computation. The datasets recorded during this project have progressed the current knowledge of velocimetry within the USGS, bringing it closer to an accepted method of computing discharge.

Cross sections surveyed during the project have shown little change caused by natural means, preserving the stage-area relation necessary for consistent discharge computation using velocimetry. Modifications made to the gauge cross-section were the only discernable differences that required a resurvey during the project. The Cross-sectional area is subject to change due to flood events, which can directly affect the computation of discharge using velocimetry especially for base-flow conditions.

Velocity data was accurately recorded when flows were greater than approximately 0.8 feet per second. Velocities below 0.8 ft per second were often less available as the velocities slowed because the measurements are close to the lower bound of the sensor's operational range and high signal to noise ratio at lower velocities. The steadiness of measured velocities is notably influenced by turbulence from bridge piers, debris, and other channel-related eddy velocities which cause fluctuations between consecutive data points.

The RQ-30 gauges are calibrated by comparing their discharge measurements with those collected in the field using Acoustic Doppler Current Profilers (ADCP). Rather than making frequent ADCP measurements, targeted stages were selected and measured to constrain the original profile. Targeted measurements include the main channel, the transition between main channel and overbank, and overbank stages. Once the targeted measurements are made, the roughness coefficient is adjusted to best fit the calibration points. Although the discovery of the targeted measurement approach to velocimetry discharge calibration has greatly reduced the time needed to calibrate a streamflow gauge, more data is needed to ensure the method is valid for all conditions. Site conditions such as high slope, variable bedforms, bridge disturbances, and backwater affected flows have not been fully assessed.

The water level and surface velocity measurements at the 80 RQ-30 stream gauge sites showed that water level and velocity do not rise and fall in lock-step with one another as a flood hydrograph passes through a gauging site. Rather, these two variables exhibit complex interactions, varying from one site to another, most often with the velocity rising ahead of the water surface elevation as the flood rises, and the reverse as the flood falls. This pattern is called hysteresis. A theoretical simulation model study, described in Chapter 6 of this report, demonstrated that this phenomenon is an anticipated consequence of the time variation of the balance of forces contained in the governing equations describing one-dimensional open channel flow. Further study using more comprehensive hydrodynamic models at multiple stream gauging sites is needed to understand this phenomenon better.

### **Flood Assessment System for TxDOT (FAST)**

At the beginning of this project, there was a significant uncertainty as to how real-time information could be delivered effectively to TxDOT during flood emergencies. What is needed is “One Water Map” – the ability to visualize the flood water impacting the road and bridge system in a context of flood inundation across the whole landscape. The base of the “One Water Map” is the real-time flood inundation mapping now being delivered by the National Weather Service to about half of Texas, with coverage of the state expected to be complete by October 2025.

The NWS flood inundation mapping is being delivered using the ESRI web map services framework, and the research team adopted the same framework for production of comparable flood map services for bridge warnings, flooded road depth and summary of impacts of road flooding over a region. To these maps are added similarly constructed maps for current and forecast precipitation and for discharge at the USGS and TxDOT gauges. These map services are collected into layers and made accessible to TxDOT through an ESRI web map services viewer. This constitutes the Flood Assessment System for TxDOT (FAST).

The design of the FAST maps has been tested in two large-scale flood emergency response exercises held in the Beaumont District in February 2022, and in the Austin District in January 2023. TxDOT Maintenance staff participated in these exercise, both Emergency Operations Center Managers and Maintenance Supervisors and field staff. They responded very positively to the FAST web map services framework and had many suggestions as to how the maps could be improved for their use. By overlaying current and forecast flood conditions on static base map layers of TxDOT roads, bridges, and jurisdictional boundaries, it was possible for Maintenance staff to zoom in to check conditions in a particular area, and to zoom out and grasp the overall picture. The ESRI web map services proved to be reliable, easy to use, and readily understood by the Maintenance staff.

A record of flood impact on the road transportation system is being maintained by TxDOT as part of its Highway Conditions Reporting System (HCRS). This contains the length of road closures due to all causes, one of which is flooding, and contains the beginning and end time of the closure. When plotted as a GIS layer, the length of the road closed is obtained. By summing these lengths at any time, the total length of roads closed is obtained, and by summing these over a flood event, the impact of this flood event on road transportation is determined. A plot of the cumulative impact of such events since the HCRS was initiated in 2014 reveals the range of significant flood events across Texas that have occurred since then.

### **Bridge Warning Service**

A particular concern for TxDOT during floods is the threat of flooding of span bridges, which become at risk if the flood waters rise above the low chord elevation of the bridge and hit the bridge support beams. Bridge overtopping and catastrophic bridge failure can follow. Once a flood has passed, the bridges on roads closed due to flooding have to be inspected to ensure that scour around the bridge foundations during the flood has not occurred.

A computer routine called Tx-Bridge has been developed in this project which surveys the LIDAR data collections across Texas and extracts all the collections of LIDAR points that are labelled as “bridge” in the data collections. At each bridge location a “bridge envelope” has been constructed that for a profile line along the road passing over the bridge records the elevation of the bridge deck, the elevation of the stream cross-section, and using a formula for bridge thickness estimates the low chord elevation. In all, Tx-Bridge identified a little more than 37,000 bridges of all types.

Of these, about 19,000 span bridges were identified as being located on National Water Model streams and thus capable of having their water conditions forecast. A demonstration Texas Flood Forecaster system was built and connected to the National Water Model forecast information accessible through the NOAA NOMADS server. A system of color codes was applied to each bridge point, denoting the height of the water as being less than 0.5 ft from the low chord, 0.5 – 2 ft, 2ft – 5ft, and more than 5ft from the low chord. The use of this system to track the movement of a storm across Texas though its impact on the bridge system was demonstrated during flood conditions occurring on 26 October 2023.

The KISTERS firm supporting this project has incorporated the same information into its Datasphere system and a map of these bridges now appears in the FAST prototype web viewer.

The state-wide demonstration bridge warning service and its translation into a prototype operational system by KISTERS is a first for TxDOT. Once the bridge warning service is moved into an operational system state-wide it will be a critical component of the Flood Assessment System for TxDOT.

### **Road Elevation Model**

A particular challenge for the research team in carrying out this project is that flood impact depends on water elevation and TxDOT has not up to this time recorded the elevation of its road and bridge assets. For the Austin District, this challenge was met by constructing a Road Elevation Model, comprising 3.8

billion LIDAR points covering the roadway surface of 38,000 miles of roads in the 11-county Austin District.

The Road Elevation Model was built using a GIS coverage of the roadway surface area defined by Artificial Intelligence interpretation of 6" Hexagon aerial imagery carried out by the Ecopia corporation of Toronto, Canada. TxDOT RTI authorized the purchase of this dataset for use in this research project, along with the road centerlines down the middle of the roadway polygon coverage. Roads constitute only 1.6% of the total landscape in area. For the 11-county Austin District, the TxGIO LIDAR coverage has several data collections of different ages and data densities, whose 1.5 TB of data were stored at the Texas Advanced Computing Center in about 10,000 spatial tiles. At the Oak Ridge National Laboratory, the LIDAR data from these tiles were filtered using the Ecopia roadway coverage. The end result is a set of LIDAR data files partitioned by Maintenance Sections that total 19 GB of data, about 1.3% of the file size of the original overlapping LIDAR data coverages.

Along with the LIDAR data points the 2D road polygons and centerlines were converted to 3D road polygons and centerlines as part of the computation. The combination of all these data constitutes the Road Elevation Model for the Austin District. The 2D and 3D road centerline and polygon data are protected by Ecopia using licensing arrangements that mean these data cannot be shared outside of TxDOT. However, the derived LIDAR points on the roadway surface are a publicly accessible and freely shared dataset.

The Road Elevation Model is a significant accomplishment, a first for TxDOT and for Texas. This is a critical asset in improving public safety during flood events by allowing more precise assessment of flood impact on the road transportation system of the Austin District.

A series of three ArcGIS tutorials have been prepared that show, respectively, (1) how to select the road elevation points located in the Shoal Creek watershed in Austin, Texas; (2) how to create a LIDAR-point based flood inundation map on Anderson Lane at Shoal Creek by subtracting the road surface elevation from the water surface elevation defined by the City of Austin's 100-year HEC-RAS model computation; and (3) the construction of a list of flooded roads impacted by a 100-year flood along Shoal Creek, indexed by road name and functional classification in the TxDOT Roadway Inventory.

This is another significant accomplishment, because it shows how the Road Elevation Model describing the road in (x,y,z), is linked to the TxDOT Roadway

Inventory representation describing the road in (x,y,m), where m is the Distance from Origin (DFO) measure value used in TxDOT roadway planning.

In this way, the technical methods needed to create the flooded roads map and the flood impact map in the Flood Assessment System for TxDOT have been demonstrated.

### **Forecast Error and Data Assimilation**

The National Water Model was found to have greater errors in areas that experienced higher precipitation, and on average, it underestimated discharge during the time period analyzed. No spatial bias is observed over the state of Texas, suggesting that the NWM does not preferentially overperform or underperform in specific areas.

A scalable solution architecture was developed utilizing KISTERS' cloud-based services to perform data assimilation computations dynamically, based on the currently available discharge measurements. This solution automatically adapts to the currently available gauges, making the system fully autonomous in updating the forecast data even if there are gauge outages..

A comprehensive Data Assimilation (DA) approach called the State-Space Muskingum method has been developed in this project to use observed streamflow data from gauges not employed by the NWS in generating the National Water Model streamflow forecasts to correct those forecasts by comparing them with observed flows at the additional gauges.

Results have been presented in Chapter 6 from two data networks – from three gauges in the TxDOT RQ-30 network in the New Year Creek watershed located near Brenham, Texas, and from six gauges in the Lower Colorado River Authority (LCRA) gauging network in the Llano watershed located west of Austin, Texas. At New Year Creek, both in terms of magnitude and timing of the flows, the DA with 6-hour and 1-hour update frequencies shows superior predictive performance to the National Water Model forecasts taken alone. Furthermore, the DA with a 1-hour update frequency enhances this predictive performance in particular, as it updates the model and assimilates sensor data more frequently, leading to a better model realization.

Similar results were achieved in the Llano basin at a much larger spatial scale (1700 stream reaches compared to about 30 at New Year Creek). It is important to note that at the beginning of the project we had designed the gage placement at HUC10 scale so as to achieve a reasonably uniform gage coverage across all basins. The DA results on the Llano watershed show that we are able to use DA at larger

HUC8 scale, thus creating a framework for improvement of discharge estimates in other regions of Texas where we have gages installed. In both the New Year Creek watershed and in the larger Llano basin, the DA method succeeded in consistently adjusting the NWM streamflow forecasts in ungauged reaches as well as in the gauged reaches.

## References

- Arcement, G.J. and Schneider V.R., 1989, Guide for Selecting Manning's Roughness Coefficients for Natural Channels and Flood Plains: U.S. Geological Survey Water-Supply Paper 2339, 1 p.
- Grzyb, S., and others, 2025, Radar-based field measurements of gage-height and surface velocity and resulting cross-sectional area and discharge from 80 U.S. Geological Survey streamgages for various locations in Texas, 2021–24, USGS ScienceBase <https://doi.org/10.5066/P14LSAMD>
- Kisters, 2023, Products – Data Acquisition, accessed October 27, 2023 at: <https://www.hyquestsolutionsamerica.com/>.
- Levesque, V.A., and Oberg, K.A., 2012, Computing discharge using the index velocity method: U.S. Geological Survey Techniques and Methods 3–A23, 148 p. (Also available at <https://pubs.usgs.gov/tm/3a23/>.)
- McCallum, A.M., Andersen, M.S., Giambastiani, B.M.S., Kelly, B.F.J., and Acworth, R.I., 2013, River–aquifer interactions in a semi-arid environment stressed by groundwater abstraction: *Hydrological Processes*, v. 27, no. 7, p. 1072–1085, accessed May 17, 2023, at <https://doi.org/10.1002/hyp.9229>
- Rantz, S.E., and others, 1982, Measurement and computation of streamflow—Volume 2. Computation of discharge: U.S. Geological Survey Water-Supply Paper 2175, 284 p.
- Turnipseed, D.P., and Sauer, V.B., 2010, Discharge measurements at gaging stations: U.S. Geological Survey Techniques and Methods book 3, chap. A8, accessed May 17, 2023, at <https://doi.org/10.3133/tm3A8>.
- U.S. Geological Survey, 2021, AreaComp Hydroacoustics Software, accessed October 27, 2023, at URL <https://www.usgs.gov/software/areacomp-hydroacoustics-software>.
- U.S. Geological Survey, 2023, National Water Information System data available on the World Wide Web (USGS Water Data for the Nation), accessed October 27, 2023, at URL <https://waterdata.usgs.gov/nwis/>.